REPUBLIQUE DU CAMEROUN
Paix – Travail – Patrie
-=-=-=-=-=-=-=-=-=-
UNIVERSITE DE YAOUNDE I
-=-=-=-=-=-=-=-=-=-
CENTRE DE RECHERCHE ET DE FORMATION DOCTORALE EN SCIENCES TECHNOLOGIQUES
-=-=-=-=-=-=-=-=-=-
UNITE DE RECHERCHE ET DE FORMATION DOCTORALE PHYSIQUE ET APPLICATIONS
-=-=-=-=-=-=-=-=-=-
BP: 812 YAOUNDE
-=-=-=-=-=-=-=-=-=-
Email: crfdstg@uy1.uninet.cm
-=-=-=-=-=-=-=-=-=-

REPUBLIC OF CAMEROON
Peace – Work – Fatherland
-=-=-=-=-=-=-=-=-=-
THE UNIVERSITY OF YAOUNDE I
-=-=-=-=-=-=-=-=-=-
POSTGRADUATE SCHOOL OF SCIENCE, TECHNOLOGY AND GEOSCIENCE
-=-=-=-=-=-=-=-=-=-
RESEARCH AND POSTGRADUATE TRAINING UNIT FOR PHYSICS AND APPLICATIONS
-=-=-=-=-=-=-=-=-=-
P.O. BOX: 812 YAOUNDE
-=-=-=-=-=-=-=-=-=-
Email: crfdstg@uy1.uninet.cm
-=-=-=-=-=-=-=-=-=-

DEPARTMENT OF PHYSICS

LABORATORY OF MECHANICS, MATERIALS AND STRUCTURES

ENERGY CONTROL TRANSMISSION IN FORBIDDEN PHONON BANDS OF FERMI-PASTA-ULAM LATTICES

Thesis submitted and defended in fulfilment of the requirements

for the degree of Doctor of Philosophy (PhD) in Physics

Speciality: Fundamental Mechanics and Complex Systems

by

SIMADJI NGAMOU Christian
Registration number : 10W0760
Master of Science in Physics

Under the supervision of

TCHAWOUA Clément,
Professor,

University of Yaounde I

2025

ENERGY CONTROL TRANSMISSION IN FORBIDDEN PHONON BANDS OF FERMI-PASTA-ULAM LATTICES

Thesis submitted and defended in fulfillment of the requirements for
the degree of Doctor of Philosophy (PhD) in Physics
Specialty: Fundamental Mechanics and Complex Systems

By
SIMADJI NGAMOU Christian
Registration number : 10W0760
Master of Science in Physics

Under the supervision of
TCHAWOUA Clément
Professor

University of Yaounde I
2025

Contents

List of Figures

List of abbreviations and acronyms

FPU : Fermi-Pasta-Ulam
NST : Nonlinear SupraTransmission
QDA : Quasi-Discrete Approximation
RWA : Rotating Wave Approximation
NSW : Nonlinear Sinusoidal Wave
FFT : Fast Fourier Transform
FT : Fourier Transform
SPD : Spectral Power Density
NLS : NonLinear Schrödinger
MATLAB : Matrix Laboratory
FORTRAN : Formula Translating

Dedications

I dedicate this thesis to my kid SIMADJI CHRISTIANNA

UNIVERSITÉ DE YAOUNDÉ I **Faculté des Sciences** Division de la Programmation et du Suivi des Activités Académiques		THE UNIVERSITY OF YAOUNDE I **Faculty of Science** Division of Programming and Follow-up of Academic Affaires
LISTE DES ENSEIGNANTS PERMANENTS		**LIST OF PERMANENT TEACHING STAFF**

ANNÉE ACADEMIQUE 2024/2025

(Par Département et par Grade)

DATE D'ACTUALISATION 16 décembre 2024

ADMINISTRATION

1. **DOYEN :** OWONO OWONO Luc Calvin, *Professeur*
2. **VICE-DOYEN / DPSAA:** NDJIGUI Paul-Désiré, *Professeur*
3. **VICE-DOYEN / DSSE :** NYEGUE Maximilienne Ascension, *Professeur*
4. **VICE-DOYEN / DRC :** NOUNDJEU Pierre, *Maître de Conférences*
5. **Chef Division Administrative et Financière :** NDOYE FOE Florentine Marie Chantal, *Maître de Conférences*
6. **Chef Division des Affaires Académiques, de la Recherche et de la Scolarité DAARS :** AJEAGAH Gideon AGHAINDUM, *Professeur*

1- DÉPARTEMENT DE BIOCHIMIE (BC) (44)

N°	NOMS ET PRÉNOMS	GRADE	OBSERVATIONS
1.	BIGOGA DAIGA Jude	Professeur	En poste
2.	FEKAM BOYOM Fabrice	Professeur	En poste
3.	KANSCI Germain	Professeur	En poste
4.	MBACHAM FON Wilfred	Professeur	En poste
5.	MOUNDIPA FEWOU Paul	Professeur	*Chef de Département*
6.	NGUEFACK Julienne	Professeur	En poste
7.	NJAYOU Frédéric Nico	Professeur	En poste
8.	OBEN Julius ENYONG	Professeur	En poste
9.	ACHU Merci BIH	Maître de Conférences	En poste
10.	AKINDEH MBUH NJI	Maître de Conférences	En poste
11.	ATOGHO Barbara MMA	Maître de Conférences	En poste
12.	AZANTSA KINGUE GABIN BORIS	Maître de Conférences	En poste
13.	BELINGA née NDOYE FOE F. M. C.	Maître de Conférences	*Chef DAF / FS*
14.	DAKOLE DABOY Charles	Maître de Conférences	En poste
15.	DONGMO LEKAGNE Joseph Blaise	Maître de Conférences	En poste
16.	DJUIDJE NGOUNOUE Marceline	Maître de Conférences	En poste
17.	DJUIKWO NKONGA Ruth Viviane	Maître de Conférences	En poste
18.	EFFA ONOMO Pierre	Maître de Conférences	*VD/FS/Univ Ebwa*
19.	EWANE Cécile Annie	Maître de Conférences	En poste
20.	KENGNE NOUEMSI Anne Pascale	Maître de Conférences	En poste
21.	KOTUE TAPTUE Charles	Maître de Conférences	En poste
22.	LUNGA Paul KEILAH	Maître de Conférences	En poste
23.	MANANGA Marlyse Joséphine	Maître de Conférences	En poste
24.	MBONG ANGIE M. Mary Anne	Maître de Conférences	En poste
25.	MOFOR née TEUGWA Clotilde	Maître de Conférences	*Doyen FS / UDs*
26.	NANA Louise épouse WAKAM	Maître de Conférences	En poste
27.	NGONDI Judith Laure	Maître de Conférences	En poste
28.	Palmer MASUMBE NETONGO	Maître de Conférences	En poste
29.	PECHANGOU NSANGOU Sylvain	Maître de Conférences	En poste
30.	TCHANA KOUATCHOUA Angèle	Maître de Conférences	En poste
31.	BEBEE Fadimatou	Chargée de Cours	En poste
32.	BEBOY EDJENGUELE Sara N.	Chargée de Cours	En poste
33.	FONKOUA Martin	Chargé de Cours	En poste
34.	FOUPOUAPOUOGNIGNI Yacouba	Chargé de Cours	En poste
35.	KOUOH ELOMBO Ferdinand	Chargé de Cours	En poste
36.	MBOUCHE FANMOE Marceline J.	Chargée de Cours	En poste
37.	OWONA AYISSI Vincent Brice	Chargé de Cours	En poste
38.	WILFRED ANGIE ABIA	Chargé de Cours	En poste
39.	BAKWO BASSOGOG Christian Bernard	Assistant	En Poste
40.	ELLA Fils Armand	Assistant	En Poste

41.	EYENGA Eliane Flore	Assistante	En Poste
42.	MADIESSE KEMGNE Eugenie Aimée	Assistante	En Poste
43.	MANJIA NJIKAM Jacqueline	Assistante	En Poste
44.	WOGUIA Alice Louise	Assistante	En Poste

2- DÉPARTEMENT DE BIOLOGIE ET PHYSIOLOGIE ANIMALES (BPA) (50)

1.	AJEAGAH Gideon AGHAINDUM	Professeur	*DAARS/FS*
2.	DIMO Théophile	Professeur	En Poste
3.	DJIETO LORDON Champlain	Professeur	En Poste
4.	DZEUFIET DJOMENI Paul Désiré	Professeur	En Poste
5.	ESSOMBA née NTSAMA MBALA	Professeur	*CD et Vice Doyen/FMSB/UYI*
6.	KEKEUNOU Sévilor	Professeur	*Chef de Département*
7.	NJAMEN Dieudonné	Professeur	En poste
8.	NOLA Moïse	Professeur	En poste
9.	TAN Paul VERNYUY	Professeur	En poste
10.	TCHUEM TCHUENTE Louis Albert	Professeur	*Inspecteur de service / Coord.Progr./MINSANTE*
11.	ZEBAZE TOGOUET Serge Hubert	Professeur	En poste

12.	ALENE Désirée Chantal	Maître de Conférences	*Vice Doyen/ Uté Ebwa*
13.	ATSAMO Albert Donatien	Maître de Conférences	En poste
14.	BILANDA Danielle Claude	Maître de Conférences	En poste
15.	DJIOGUE Séfirin	Maître de Conférences	En poste
16.	GOUNOUE KAMKUMO Raceline épse FOTSING	Maître de Conférences	En poste
17.	JATSA BOUKENG Hermine épse MEGAPTCHE	Maître de Conférences	En Poste
18.	KANDEDA KAVAYE Antoine	Maître de Conférences	En poste
19.	LEKEUFACK FOLEFACK Guy B.	Maître de Conférences	En poste
20.	MAHOB Raymond Joseph	Maître de Conférences	En poste
21.	MBENOUN MASSE Paul Serge	Maître de Conférences	En poste
22.	MEGNEKOU Rosette	Maître de Conférences	En poste
23.	MOUNGANG Luciane Marlyse	Maître de Conférences	En poste
24.	NOAH EWOTI Olive Vivien	Maître de Conférences	En poste
25.	MONY Ruth épse NTONE	Maître de Conférences	En Poste
26.	MVEYO NDANKEU Yves Patrick	Maître de Conférences	En poste
27.	NGUEGUIM TSOFACK Florence	Maître de Conférences	En poste
28.	NGUEMBOCK	Maître de Conférences	En poste
29.	TAMSA ARFAO Antoine	Maître de Conférences	En poste
30.	TOMBI Jeannette	Maître de Conférences	En poste

31.	AMBADA NDZENGUE GEORGIA ELNA	Chargé de Cours	En poste
32.	BASSOCK BAYIHA Etienne Didier	Chargé de Cours	En poste
33.	ETEME ENAMA Serge	Chargé de Cours	En poste
34.	FEUGANG YOUMSSI François	Chargé de Cours	En poste
35.	FOKAM Alvine Christelle Epse KENGNE	Chargée de Cours	En poste
36.	FOSSI TANKOUA Olivia Epse DJEUTCHOUANG SAYANG	Chargée de Cours	En poste (transfert Uté de Dla)
37.	GONWOUO NONO Legrand	Chargé de Cours	En poste
38.	KOGA MANG DOBARA	Chargé de Cours	En poste

39.	LEME BANOCK Lucie	Chargée de Cours	En poste
40.	MAPON NSANGOU Indou	Chargé de Cours	En poste
41.	METCHI DONFACK MIREILLE FLAURE EPSE GHOUMO	Chargée de Cours	En poste
42.	NGOUATEU KENFACK Omer Bébé	Chargé de Cours	En poste
43.	NJUA Clarisse YAFI	Chargée de Cours	*Chef Div. Uté Bamenda*
44.	NWANE Philippe Bienvenu	Chargé de Cours	En poste
45.	TADU Zephyrin	Chargé de Cours	En poste
46.	YEDE	Chargé de Cours	En poste
47.	YOUNOUSSA LAME	Chargé de Cours	En poste

48.	KODJOM WANCHE Jacguy Joyce	Assistante	En poste
49.	NDENGUE Jean De Matha	Assistant	En poste
50.	ZEMO GAMO Franklin	Assistant	En poste

3- DÉPARTEMENT DE BIOLOGIE ET PHYSIOLOGIE VÉGÉTALES (BPV) (32)

1.	AMBANG Zachée	Professeur	*Chef de Département*
2.	DJOCGOUE Pierre François	Professeur	En poste
3.	MBOLO Marie	Professeur	En poste
4.	MOSSEBO Dominique Claude	Professeur	En poste
5.	NDONGO BEKOLO	Professeur	En poste
6.	ZAPFACK Louis	Professeur	En poste

7.	ANGONI Hyacinthe	Maître de Conférences	En poste
8.	BIYE Elvire Hortense	Maître de Conférences	En poste
9.	MAHBOU SOMO TOUKAM. Gabriel	Maître de Conférences	En poste
10.	MALA Armand William	Maître de Conférences	En poste
11.	MBARGA BINDZI Marie Alain	Maître de Conférences	*DDES/MINESUP*
12.	NGALLE Hermine BILLE	Maître de Conférences	En poste
13.	NGONKEU MAGAPTCHE Eddy L.	Maître de Conférences	*CT / MINRESI*
14.	TONFACK Libert Brice	Maître de Conférences	En poste
15.	TSOATA Esaïe	Maître de Conférences	En poste
16.	ONANA JEAN MICHEL	Maître de Conférences	En poste

17.	DJEUANI Astride Carole	Chargé de Cours	En poste
18.	GONMADGE CHRISTELLE	Chargé de Cours	En poste
19.	MAFFO MAFFO Nicole Liliane	Chargé de Cours	En poste
20.	MANGA NDJAGA JUDE	Chargé de Cours	En poste
21.	NNANGA MEBENGA Ruth Laure	Chargée de Cours	En poste
22.	NOUKEU KOUAKAM Armelle	Chargée de Cours	En poste
23.	NSOM ZAMBO EPSE PIAL ANNIE CLAUDE	Chargée de Cours	*En détachement/UNESCO MALI*
24.	GODSWILL NTSOMBOH NTSEFONG	Chargé de Cours	En poste
25.	KABELONG BANAHO Louis-Paul-Roger	Chargé de Cours	En poste
26.	KONO Léon Dieudonné	Chargé de Cours	En poste
27.	LIBALAH Moses BAKONCK	Chargé de Cours	En poste
28.	LIKENG-LI-NGUE Benoit C	Chargé de Cours	En poste
29.	TAEDOUNG Evariste Hermann	Chargé de Cours	En poste
30.	TEMEGNE NONO Carine	Chargée de Cours	En poste
31.	DIDA LONTSI Sylvere Landry	Assistant	En poste
32.	METSEBING Blondo-Pascal	Assistant	En poste

4- DÉPARTEMENT DE CHIMIE INORGANIQUE (CI) (27)

1.	GHOGOMU Paul MINGO	Professeur	*Ministre Chargé de Mission PR*
2.	NANSEU NJIKI Charles Péguy	Professeur	En poste
3.	NDIFON Peter TEKE	Professeur	*CT MINRESI*
4.	NENWA Justin	Professeur	En poste
5.	NGOMO Horace MANGA	Professeur	*Vice Chancelor/UB*
6.	NJIOMOU C. épse DJANGANG	Professeur	En poste
7.	NJOYA Dayirou	Professeur	En poste

8.	ACAYANKA Elie	Maître de Conférences	En poste
9.	EMADAK Alphonse	Maître de Conférences	En poste
10.	KAMGANG YOUBI Georges	Maître de Conférences	En poste
11.	KEMMEGNE MBOUGUEM Jean C.	Maître de Conférences	En poste
12.	KENNE DEDZO GUSTAVE	Maître de Conférences	En poste
13.	MBEY Jean Aimé	Maître de Conférences	En poste
14.	NDI NSAMI Julius	Maître de Conférences	*Chef de Département*
15.	NEBAH Née NDOSIRI Bridget NDOYE	Maître de Conférences	*Sénatrice/SENAT*
16.	NYAMEN Linda Dyorisse	Maître de Conférences	En poste
17.	PABOUDAM GBAMBIE AWAWOU	Maître de Conférences	En poste
18.	TCHAKOUTE KOUAMO Hervé	Maître de Conférences	En poste
19.	BELIBI BELIBI Placide Désiré	Maître de Conférences	*Chef Service/ ENS Bertoua*
20.	CHEUMANI YONA Arnaud M.	Maître de Conférences	En poste
21	KOUOTOU DAOUDA	Maître de Conférences	En poste

22.	MAKON Thomas Beauregard	Chargé de Cours	En poste
23.	NCHIMI NONO KATIA	Chargée de Cours	En poste
24.	NJANKWA NJABONG N. Eric	Chargé de Cours	En poste
25.	PATOUOSSA ISSOFA	Chargé de Cours	En poste
26.	SIEWE Jean Mermoz	Chargé de Cours	En Poste
27.	BOYOM TATCHEMO Franck W.	Assistant	En Poste

6- DÉPARTEMENT DE CHIMIE ORGANIQUE (CO) (33)			
1.	Alex de Théodore ATCHADE	Professeur	*DEPE/Univ. Bertoua*
2.	DONGO Etienne	Professeur	*Vice-Doyen/FSE/UYI*
3.	NGOUELA Silvère Augustin	Professeur	*Chef de Département UDS*
4.	PEGNYEMB Dieudonné Emmanuel	Professeur	*Recteur UBertoua/ Chef de Département*
5.	MBAZOA née DJAMA Céline	Professeur	En poste
6.	MKOUNGA Pierre	Professeur	En poste
7.	AMBASSA Pantaléon	Maître de Conférences	En poste
8.	EYONG Kenneth OBEN	Maître de Conférences	En poste
9.	FOTSO WABO Ghislain	Maître de Conférences	En poste
10	KAMTO Eutrophe Le Doux	Maître de Conférences	En poste
11	KENMOGNE Marguerite	Maître de Conférences	En poste
12	MVOT AKAK CARINE	Maître de Conférences	En poste
13	NGO MBING Joséphine	Maître de Conférences	*Chef de Cellule MINRESI*
14	NGONO BIKOBO Dominique Serge	Maître de Conférences	*C.E.A/ MINESUP*
15	NOTE LOUGBOT Olivier Placide	Maître de Conférences	*Dir ENS/Uté Bertoua*
16	NOUNGOUE TCHAMO Diderot	Maître de Conférences	En poste
17	TABOPDA KUATE Turibio	Maître de Conférences	En poste
18	TAGATSING FOTSING Maurice	Maître de Conférences	En poste
19	OUAHOUO WACHE Blandine M.	Maître de Conférences	En poste
20	ZONDEGOUMBA Ernestine	Maître de Conférences	En poste
21.	MESSI Angélique Nicolas	Chargé de Cours	En poste
22.	MUNVERA MFIFEN Aristide	Chargé de Cours	En poste
23.	NGNINTEDO Dominique	Chargé de Cours	En poste
24.	NGOMO Orléans	Chargée de Cours	En poste
25.	NONO NONO Éric Carly	Chargé de Cours	En poste
26.	OUETE NANTCHOUANG Judith Laure	Chargée de Cours	En poste
27.	SIELINOU TEDJON Valérie	Chargé de Cours	En poste
28.	TCHAMGOUE Joseph	Chargé de Cours	En poste
29.	TSAFFACK Maurice	Chargé de Cours	En poste
30.	TSAMO TONTSA Armelle	Chargée de Cours	En poste
31.	TSEMEUGNE Joseph	Chargé de Cours	En poste
32	NDOGO ETEME Olivier	Assistant	En poste
33	NGUEMDJO CHIMEZE Valery Wilfried	Assistant	En poste

6- DEPARTEMENT DES ENERGIES RENOUVELABLES (ER) (1)			
1.	BODO Bertrand	Professeur	*Chef de Département*

7- DÉPARTEMENT D'INFORMATIQUE (IN) (22)

1.	ATSA ETOUNDI Roger	Professeur	*Chef de Division des SI/ MINESUP*
2.	FOUDA NDJODO Marcel Laurent	Professeur	*Inspecteur Général Académique/ MINESUP*

3.	NDOUNDAM Réné	Maître de Conférences	En poste
4.	TSOPZE Norbert	Maître de Conférences	En poste

5.	ABESSOLO ALO'O Gislain	Chargé de Cours	*Chef de Cellule MINFOPRA*
6.	AMINOU HALIDOU	Chargé de Cours	*Chef de Département*
7.	DJAM Xaviera YOUH - KIMBI	Chargée de Cours	En Poste
8.	DOMGA KOMGUEM Rodrigue	Chargé de Cours	En poste
9.	EBELE Serge Alain	Chargé de Cours	En poste
10.	EKODECK Stéphane Gaël Raymond	Chargé de Cours	En poste
11.	HAMZA Adamou	Chargé de Cours	En poste
12.	JIOMEKONG AZANZI Fidel	Chargé de Cours	En poste
13.	KOUOKAM KOUOKAM E. A.	Chargé de Cours	En poste
14.	MELATAGIA YONTA Paulin	Chargé de Cours	En poste
15.	MESSI NGUELE Thomas	Chargé de Cours	En poste
16.	MONTHE DJIADEU Valery M.	Chargé de Cours	En poste
17.	NZEKON NZEKO'O Armel Jacques	Chargé de Cours	En poste
18.	OLLE OLLE Daniel Claude Georges Delort	Chargé de Cours	*Directeur Adjoint ENSET Ebolowa*
19.	TAPAMO Hyppolite	Chargé de Cours	En poste

20.	BAYEM Jacques Narcisse	Assistant	En poste
21.	MAKEMBE. S. Oswald	Assistant	*Directeur CUTI*
22.	NKONDOCK. MI BAHANACK. N.	Assistant	En poste

8- DÉPARTEMENT DE MATHÉMATIQUES (MA) (34)			
1.	AYISSI Raoult Domingo	Professeur	*Chef de Département/D. ENSPY*
2.	KIANPI Maurice	Maître de Conférences	En poste
3.	MBANG Joseph	Maître de Conférences	En poste
4.	MBEHOU Mohamed	Maître de Conférences	*Chef de Division/ENSPY*
5.	MBELE BIDIMA Martin Ledoux	Maître de Conférences	En poste
6.	NOUNDJEU Pierre	Maître de Conférences	*VDRC/FS/UYI*
7.	TAKAM SOH Patrice	Maître de Conférences	En poste
8.	TCHAPNDA NJABO Sophonie B.	Maître de Conférences	*Directeur/AIMS Rwanda*
9.	TCHOUNDJA Edgar Landry	Maître de Conférences	En poste
10.	AGHOUKENG JIOFACK Jean Gérard	Chargé de Cours	*Chef Cellule MINEPAT*
11.	BOGSO ANTOINE Marie	Chargé de Cours	En poste
12.	BITYE MVONDO Esther	Chargé de Cours	En poste
13.	CHENDJOU Gilbert	Chargé de Cours	En poste
14.	DJIADEU NGAHA Michel	Chargé de Cours	En poste
15.	DOUANLA YONTA Herman	Chargé de Cours	En poste
16.	KIKI Maxime Armand	Chargé de Cours	En poste
17.	KOKOMO AYISSI Eric Brice	Chargé de Cours	En poste(transfert de l'université de Douala)
18.	LOUMNGAM KAMGA Victor	Chargé de Cours	En poste
19.	MBAKOP Guy Merlin	Chargé de Cours	En poste
20.	MBATAKOU Salomon Joseph	Chargé de Cours	En poste
21.	MENGUE MENGUE David Joël	Chargé de Cours	*Chef Dpt /ENS Université d'Ebolowa*
22.	MBIAKOP Hilaire George	Chargé de Cours	En poste
23.	NGUEFACK Bernard	Chargé de Cours	En poste
24.	NIMPA PEFOUKEU Romain	Chargée de Cours	En poste
25.	OGADOA AMASSAYOGA	Chargée de Cours	En poste
26.	POLA DOUNDOU Emmanuel	Chargé de Cours	*En stage*
27.	TENKEU JEUFACK Yannick Léa	Chargé de Cours	En poste
28.	TCHEUTIA Daniel Duviol	Chargé de Cours	En poste
29.	TETSADJIO TCHILEPECK M. Eric.	Chargé de Cours	En poste
30.	FOKAM Jean Marcel	Assistant	En poste
31.	GUIDZAVAI KOUCHERE Albert	Assistant	En poste
32.	MANN MANYOMBE Martin Luther	Assistant	En poste
33.	MEFENZA NOUNTU Thiery	Assistant	En poste
34.	NYOUMBI DLEUNA Christelle	Assistant	En poste

9- DÉPARTEMENT DE MICROBIOLOGIE (MIB) (24)

1.	ESSIA NGANG Jean Justin	Professeur	*Chef de Département*
2.	NYEGUE Maximilienne Ascension	Professeur	*Vice-Doyen / DSSE*
3.	SADO KAMDEM Sylvain Leroy	Professeur	En poste
4.	ASSAM ASSAM Jean Paul	Maître de Conférences	En poste
5.	BOUGNOM Blaise Pascal	Maître de Conférences	En poste
6.	KOUITCHEU MABEKU Epse KOUAM Laure Brigitte	Maître de Conférences	En poste
7.	MUNE MUNE Martin Alain	Maître de Conférences	En poste
8.	RIWOM Sara Honorine	Maître de Conférences	En poste
9.	NJIKI BIKOÏ Jacky	Maître de Conférences	En poste
10.	TCHIKOUA Roger	Maître de Conférences	*Chef de Service de la Scolarité*
11	ESSONO Damien Marie	Chargé de Cours	En poste
12	LAMYE Glory MOH	Chargé de Cours	En poste
13	MEYIN A EBONG Solange	Chargée de Cours	En poste
14	MONI NDEDI Esther Del Florence	Chargée de Cours	En poste
15	NKOUDOU ZE Nardis	Chargé de Cours	En poste
16	NKOUE TONG Abraham	Chargé de Cours	En poste
17	TAMATCHO KWEYANG Blandine Pulchérie	Chargée de Cours	En poste
18	SAKE NGANE Carole Stéphanie	Chargée de Cours	En poste
19	TOBOLBAÏ Richard	Chargé de Cours	En poste
20.	EZO'O MENGO Fabrice Télésfor	Assistant	En poste
21.	EHETH Jean Samuel	Assistant	En poste
22.	MAYI Marie Paule Audrey	Assistante	En poste
23.	NGOUENAM Romial Joël	Assistant	En poste
24.	NJAPNDOUNKE Bilkissou	Assistant	En poste

10. DEPARTEMENT DE PHYSIQUE (PHY) (42)

1.	BEN- BOLIE Germain Hubert	Professeur	En poste
2.	BIYA MOTTO Frédéric	Professeur	*DG/HYDRO Mekin*
3.	DJUIDJE KENMOE ép. ALOYEM	Professeur	En poste
4.	EKOBENA FOUDA Henri Paul	Professeur	*Vice-Recteur. Uté Ngaoundéré*
5.	ESSIMBI ZOBO Bernard	Professeur	En poste
6.	EYEBE FOUDA Jean sire	Professeur	En poste
7.	HONA Jacques	Professeur	En poste
8.	NANA ENGO Serge Guy	Professeur	En poste
9.	NANA NBENDJO Blaise	Professeur	*Chef de Département/Uni. Bertoua*
10.	NDJAKA Jean Marie Bienvenu	Professeur	*Chef de Département*
11.	NJANDJOCK NOUCK Philippe	Professeur	En poste
12.	SAIDOU	Professeur	*Chef de centre/IRGM/MINRESI*
13.	SIMO Elie	Professeur	En poste
14.	TABOD Charles TABOD	Professeur	*Doyen FS/Univ/Bda*
15.	TCHAWOUA Clément	Professeur	En poste
16.	WOAFO Paul	Professeur	En poste
17.	ZEKENG Serge Sylvain	Professeur	En poste

18.	ENYEGUE A NYAM épse BELINGA	Maître de Conférences	*Chef de Division de la formation continue et à distance/ENSPY*
19.	FEWO Serge Ibraïd	Maître de Conférences	En poste
20.	FOUEJIO David	Maître de Conférences	*Chef Cell/ MINADER*
21.	MBINACK Clément	Maître de Conférences	En poste
22.	MBONO SAMBA Yves Christian U.	Maître de Conférences	En poste
23.	MELI'I Joelle Larissa	Maître de Conférences	En poste
24.	MVOGO ALAIN	Maître de Conférences	En poste
25.	NDOP Joseph	Maître de Conférences	En poste
26.	SIEWE SIEWE Martin	Maître de Conférences	En poste
27.	VONDOU Derbetini Appolinaire	Maître de Conférences	En poste
28.	WAKATA née BEYA Annie Sylvie	Maître de Conférences	*DAAC/UYII*
29.	WOULACHE Rosalie Laure	Maître de Conférences	*En stage depuis février 2023*
30.	ABDOURAHIMI	Chargé de Cours	En poste
31.	AYISSI EYEBE Guy François Valérie	Chargé de Cours	En poste
32.	CHAMANI Roméo	Chargé de Cours	En poste
33.	DJIOTANG TCHOTCHOU Lucie Angennes	Chargée de Cours	En poste
34.	EDONGUE Hervais	Chargé de Cours	En poste

35.	KAMENI NEMATCHOUA Modeste	Chargé de Cours	En poste
36.	LAMARA Maurice	Chargé de Cours	En poste
37.	NGA ONGODO Dieudonné	Chargé de Cours	En poste
38.	OTTOU ABE Martin Thierry	Chargé de Cours	*Directeur Unité de production des réactifs/IMPM*
39.	TEYOU NGOUPO Ariel	Chargé de Cours	En poste
40.	TOGUEU MOTCHEYO Alain Bertrand	Chargé de Cours	En poste
41.	WANDJI NYAMSI William	Chargé de Cours	En poste
42.	SOUFFO TAGUEU Merimé	Assistant	En poste

11- DÉPARTEMENT DE SCIENCES DE LA TERRE (ST) (34)			
1.	EKOMANE Emile	Professeur	*Chef Div./Uté Ebolowa*
2.	GANNO Sylvestre	Professeur	En poste
3.	NDJIGUI Paul-Désiré	Professeur	*Vice-Doyen /DPSAA*
4.	NGOS III Simon	Professeur	En poste
5.	NKOUMBOU Charles	Professeur	En poste
6.	ONANA Vincent Laurent	Professeur	*Chef de Département/Uté. Eb.*
7.	YENE ATANGANA Joseph Q.	Professeur	*Chef Div. /MINTP*
8.	BISSO Dieudonné	Maître de Conférences	*Chef de Département*
9.	Elisé SABABA	Maitre de Conférences	En poste
10.	EYONG John TAKEM	Maître de Conférences	En poste
11.	FUH Calistus Gentry	Maître de Conférences	*Sec. D'Etat/MINMIDT(ai)*
12.	MBIDA YEM	Maitre de Conférences	En poste
13.	MBESSE Cécile Olive	Maitre de Conférences	En poste
14.	METANG Victor	Maître de Conférences	En poste
15.	NGO BIDJECK Louise Marie	Maître de Conférences	En poste
16.	NGUEUTCHOUA Gabriel	Maître de Conférences	*CEA/MINRESI*
17.	NJILAH Isaac KONFOR	Maître de Conférences	En poste
18.	TCHAKOUNTE Jacqueline épse NUMBEM	Maître de Conférences	*Chef. Cell /MINRESI*
19.	TCHOUANKOUE Jean-Pierre	Maître de Conférences	En poste
20.	TEMGA Jean Pierre	Maître de Conférences	En poste
21.	ZO'O ZAME Philémon	Maître de Conférences	*DG/ART*
22.	ANABA ONANA Achille Basile	Chargé de Cours	En poste
23.	MAMDEM TAMTO Lionelle Estelle, épouse BITOM	Chargée de Cours	En poste
24.	NGO BELNOUN Rose Noël	Chargée de Cours	En poste
25.	NGO'O ZE ARNAUD	Chargé de Cours	En poste
26.	NOMO NEGUE Emmanuel	Chargé de Cours	En poste
27.	NTSAMA ATANGANA Jacqueline	Chargée de Cours	En poste
28.	TCHAPTCHET TCHATO De P.	Chargé de Cours	En poste
29.	TEHNA Nathanaël	Chargé de Cours	En poste
30.	FEUMBA Roger	Chargé de Cours	En poste
31.	MBANGA NYOBE Jules	Chargé de Cours	En poste
32.	KOAH NA LEBOGO Serge P.	Assistant	En poste
33.	TENE DJOUKAM Joëlle Flore, épouse KOUANKAP NONO	Assistante	En poste

Répartition chiffrée des Enseignants de la Faculté des Sciences de l'Université de Yaoundé I

NOMBRE D'ENSEIGNANTS					
DÉPARTEMENT	**Professeurs**	**Maîtres de Conférences**	**Chargés de Cours**	**Assistants**	**Total**
BCH	08 (01)	22 (13)	08 (03)	06 (04)	**44 (20)**
BPA	11 (01)	19 (09)	16 (05)	03 (01)	**49 (16)**
BPV	06 (01)	10 (02)	14 (07)	02 (00)	**32 (10)**
CI	07 (01)	14 (03)	05 (01)	01 (00)	**27 (05)**
CO	06 (01)	14 (05)	11 (03)	02 (00)	**33 (09)**
ER	01 (00)		/	/	**01 (0)**
IN	02 (00)	02 (00)	15 (01)	03 (00)	**22 (01)**
MAT	01 (00)	08 (00)	20 (01)	05 (01)	**34 (02)**
MIB	03 (01)	07 (03)	09 (05)	05 (02)	**24 (11)**
PHY	17 (01)	12 (04)	12 (01)	01 (00)	**42 (06)**
ST	07 (00)	14 (03)	11 (03)	02 (01)	**34 (07)**
Total	**69 (07)**	**122 (42)**	**121 (30)**	**30 (09)**	**342 (88)**

Soit un total de **342 (88)** dont :

- Professeurs **69 (07)**
- Maîtres de Conférences **123 (41)**
- Chargés de Cours **120 (30)**
- Assistants **30 (09)**

( ) = Nombre de Femmes **88**

Acknowledgment

I want express my gratefulness to :

- *Professor* ***TCHAWOUA Clément*** for his scientific perfectionism, his availability, and his guidance during these years of research.
- *The Dean of the faculty of Science, Professor* ***Luc Calvin OWONO OWONO*** for his leadership skills and efficient management of the institution entrusted to him.
- *Head of the department, Professor* ***NDJAKA Jean Marie Bienvenu*** for the quality of his teaching at the undergraduate level.
- *Members of the jury*, Professor **ESSIMBI ZOBO Bernard**, Professor **DJUIDJE KENMOE Germaine**, Professor **TCHOFFO Martin** and Professor **HONA Jacques** for their valuable criticisms and observations to improve this thesis.
- *All teachers in the Department of Physics* for their dedication to research and student training.
- *Doctor* ***NDJOMATCHOUA Thomas Frank*** for initiating me into scientific research.
- *My parents,* ***THICHI Jean Marie*** *and* ***NGANDJUI Véronique****, and my aunt* ***Dja'ankam Henriette*** for their love and unwavering support.
- *My siblings, especially* ***NJINE Michel, DZIAHA Cédric, KEBIWA Ivan, NGUEKAM Loïc, KAMOU Mauriant, NGUENKAM Charlie, SONDI***

Jeanne, NGASSEU Gilles, AZAMO Dominique, MEBE GUELE Russel, for their encouragement and their support throughout the most challenging phases of this work.

- *My friends,* ***MEKONTCHOU Michael, TABAPSI Rostant, KAMGA Samuel, SIGNE Eric, NDOGMO Ragil, ZANGA Dieudonné, MAGUIABOU Daura, Gbouli Aïcha, NDZIA Lina, YOUMBISSI Alex*** *and* ***MOUAJI Malik***, for their solidarity and intellectual contributions.
- *All members of my family* for their unconditional support.
- *Everyone who contributed, near or far, to the elaboration of this work, I am infinitely grateful.*

Résumé

La transmission d'énergie dans les bandes interdites des réseaux Fermi-Pasta-Ulam (FPU) est étudiée. En appliquant à l'une des extrémités d'un réseau FPU, un signal dont la fréquence se situe dans la bande interdite, deux types de contrôle ont été mis en évidence. Premièrement, pour un réseau diatomique FPU excité par un signal sinusoïdal dont la fréquence est prise soit dans la bande interdite supérieure soit dans la bande interdite entre les modes acoustique et optique, nous déterminons analytiquement l'amplitude seuil de supratransmission. Pour chaque cas, cette détermination repose sur l'utilisation d'un ansatz de découplage combiné soit à l'approximation des milieux continus, soit à l'approximation semi-discrète. La valeur estimée du seuil de supratransmission diffère selon que la particule excitée soit la plus lourde ou la plus légère, offrant la possibilité d'obtenir, dans chaque bande interdite, deux seuils en permutant l'ordre des particules lourdes et légères. Par ailleurs, cela met en évidence l'influence de la masse de la particule excitée sur le phénomène de supratransmission, et sur la transmission d'énergie en général.

Dans la bande interdite inférieure, la dépendance du seuil au rapport des masses ($\mu = m/M$) des deux particules a été établie et il en ressort que pour des valeurs élevées (resp. faibles) du rapport de masse μ ($\mu \geq 60\%$), le couplage entre les deux modes doit (resp. ne doit pas) être considéré.

Un deuxième contrôle de la transmission d'énergie a été mis en évidence dans le réseau monoatomique FPU. En utilisant une excitation périodique déformable plutôt qu'une excitation sinusoïdale, nous démontrons qu'une forme optimale d'excitation périodique non sinusoïdale peut induire (resp. inhiber) la transmission d'énergie à travers le réseau en dessous (resp. au-dessus) de l'amplitude seuil de supratransmission, révélant ainsi que le phénomène de supratransmission est lié non seulement à

l'amplitude de l'onde excitatrice, mais aussi à sa forme; et plus généralement, que la transmission d'énergie peut être contrôlée par la forme du signal excitateur.

Des analyses numériques ont ensuite été réalisées en mettant l'accent sur la dépendance du seuil à la fréquence du signal excitateur ainsi qu'à la masse de la particule excitée (légère ou lourde) pour le réseau diatomique; et en faisant varier la forme du signal excitateur pour le réseau monoatomique étudié. Une bonne concordance a été observée entre les seuils numériques et analytiques. Pour le cas particulier du réseau diatomique où toutes les particules ont la même masses, et en annulant le paramètre de déformation pour le réseau monoatomique excité par un signal déformable, les résultats de la littérature relatifs au réseau FPU monoatomique sont retrouvés.

Mots-clés: Supratransmission, réseau FPU, ansatz de découplage, approximation semi-discrète, bande interdite, seuil de supratransmission, excitation déformable.

Abstract

The energy transmission in forbidden bands of Fermi-Pasta-Ulam (FPU) lattices is investigated. When applying at one end of an FPU lattice a signal whose frequency lies in the forbidden band, two types of control have been evidenced. Firstly, for an FPU diatomic lattice driven by a sinusoidal signal with frequency in the upper forbidden band (lower forbidden band between acoustic and optical modes), we derived analytically, using a decoupling ansatz for the motion of the two different sub-lattices combined with the continuum (quasi-discrete) approximation, the threshold amplitudes of energy transmission occurrence. The estimated value of the supratransmission threshold differs depending on whether the excited particle is the heaviest or the lightest, offering the possibility of obtaining, in each band gap, two thresholds by switching the order of heavy and light particles. Furthermore, this highlights the influence of the mass of the driven particle on the supertransmission phenomenon, and on energy transmission in general.

In the lower forbidden band, the dependence of the supratransmission threshold on the mass ratio ($\mu = m/M$) has been evidenced and it appears that for large (small) values of μ, that is $\mu > 60\%$, the coupling between the two modes must (must not) be considered.

A second energy transmission control has been evidenced in the FPU monoatomic lattice. When using instead of a sinusoidal driving, a periodic variable shape signal, we show that an optimal shape of a periodic non-sinusoidal excitation may induce (or inhibit) energy flow through the lattice below (or above) the NST threshold, demonstrating that nonlinear supratransmission is reliant not only on driving amplitude but also on its shape, and more generally that energy transmission can be controlled by the shape of the driving signal.

Numerical explorations were subsequently performed with an emphasis, on the dependence of the threshold on the driving frequency and also on the mass of the driven particle (light or heavy) for the diatomic lattice; and by varying the excitation signal shape in the monoatomic lattice studied. A good agreement is found between the numerical and analytical thresholds. For the limit case of the diatomic lattice where all the masses are identical, and when setting the shape parameter to zero in the monoatomic lattice, the results of the monoatomic FPU previously found in the literature are recovered.

Keywords: Supratransmission, FPU lattice, decoupling ansatz, quasi-discrete approximation, forbidden band, threshold, variable shape, non-sinusoidal.

General introduction

Periodic structures represent a fascinating realm of study within the field of physics, showcasing a rich tapestry of complex behaviors and applications that extend across various disciplines. They are commonly encountered in condensed matter physics [1,5–12], crystallography [13–15], and materials science [16–19]. The presence of nonlinearity in these structures often leads to unique and unexpected phenomena, laying the foundation for groundbreaking applications. They serve as models for understanding the behavior of certain materials, including their thermal [16], and mechanical [8, 15] properties. Additionally, periodic structures find applications in the design of novel materials with tailored properties [20–25], influencing advancements in materials engineering. The interplay of nonlinearity and dispersion gives rise to phenomena such as modulational instability [26–32], soliton propagation [33–37], breathers generation [38–42], and chaotic dynamics [43–46]. These nonlinear effects contribute to the understanding of energy localization, wave propagation, and stability in lattice structures. Investigating these phenomena not only deepens our understanding of the underlying physics but also unlocks potential applications in diverse fields. One particularly captivating phenomenon within nonlinear lattices is supratransmission. This phenomenon involves the transmission of energy in a lattice structure beyond what is classically expected with linear waves. Under certain conditions, a threshold amplitude is surpassed, leading to the supratransmission of energy through the lattice. This intriguing phenomenon has implications in information transmission [47–50], signal processing [51, 52], energy transport, ultrasensitive detector's conception [53, 54] and eventually the development of heat pump [55]. Nonlinear supratransmission (NST) occurs when nonlinear structures known as gap solitons are produced in a medium with a naturally occur-

ring forbidden band gap [56–59], induced by applying a periodic boundary condition at a frequency within the band gap. Initially observed in the pendula chain (sine-Gordon model) [2], NST has been further investigated in various fields, including Bragg media (employing coupled mode equations in the Kerr regime) [60], Josephson junction [61,62], electrical lines [4,63], wave-guide arrays (modeled by the nonlinear Schrödinger equation) [1, 64, 65], Fermi-Pasta-Ulam models [3, 66] and many others [67–69]. Supratransmission has been observed in a variety of complex spatially discrete structures, including disordered [70], structures with on-site potential [71], two-dimensional [72], and transversally coupled [67, 73, 74] lattices.

The emergence of NST stems from the instability of the evanescent wave profile caused by the sinusoidal or harmonic driving force, becoming evident above a certain threshold amplitude. Nowadays, determining this threshold in 1D lattices formed by identical cells systems is achieved by utilizing the explicit solution of the model equation and identifying its maximum allowable amplitude at the boundary [2–4,71]. Accurately predicting the threshold value holds paramount importance for physical applications such as soliton generation or the development of highly sensitive detectors. The existence of lattices possessing more than one degree of freedom per unit cell [75–77], and the study of nonlinear phenomena within these lattices [78,79], provide a better understanding of real physical and biological systems modeled by these lattices and enable the attainment of results increasingly closer to reality. The complex nature of discrete lattices representing real systems, including the presence in their internal structures of non-identical cells such as granular crystals [56, 80], chain of coupled pendulums [81] and electrical transmission lines [82–84], generated the question of the existence of NST and its specificity in such lattices. The specific case of the NST in a lattice possessing two degrees of freedom per unit cell shall the first query to investigate in this thesis.

Otherwise, despite the number of studies on periodic structures conducted through sinusoidal signals [2–4, 62, 65, 70–73, 85–93], a great amount of periodic signals encountered in the nature present a non-sinusoidal profile [94–98], the question of the occurrence of NST through such signals becomes of fundamental interest and will be the second focus of this work. The rest of the work is organized as follow: in chapter I, we make a literature review on periodic structures and the NST phenomenon;

chapter II is devoted to the models, the different analytical and numerical methods used to investigate the NST phenomenon, and also to the derivation of analytical threshold for each scenario met; in chapter III, we present and discuss the results obtained. The work is closed with a conclusion and perspectives for future works.

Chapter I

LITERATURE REVIEW

1.1 Introduction

In this chapter, we explicitly outline the fundamental concepts that will be used throughout this thesis. We will focus on nonlinear lattices, their modeling, and their dynamics. Subsequently, our attention will shift to the supratransmission phenomenon. Several examples of nonlinear lattices will be presented, and a literature review on the supratransmission phenomenon will be conducted.

1.2 Generalities on nonlinear lattices

1.2.1 Discrete lattices

A lattice is a connection of a number N of elementary cells, which can be identical or not. When the nonlinear part of the response of these cells to external solicitations is non-negligible, the lattice is considered as nonlinear. Nonlinear lattices model real systems (biological, physical, chemical, etc.) to understand and describe their behavior. In what follows, we give some examples of 1D, 2D, and 3D nonlinear lattices.

1.2.1.1 Example of 3D lattice: Network of neurons:

A lattice is considered as tri-dimensional (3D) when the unit cells extend along the three directions of space. Networks of neurons are typical examples of real systems modeled by 3D lattices. A network of neurons, commonly known as neural network, is a complex interconnected system of biological neurons in the brain or an artificial system designed to emulate the structure and function of the brain's neural networks.

Each elementary cell here is a neuron, and for the study of nonlinear phenomena such that chaos, synchronization, bursting and pattern formation [99–101], the authors have considered that all the cells are identical.

Figure 1.1: Network of neuron. https://www.bioedonline.org/lessons-and-more/lessons-by-topic/brain-and-behavior/the-brain-neurons-and-brain-chemistry/neural-network-signals

1.2.1.2 Example of 2D lattice: Network of graphene carbon:

A lattice is considered as two-dimensional (2D) when the unit cells extend along two of the three directions of space. A well known example of 2D lattice is the network of graphene.

Graphene, a two-dimensional material composed of a single layer of carbon atoms arranged in a hexagonal lattice, can be conceptualized as a nonlinear lattice. While the term "nonlinear lattice" is often associated with physical structures like di-atomic chains, the unique electronic and vibrational properties of graphene can be analogously described using concepts from nonlinear lattice models.

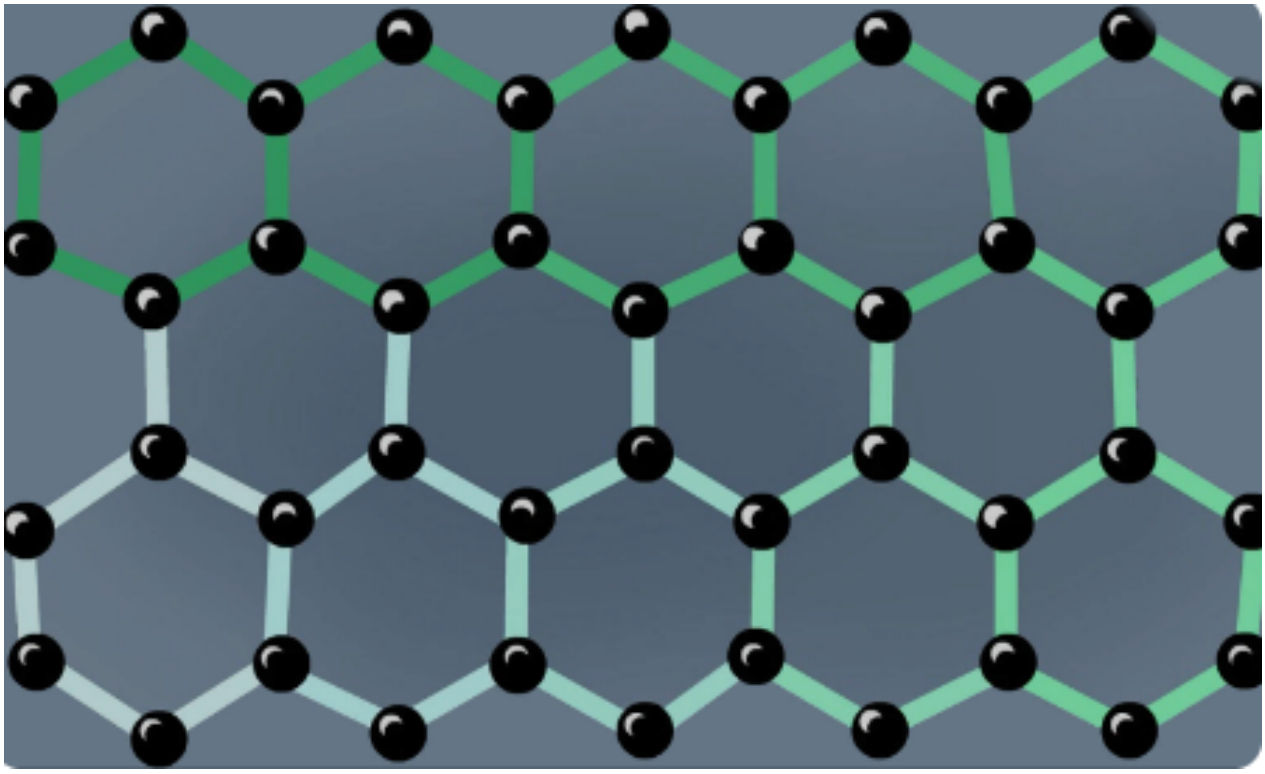

Figure 1.2: Atomic modeling of a network of graphene. https://www.sciencedirect.com/topics/nursing-and-health-professions/graphene

1.2.1.3 Examples of 1D lattices

A lattice is considered as one-dimensional (1D) when the unit cells extend along one of the three directions of space. During the last decades, several 1D lattices are developed for the modeling of real systems encountered in the nature. One can list:

- **the α and β Fermi-Pasta-Ulam lattices**
  They are junctions of N identical masses m, any mass being connected to its two nearest neighbors by identical nonlinear springs. FPU lattices can model the nonlinear dynamics of solids including lattice vibration and phonon interaction [32], the dynamics of biological systems such as proteins folding and DNA dynamics [102]; they can also simulate the behavior of granular materials [103], and can be adapted to model nonlinear optical phenomena such as soliton propagation in optical fiber [104].

The Hamiltonian FPU these is given by

$$H = \sum_{i=1}^{N} \frac{1}{2} m \left(\frac{du_i}{dt} \right)^2 + \Phi \left(u_{i+1} - u_i \right), \tag{1.1}$$

where u_i is the displacement from its equilibrium position of the nth particle, and Φ the potential energy.

- For the α-FPU lattice, the potential Φ is cubic and is given by $\Phi(r) = \frac{1}{2}K_2 r^2 + \frac{1}{3}K_3 r^3$;
- For the β-FPU lattice, the potential Φ is quartic and is given by $\Phi(r) = \frac{1}{2}K_2 r^2 + \frac{1}{4}K_4 r^4$,

r being the spring elongation, K_2 and K_4 are positive constants representing harmonic and quartic potentials, respectively; $u_i = u_i(t)$ is the displacement from its equilibrium position of the ith particle.

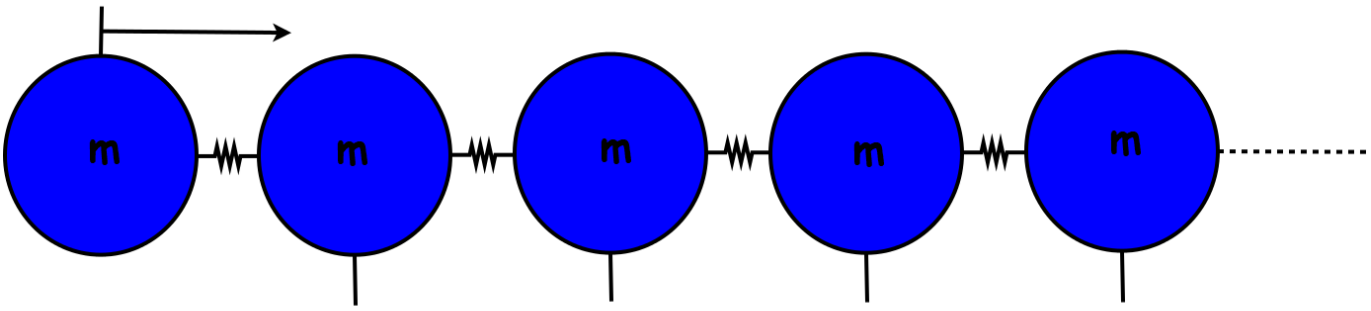

Figure 1.3: Monoatomic FPU lattice.

- **Toda Lattice**

The Toda lattice is a simple model for a one-dimensional crystal in solid state physics where particles interact with their nearest neighbors via an exponential potential. The Toda potential energy $V(q)$ associated with the Toda lattice is given by [105, 106]:

$$V(q) = e^{-q} + q + 1, \tag{1.2}$$

and the Hamiltonian of the system is:

$$H(p,q) = \sum_{n=1}^{N} \left(\frac{1}{2} m \left(\frac{du_n}{dt} \right)^2 + V\left(u_{n+1} - u_n\right) \right), \tag{1.3}$$

where u_n denotes the displacement of the nth particle from its equilibrium position. Toda lattices find applications in various fields of physics and behond, such that the study of dynamics of atoms in crystal lattices [107], the modeling of biological systems such as protein dynamics and DNA interaction [102], and the study of phenomena in condensed matter physics, including phase transitions [108]. The modeling of Toda lattice is similar to FPU lattices (Fig.1.3) and differs by the form of the potential energy.

- **Josephson Junction Arrays**

  The network of Josephson junctions comprises a series of interconnected superconducting elements, typically formed by two superconductors separated by a thin insulating barrier or a weak link. These junctions exhibit the Josephson effect, allowing for the flow of a supercurrent without the application of voltage [109, 110].

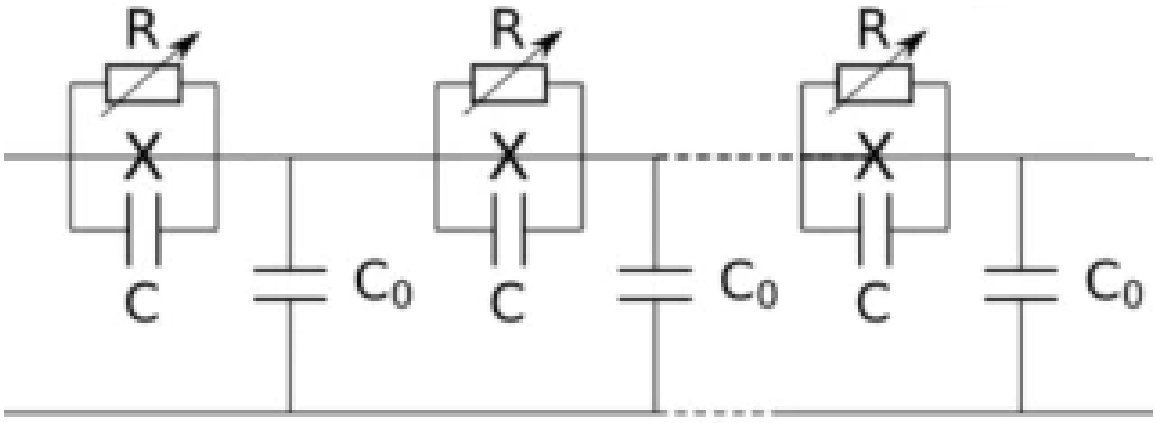

Figure 1.4: Circuit model of the one-dimensional Josephson junction chain.

In Fig.1.4, C is the junction capacitance; C_0 the shunt capacitance, R the variable resistance of each the junction. These networks find applications in multiple systems such as ultrasensitive detection. [53, 54].

- **Nonlinear Electrical Transmission Lines**

Electrical transmission lines and more specifically LC transmission lines comprise a series of inductance and capacitors connected in a repetitive pattern along its length. Each inductance stores energy in the form of a magnetic field, while each capacitor stores energy in an electric field. Most of the time, the capacitor is nonlinear (varicap diode). The combination of inductance L_1 and nonlinear capacitors C_1 creates a distributed circuit, which allows the observation of complex phenomena such as modulational instability [111], soliton propagation [37, 112, 113] and supratransmission [4, 63, 114].

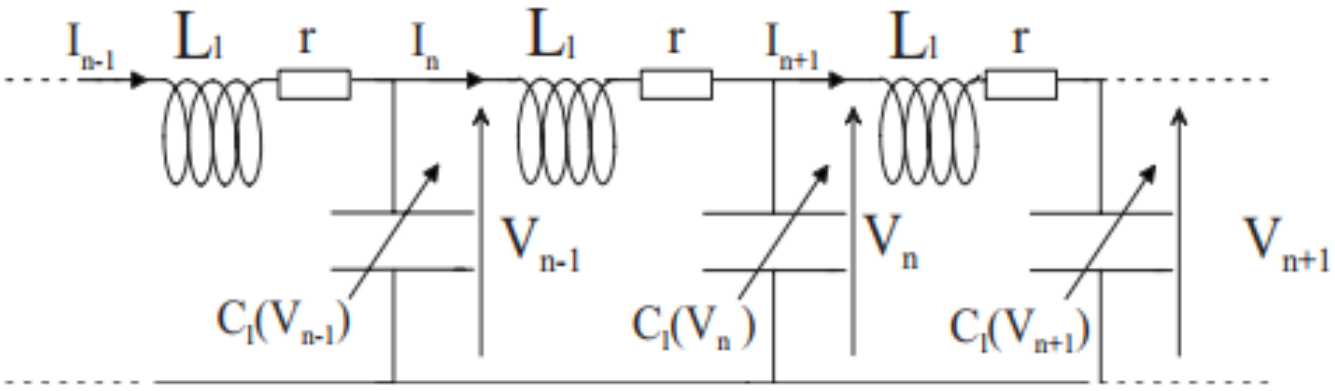

Figure 1.5: LC electrical transmission line

r denotes the inductor resistance, I_n the current crossing the nth inductance, and V_n the voltage of the nth capacitor.

- **The network of waveguides**
  It refers to a complex interconnected system of channels designed to guide and manipulate the propagation of electromagnetic waves or other types of waves, such as acoustic or optical waves [1, 115].

A model of network of waveguides is proposed by Khomeriki et al [1]; in this work, a beam is injected into the boundary waveguide $j = 0$ and can propagates along the array. This is schematized in Fig. 1.6, where Q_0 is a linear coupling between boundary and the first waveguide, Q the constant coupling between the waveguides in the array, n_0 and n are linear refractive indexes of the boundary and array waveguides, respectively. Z is the longitudinal space dimension.

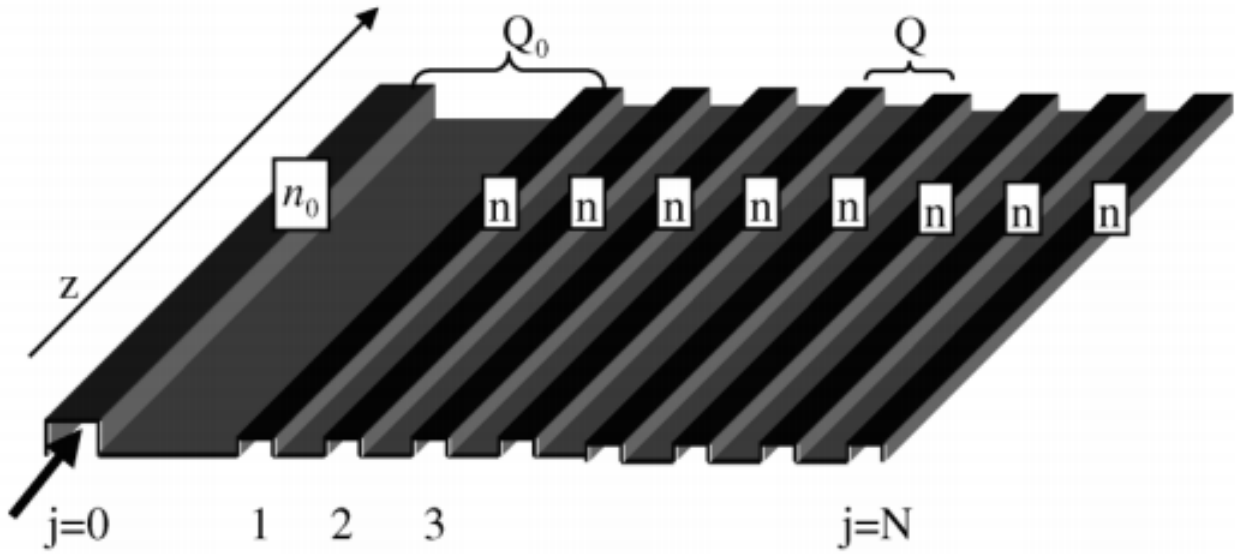

Figure 1.6: Modeling of a network of wave guide. [1]

1.2.2 Forbidden band and evanescent wave in 1D nonlinear lattices

To illustrate the concept of forbidden band, we consider the β-FPU lattice described in section (1.2.1.3) whose Hamiltonian is given by:

$$H = \sum_j \left[\frac{1}{2} m \left(\frac{du_j}{dt} \right)^2 + \Phi(u_{j+1} - u_j) \right] \tag{1.4}$$

$\Phi(r) = \frac{1}{2}K_2 r^2 + \frac{1}{4}K_4 r^4$; r denotes the spring elongation, K_2 and K_4 are positive constants representing harmonic and quartic potentials, respectively; $u_j = u_j(t)$. When neglecting the nonlinear response of the system ($K_4 = 0$), we obtain the following equation of the motion of the nth particle:

$$m\ddot{u}_n = K_2(u_{n-1} + u_{n+1} - 2u_n), \quad n = 1, 2, 3, ... \tag{1.5}$$

where u_n denotes the displacement from its equilibrium position of the nth mass. The solutions of Eq. (1.5) can be sought as plane wave solution on the form

$$u_n = A_0 e^{i[qnd - \omega t]}, \tag{1.6}$$

where d is the lattice spacing, q the wave vector, ω the angular frequency of the

incident wave, and A_0 its amplitude. When inserting Eq. (1.6) into Eq. (1.5), we obtain the following relation:

$$\omega = \sqrt{\frac{4K_2}{m}} \sin\left(\frac{qd}{2}\right), \tag{1.7}$$

which is known as **linear dispersion relation** and displayed on [Fig. 1.7].

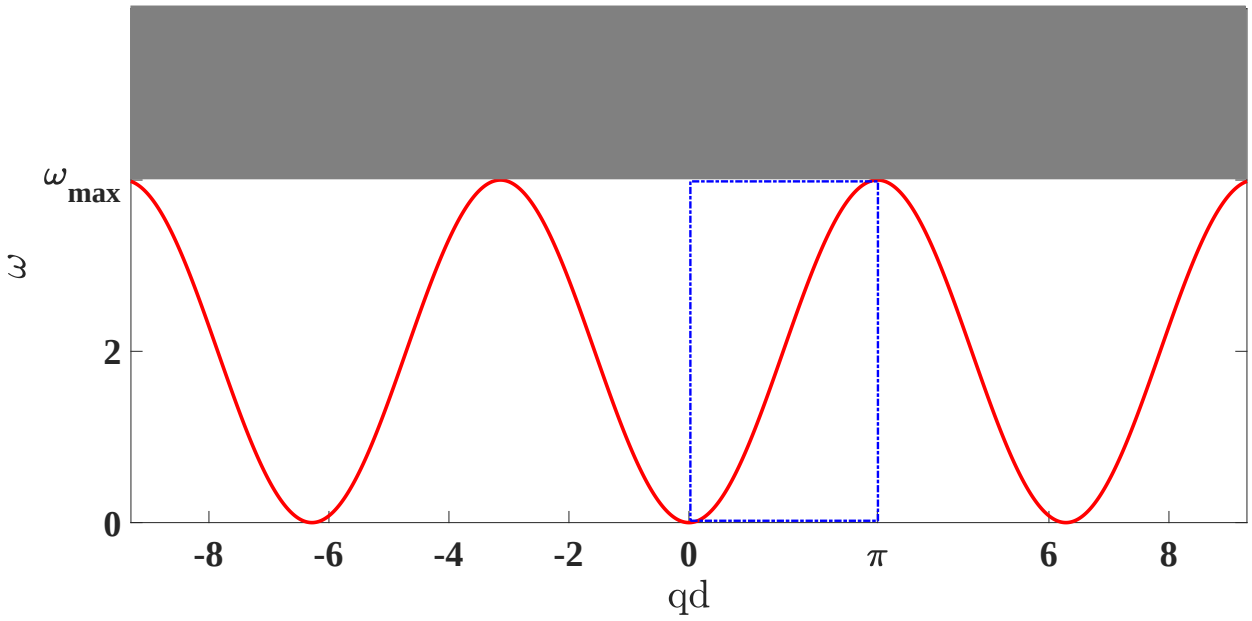

Figure 1.7: linear dispersion relation, $d = 1$, $m = 1$, $K_2 = 1$. Due to the k-space periodicity the study can be limited to the first Brillouin zone ($-\pi \leq qd \leq \pi$) where k=0 is at the center. Moreover, due to the parity of ω ($\omega(-q) = \omega(q)$) the study shall be limited to the half of the first Brillouin zone ($0 \leq qd \leq \pi$) delimited by the blue dashed box.

From the dispersion relation, we derive the phase and the group velocity:

$$v_{ph} = \frac{\omega}{q} = \sqrt{\frac{K_2 d^2}{m}} \frac{\sin\left(\frac{qd}{2}\right)}{\frac{qd}{2}}, \tag{1.8}$$

$$v_g = \frac{d\omega}{dq} = \sqrt{\frac{K_2 d^2}{m}} \cos\left(\frac{qd}{2}\right), \tag{1.9}$$

respectively. Moreover, we derived the condition for a plane wave to be solution of Eq. (1.5) as $0 < \omega < \omega_{max}$, resulting in the splitting of the frequency's spectrum into two zones.

- **a pass band** $0 < \omega < \omega_{max}$: the wave number q is real and the wave can propagates within the lattice without attenuation;
- **a forbidden band** $\omega > \omega_{max}$: the wave number becomes complex $q = q_r + iq_i$, the real part of the wave number q_r has the value of the wave number at the limit of the first Brillouin zone ($q_r = \pi/d$). When propagating within the lattice, the signal becomes $u_n = A_0 e^{-q_i nd} e^{i[n\pi - \omega_{max} t]}$, which exponentially decreases until the value *zero*. This decreasing is known as wave evanescence [116].

This property of the lattices to split the spectrum into pass band and forbidden band is a consequence of their discrete nature which makes them pass-band filters.

The effect of driving frequency on the up-described lattice is displayed on Fig. 1.8 where a chain of 100 particles driven at one end by the sinusoidal signal $u = A\cos(\omega t)$ have been considered.

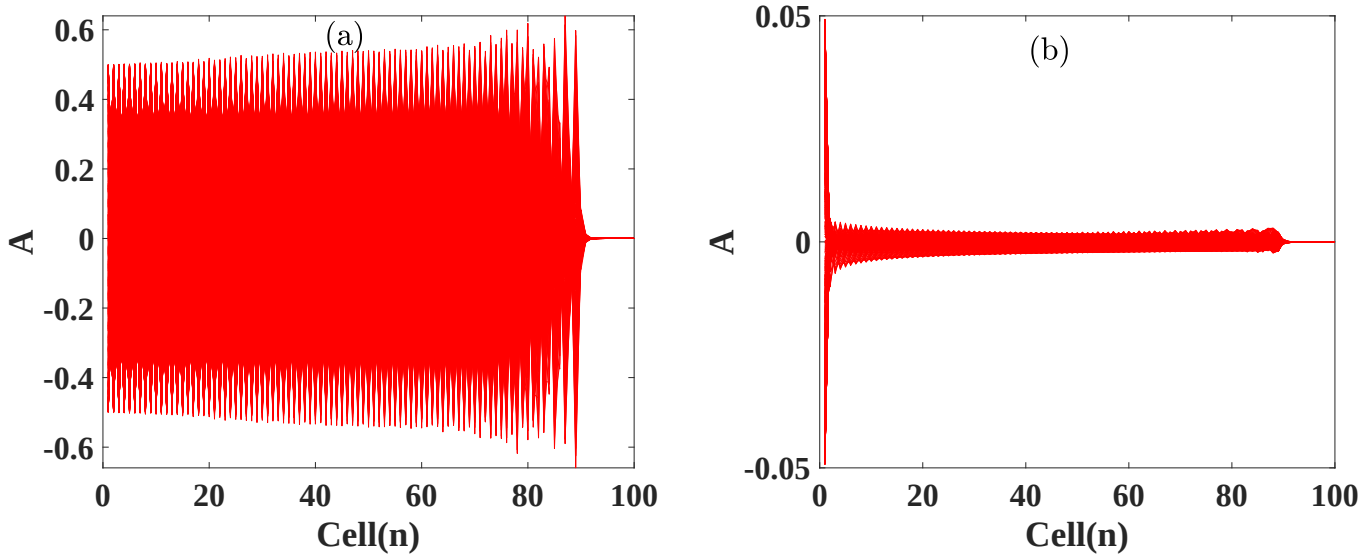

Figure 1.8: Propagating wave (a) and evanescent wave (b) within the linear lattice described by Eq. (1.5). $\omega = 1.5 < \omega_{max}$ (a) and $\omega = 3.5 > \omega_{max}$ (b). $A = 0.5$ for the two cases.

1.2.3 Supratransmission phenomenon

When the nonlinear response of a lattice to external solicitations is non-negligible ($K_4 \neq 0$ in the previous case), the lattice is considered as nonlinear; this property strongly modifies the dynamics of the system and gives birth to several phenomena. Among them, the nonlinear supratransmission.

For a nonlinear lattice driven by a signal which frequency lies in the forbidden band, the following observations have been done:

- When the driving amplitude is sufficiently small, the wave's evanescence occurs as describe in section (1.2.2),
- when the driving amplitude is greater or equal to a certain value called *threshold*, an instability on the evanescent wave's profile occurs resulting in the generation of nonlinear structures which can propagate along the lattice, allowing the energy propagation although the frequency lies in the forbidden band. This phenomenon has been termed as **nonlinear supratransmission phenomenon.**

Firstly discovered by Geniet et Leon [2] in early 2000's, the phenomenon has been widely studied in diverse physical as well as biological systems through various process. In the following we shall present some of them.

1.3 Sine Gordon model

The Sine-Gordon model describes the behavior of a coupled chain of pendulum as indicated in Fig. 1.9.

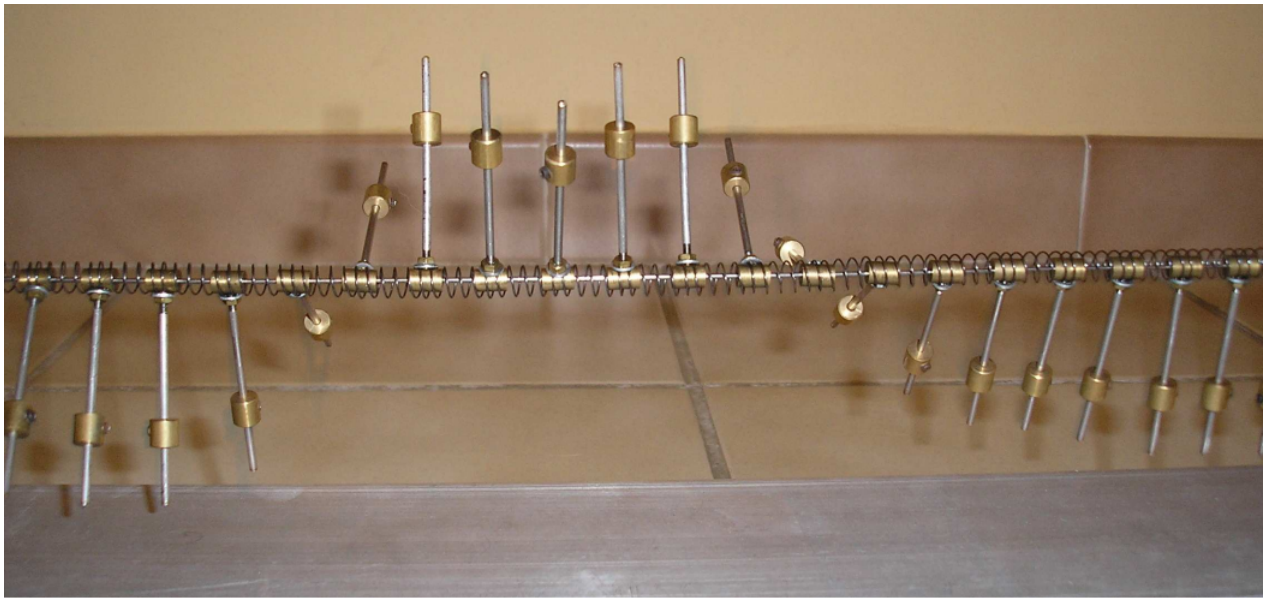

Figure 1.9: Coupled chain of pendulum [2].

The dynamic of this lattice is described by [2]:

$$\ddot{\theta}_n - \omega_1^2 \left(\theta_{n+1} - 2\theta_n + \theta_{n-1}\right) + \omega_0^2 \sin\theta_n = 0, \tag{1.10}$$

$n = 1, ..., N$, where N is the total number of pendulum, $\omega_0^2 = \frac{g}{l}$ is the eigen frequency of each unit, ω_1^2 the coupling between two consecutive pendula, and θ_n denotes the displacement from its equilibrium position of the nth pendulum.

1.3.1 Dispersion law

By considering the limit case of small amplitudes ($\theta_n \ll 2\pi$), the approximation $\sin\theta_n = \theta_n$ can be done and Eq. (1.10) yields to the linear form:

$$\ddot{\theta}_n - \omega_1^2 \left(\theta_{n+1} - 2\theta_n + \theta_{n-1}\right) + \omega_0^2 \theta_n = 0. \tag{1.11}$$

When seeking the solution of Eq. (1.11) on the form $\theta_n(t) = \theta_0 e^{i(knd-\omega t)} + cc$, we derive the linear dispersion law as:

$$\omega^2 = \omega_0^2 + \omega_{max}^2 \sin^2\left(\frac{kd}{2}\right), \tag{1.12}$$

$\omega_{max}^2 = 4\omega_1^2$. The dispersion law is plotted and displayed on Fig. 1.10 where we distinguish the upper and the lower cuttoff frequencies ω_0 and ω_{max}, respectively.

1.3.2 Supratransmission in Sine Gordon model

The supratransmission in Sine Gordon model has been investigated by Geniet et al [2] in the lower forbidden band of the chain of coupled pendulum (light gray band of Fig. 1.10). They have considered for this effect the continuous approximation ($\theta_n(t) \to \theta(x,t)$) and the Taylor expansion $\theta_{n\pm1} = \theta \pm \frac{\partial\theta}{\partial x} + \frac{\partial^2\theta}{\partial x^2}$; and derived the continuous version of the Sine-Gordon equation as:

$$\frac{\partial^2\theta}{\partial t^2} - c^2\frac{\partial^2\theta}{\partial x^2} + \omega_0^2 \sin(\theta) = 0, \tag{1.13}$$

where $c = \omega_1 d$.

By submitting the lattice at $x = 0$ to the periodic signal $\theta(t) = \theta_0 \sin(\omega t)$, the derived static breather solution of Eq.(1.13) which is given by [2, 117]:

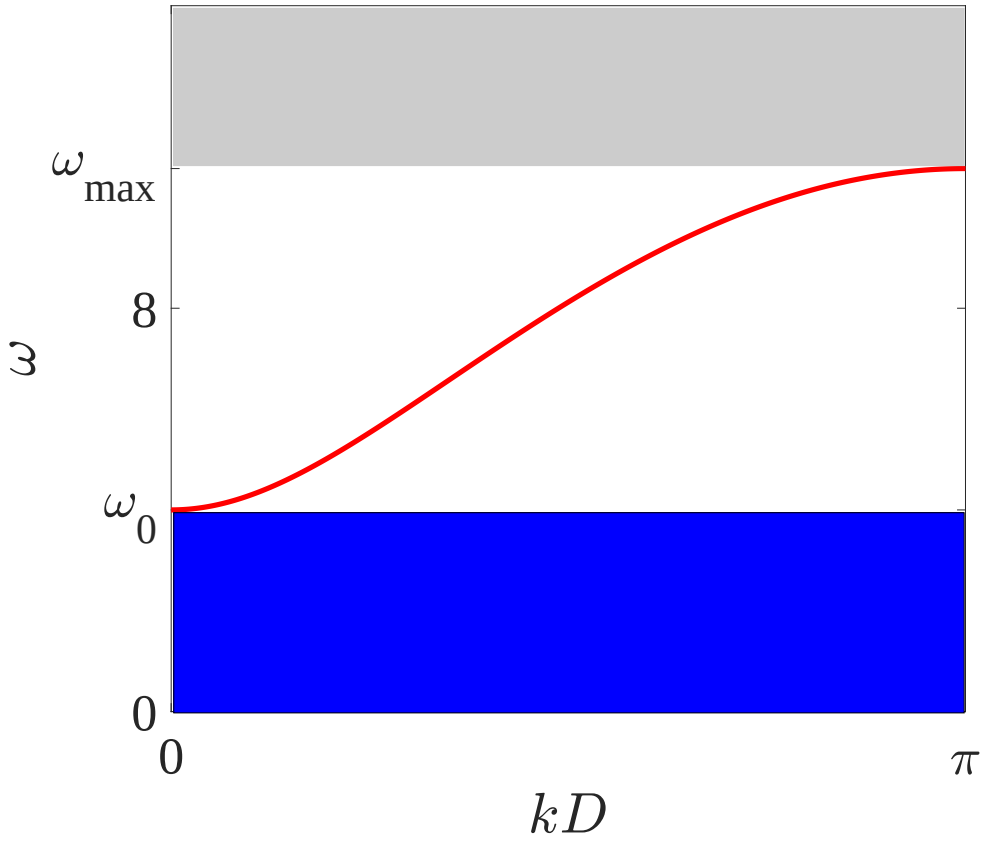

Figure 1.10: Linear dispersion law. Light gray and dark gray bands represent the forbidden bands gap frequencies. $\omega_0 = 4$, $\omega_1 = 5$.

$$\theta_b(x,t) = 4\arctan\left[\frac{\lambda c\cos(\omega t)}{\omega\cosh[\lambda(x-x_0)]}\right]. \tag{1.14}$$

The supratransmission threshold which is the maximum amplitude of the static breather solution is then found and is given by:

$$\theta_{th} = 4\arctan\left[\frac{\lambda c}{\omega}\right], \tag{1.15}$$

1.4 β-Fermi-Pasta-Ulam Monoatomic lattice

1.4.1 Model and dispersion relation

The β-FPU lattice is formed by N identical masses m, each mass being connected to its two nearest neighbors by a nonlinear spring as indicated on Fig. 1.3.

The Hamiltonian of the system is given by :

$$H = \sum_j \left[\frac{1}{2} m \left(\frac{du_j}{dt} \right)^2 + \phi(u_{j+1} - u_j) \right], \tag{1.16}$$

where $\phi(r) = \frac{1}{2}K_2 r^2 + \frac{1}{4}K_4 r^4$, K_2 and K_4 are positive constants representing harmonic and quartic potentials respectively, u_i is the displacement from the equilibrium position of the ith particle. The derived equation of the motion is given by

$$\ddot{u}_n = L_2 \left(u_{n+1} + u_{n-1} - 2u_n \right) + L_4 \left[(u_{n+1} - u_n)^3 - (u_n - u_{n-1})^3 \right], \tag{1.17}$$

where $L_2 = K_2/m$ and $L_4 = K_4/m$. When taking the linear form of Eq. (3.6) and seeking plane wave solution on the form $u_n(t) = u_0 exp[i(knD - \omega t)]$, where $i^2 = -1$, k being the wave vector and ω the phonon frequency; we can derive the linear dispersion relation as:

$$\omega(k) = \omega_c \sin\left(\frac{kD}{2} \right), \tag{1.18}$$

where $\omega_c = 2\sqrt{L_2}$ is the cuttoff frequency of the phonon band. The plotting of the dispersion relation [Eq. (1.18)] displays a phonon band (red curve) and a forbidden band (gray band)) [Fig. 1.11].

1.4.2 Supratransmission in β-FPU monoatomic lattice

The nonlinear supratransmission in a β-FPU lattice has been investigated by Khomeriki et al [3]. The phenomenon has been studied analytically by splitting the forbidden band into two domains (with respect to whether the driving frequency lies close or far from the cutoff frequency ω_c).

1.4.2.1 Forbidden band frequencies close to the cutoff frequency ω_c

The parameters have been taken as $m = 1$, $K_2 = 1$ and $K_4 = 1$. For driving frequencies close to the cutoff frequency ($0 < \omega - 2 \ll 1$), the solution of Eq. (3.6) has been sought on the form [3]:

$$u_n = (-1)^n \frac{1}{2} \left[\psi_n e^{i\omega t} + \psi_n^* e^{-i\omega t} \right]. \tag{1.19}$$

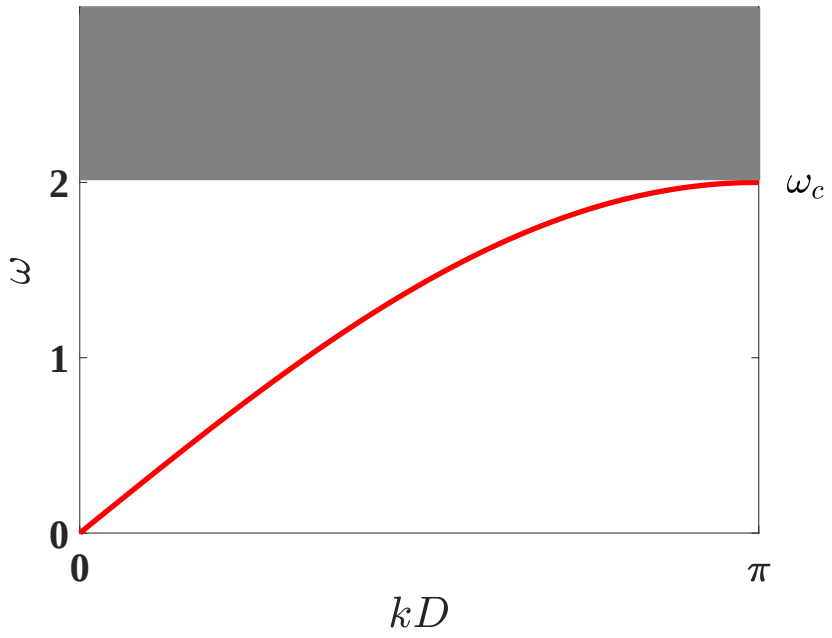

Figure 1.11: Linear dispersion relation. $m = 1$, $K_2 = 1$, $K_4 = 1$.

When considering the rotating wave approximation and the slowly varying envelop (in space and time), the nonlinear Schrödinger equation has been derived as

$$2im\omega\dot{\psi} = \left(\omega^2 - 4\right) - \psi_{xx} - 12\psi|\psi|^2. \tag{1.20}$$

The static breather solution of Eq. (1.20) has therefore been found and is given by [3]:

$$u_n = (-1)^n \sqrt{\frac{\omega^2 - 4}{6}}\,\mathrm{sech}\left[\sqrt{\frac{\omega^2 - 4}{6}}(x - x_0)\right], \tag{1.21}$$

and the NST threshold is then given by

$$A_{th} = \sqrt{\frac{\omega^2 - 4}{6}}. \tag{1.22}$$

1.4.2.2 Forbidden band frequencies far from the cutoff frequency ω_c

As far is the driving frequencies from the cutoff frequency as large is the driving amplitude necessary to trigger the supratransmission phenomenon. The slowly varying envelop approximation, accurate for small amplitude excitations, becomes less and

less accurate; a large amplitude static discrete breather solution has been obtained, through the nonlinear sinusoidal wave ansatz [118], and is given by:

$$u_n = a(-1)^n cos\left[\omega_B(a)t\right] \cos\left(\frac{\pi}{3}n \pm x_0\right), \tag{1.23}$$

where ω_B stands for the breather frequency, $x_0 = a\cos(A/a)$, A being the driving amplitude and a the breather's amplitude.

The supratransmission threshold has been derived through the resonance's condition $\omega = \omega_B(A_{th})$, and the following relation has been found:

$$\omega = 1.03\frac{\sqrt{3\pi^2\left(4 + 9A_{th}^2\right)}}{4K(s)}, \tag{1.24}$$

where $K(s)$ is the complete elliptic integral of the first kind with argument

$$s = 3A_{th}/\sqrt{2\left(9A_{th}^2 + 4\right)}.$$

1.4.3 Numerical study

The supratransmission phenomenon in β-FPU model has been investigated by Khomeriki [3] in a lattice of 512 particles submitted at one end to the sinusoidal signal $u = Acos(\omega t)$ which frequency lies in the forbidden band ($\omega > 2$). To avoid the reflexive signals to propagate in the lattice, the last 10% of particles are submitted to a strong dissipation $\gamma\dot{u}$.

The onset of the supratransmission is observe through the avaraged energy flux

$$j = \sum_N j_n, \tag{1.25}$$

where $j_n = \frac{1}{2}\left(\dot{u}_n + \dot{u}_{n+1}\right)\left[u_{n+1} - u_n + \left(u_{n+1} - u_n\right)^3\right]$

For a driving frequency $\omega = 3.5$, the ploting of the time averages of energy flux as a function of driving amplitude reveals the supratransmission threshold as a sharp increase of these averages when increasing the driving amplitude [see Fig 1.12].

The numerical study of the supratransmission as a function of driving frequency shows a good agreement with the analytical results, for small (Eq. 1.22) and large (Eq. 1.24) amplitude, as displayed in Fig. 1.13.

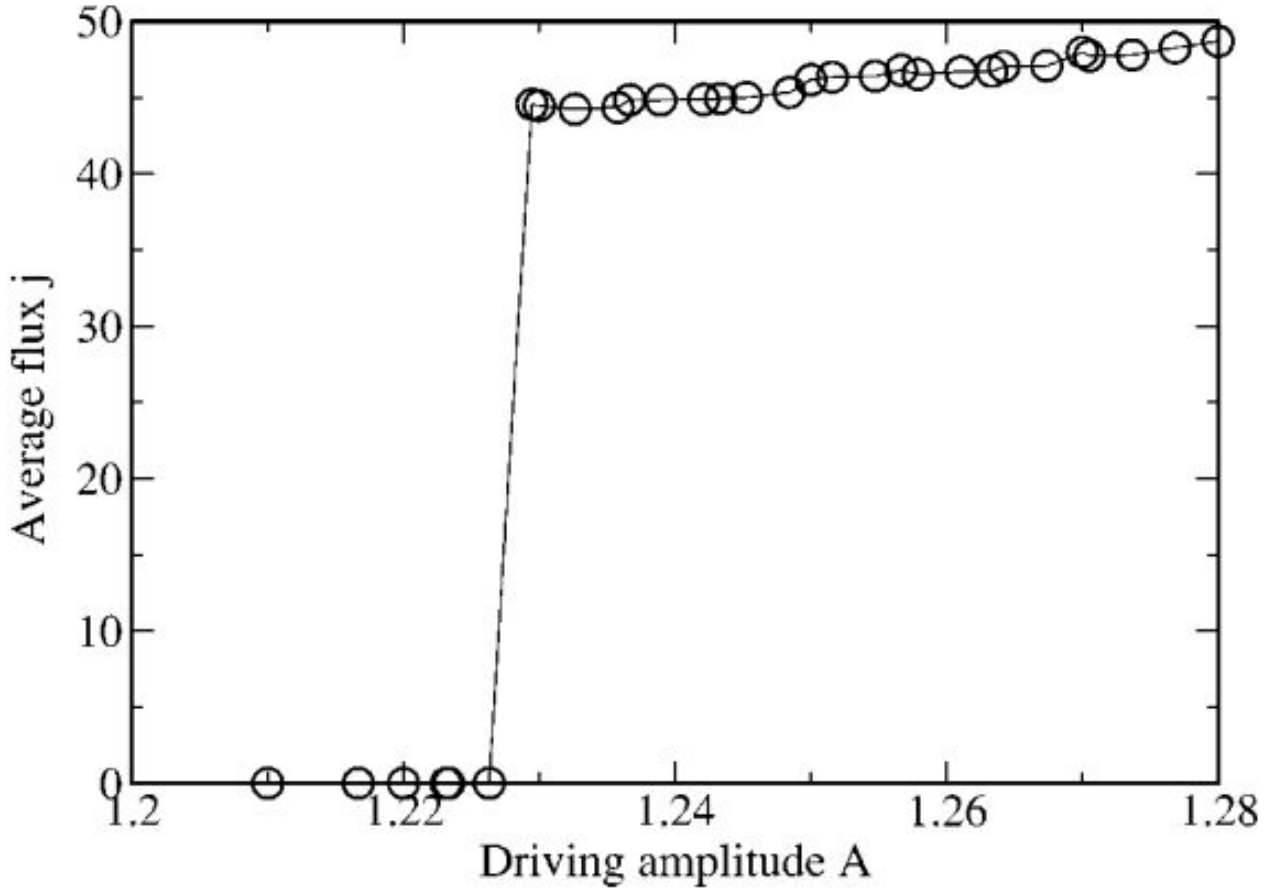

Figure 1.12: Average energy flux Vs driving amplitude for out-band forcing; $\omega = 3.5$ and $\gamma = 5$ [3].

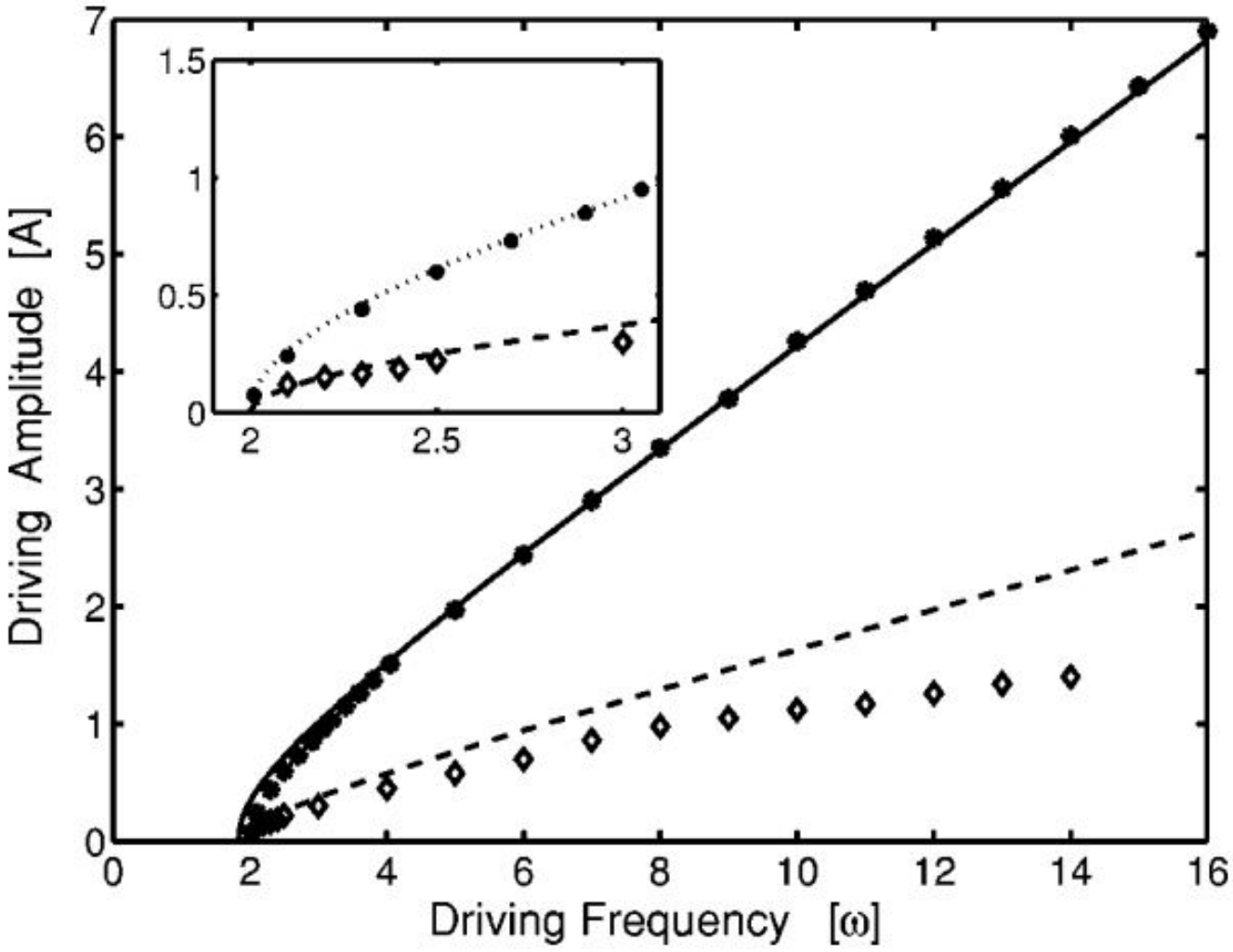

Figure 1.13: Comparison between analytic estimates and numerical values of threshold amplitudes Vs the driving frequency. Main plot: the full dots are the numerical values of A_{th} and the solid line is a plot of Eq. (1.22) and Eq. (1.24), which are valid for large amplitudes. The inset shows an enlargement of the small A_{th} region, in order to illustrate the accuracy of the small-amplitude approximation Eq. (1.22) (dotted line). The diamonds and the dashed line are numerical and analytical simulation data for the lower transmission threshold A_{th}^{-}, respectively.

1.5 Discrete nonlinear electrical transmission line

1.5.1 The model

The discrete nonlinear electrical transmission line here considered is formed by a junction of N elementary cells. Each cell consisting of a nonlinear capacitor $C(v)$ in the shunt branch and a linear inductance L in serial with a resistance r in the direct branch [Fig. 1.14]. The nonlinear capacitance is defined as

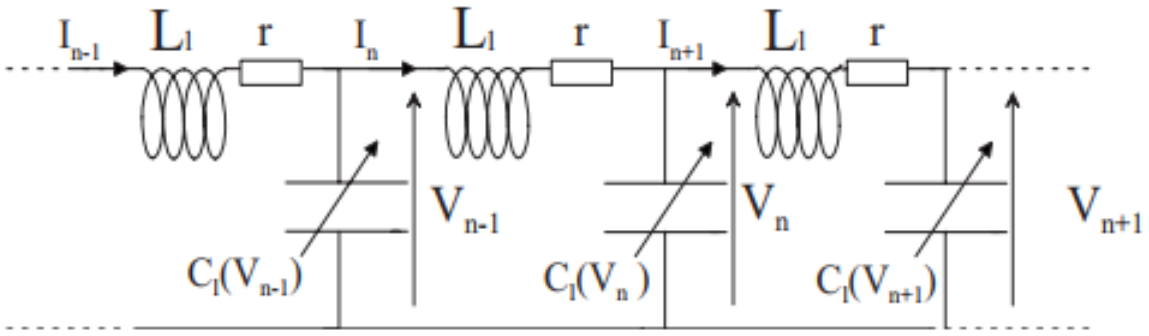

Figure 1.14: LC electrical transmission line [4].

$$C\left[V_0 + V_n\right] = C_0 \times \left[1 - 2\alpha V_n + 3\beta V_n^2\right], \tag{1.26}$$

where $V_0 = 2$ is the dc bias voltage, $C_0 = 320pF$, $\alpha = 0.21V^{-1}$ and $\beta = 0.0197V^{-2}$; The inductance shall be taken as $L = 220\mu H$.

The Kirchoff's laws applied to the system yield to the propagation's equation [4]

$$\left[\frac{d^2}{dt^2} + \frac{r}{L}\frac{d}{dt}\right]\left(V_n - \alpha V_n^2 + \beta V_n^3\right) = \frac{1}{LC}\left(V_{n+1} + V_{n-1} - 2V_n\right), \tag{1.27}$$

V_n being the voltage of the nth capacitor, $n = 1, 2, ..., N$.

When linearizing Eq. (1.27) and seeking the solution on the form of a plane wave $V_n = A_0 e^{[i(kn-\omega t)]}$, where ω and k are the angular frequency and the wave number, respectively, we derived the linear dispersion law:

$$\omega = \frac{2}{\sqrt{LC}}\sin\left(\frac{k}{2}\right) \tag{1.28}$$

The above relation admits an upper cuttoff frequency $\omega = \omega_{max} = 2/\sqrt{LC}$ at $k = \pi$. The existence of the cuttoff ω_{max} is the consequence of the discreteness of the electrical transmission line, this means that it does not exist in the continuum limit. The plotting of Eq. (1.28) is similar to the figure obtained for the β-FPU monoatomic lattice which displays a pass band and a forbidden band [Fig. 1.18].

1.5.2 Supratransmission in an electrical transmission line

To investigate the NST in the given electric transmission line, Koon et al [4] have sought solution of Eq.(1.27) on the form :

$$V_n(t) = \epsilon \left[\psi(\eta,\tau)e^{i\theta} + cc\right] + \epsilon^2 \left[\Phi(\eta,\tau) + B(\eta,\tau)e^{2i\theta} + cc\right] + ..., \tag{1.29}$$

where cc stands for the complex conjugate of the nearest preceding term, $\eta = \epsilon(n - v_g t)$, $\tau = \epsilon^2 t$, $\theta = kn - \omega t$. ϵ is a small parameter and v_g the group velocity, the resistance r is supposed negligible ($r = 0$).

$\Phi(\eta,\tau)$, $\Phi(\eta,\tau)$ and $B(\eta,\tau)$ are slowly spatial and temporal varying envelops. when inserting Eq. (1.29) into Eq. (1.27), the nonlinear Schrödinger equation is derived at the limit $k = \pi$ of the first Brillouin zone, for the first harmonic envelop Ψ:

$$i\frac{\partial \Psi}{\partial t} + \frac{\omega_c}{8}\frac{\partial \Psi}{\partial x^2} + \frac{1}{2}\omega_c \left(2\alpha^2 - 3\beta\right)|\Psi|^2\Psi = 0, \tag{1.30}$$

where $\Psi = \epsilon\psi$, $x = \eta/\epsilon$, $t = \tau/\epsilon^2$, $\omega_c = 1/\sqrt{LC}$.

The static breather solution of Eq. (1.30) is found as:

$$\Psi(x,t) = Ae^{-i\omega_s t}\,\mathrm{sech}\left[\lambda\left(x - x_0\right)\right], \tag{1.31}$$

where

$$A = \sqrt{\frac{4\omega_s}{\omega_c(2\alpha^2 - 3\beta)}},$$

$$\lambda = \frac{8\omega_s}{\omega_c},$$

$$\omega_s = \omega - \omega_c.$$

The supratransmission threshold (the maximum amplitude of the static solution)

is then given by:

$$A_{th} = 2\sqrt{\frac{\omega - \omega_c}{\omega_c\,(2\alpha^2 - 3\beta)}} \tag{1.32}$$

1.5.3 Numerical simulations

To investigate numerically the supratransmission phenomenon in an LC transmission line, a chain of 2000 cell has been considered [4]. The line is driven at one end by a sinusoidal signal which frequency lies in the forbidden band ($f > 1.1997$ MHz).

For a driving frequency $\omega = 1.2MHz$, the lattice allows energy propagation (supratransmission) for a driving amplitude $A = 0.37V$ whereas the wave vanishes during its propagation within the lattice for $A = 0.36V$ [Fig. 1.15] [4].

The the plotting of numerical supratransmission threshold as a function of driving frequency shows a good agreement with the analytical results Eq. (1.32) as displayed in Fig. 1.16.

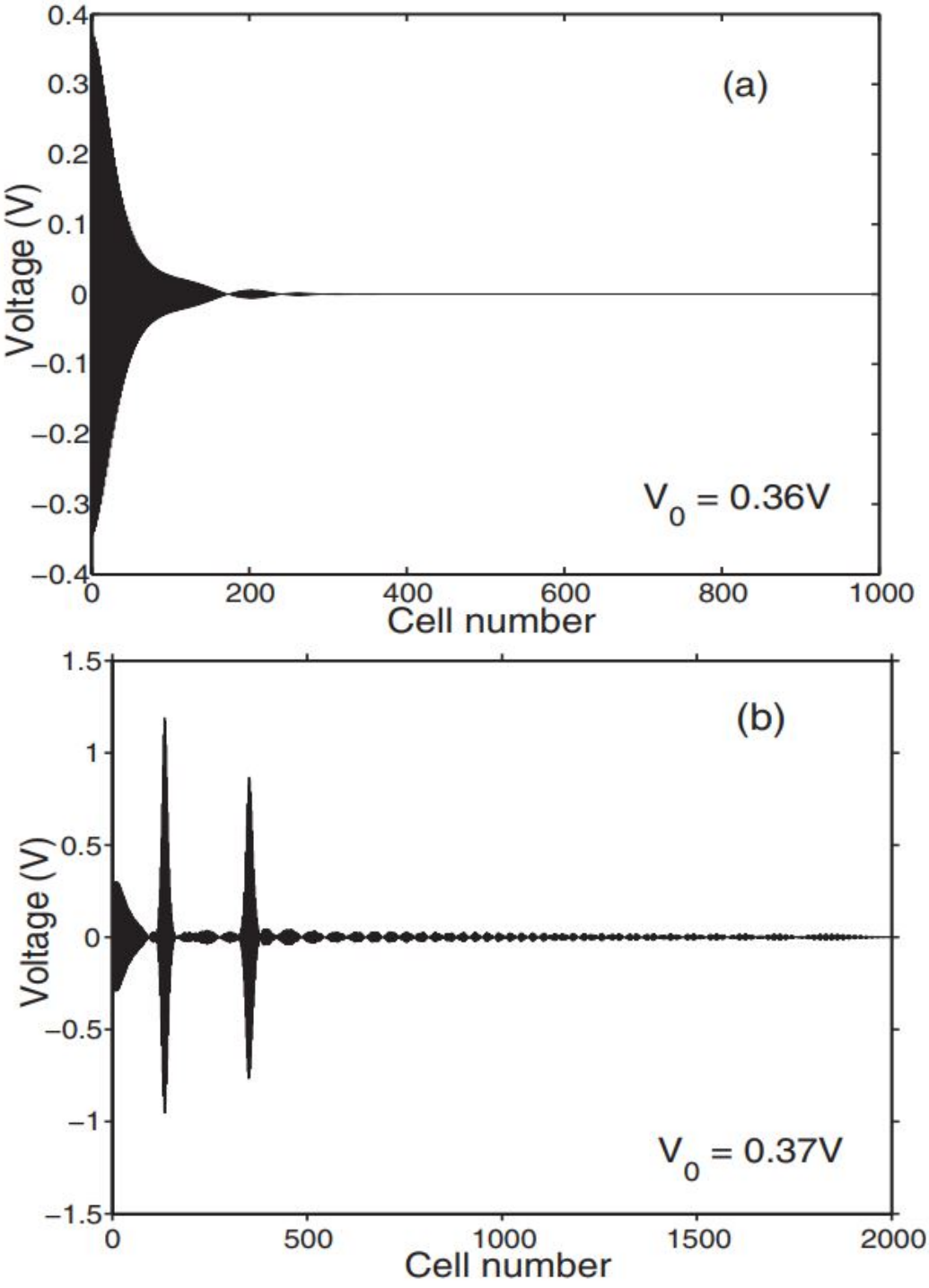

Figure 1.15: Final state at the time t=5 ms, of the electrical line for a driving frequency $\omega = 1.2MHz$ and a driving amplitudes (a) $A = 0.36V$ and (b) $A = 0.37V$, both obtained for $N = 2000cells$. The figure (b) shows energy transmission above the threshold 0.37 V as predicted by Eq.(1.32).

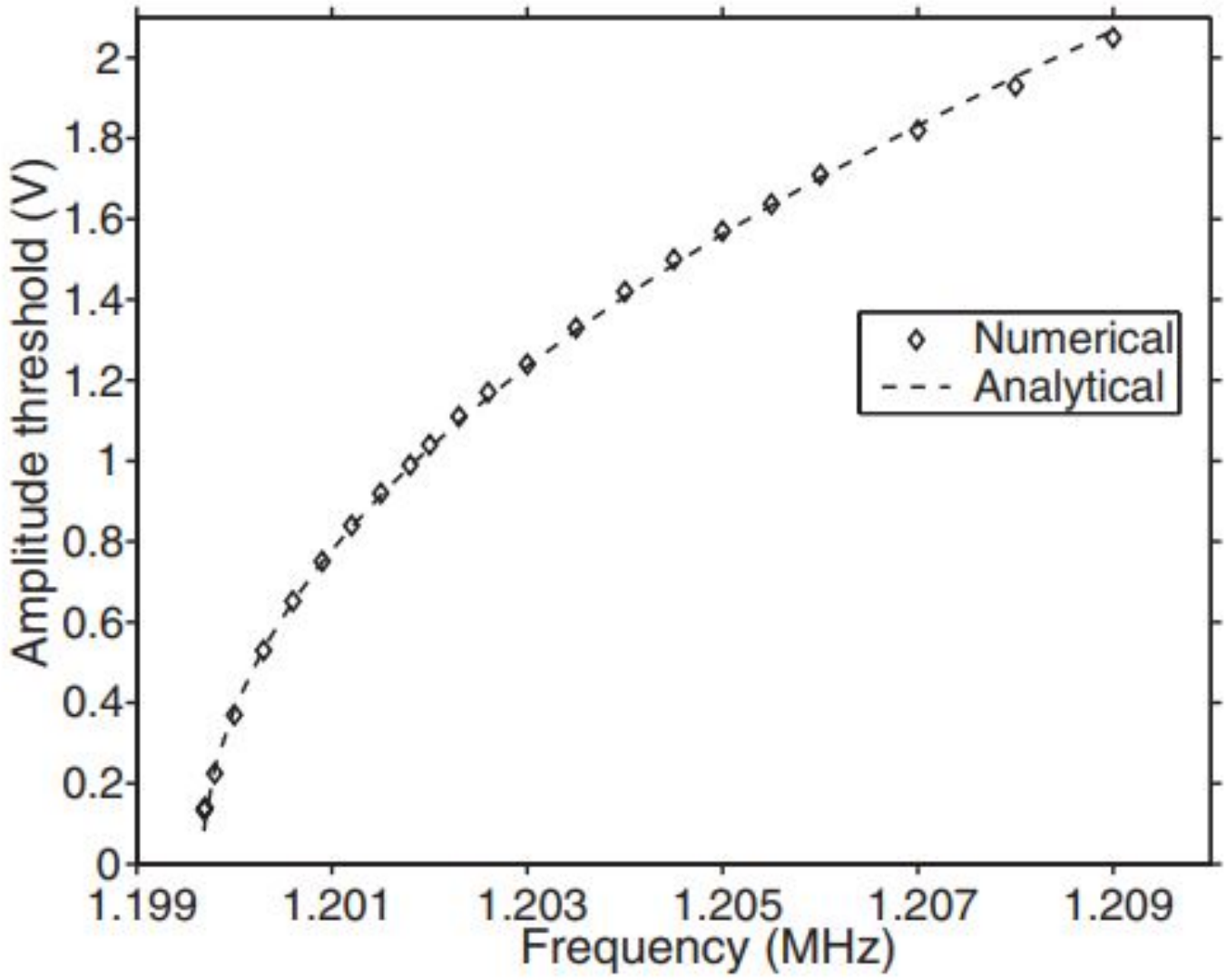

Figure 1.16: Comparision between numerical supratransmission threshold (diamonds) with its analytical analog Eq. (1.32)(dashed line).

1.6 Plasma dust

For over thirty years, the study of dusty plasma crystals has gained significant momentum due to their expanding range of applications, including in asteroid belts, planetary rings, cometary tails, and magnetospheres. Two primary models of dusty plasma crystals have been identified: the dust-acoustic model and the dust-lattice model. The latter is characterized as a strongly coupled plasma and exhibits dispersive properties, except at very long wavelengths relative to the inter-grain distance. Since their discovery, these models have captivated plasma physicists, revealing numerous novel phenomena such as intrinsic localized modes and modulational instability.

Dust grains can be analyzed in both longitudinal and transverse directions. Recently, Togueu Motcheyo et al. highlighted nonlinear wave propagation in transverse dust grain oscillations. In this section, we will investigate longitudinal dust grain oscillations.

In longitudinal oscillations, a cutoff frequency is observed at the end of the first Brillouin zone, indicating the presence of a forbidden band.

1.6.1 The model

A 1D plasma dust model here considered is the longitudinal dust grain oscillations in dusty plasma crystals modeled by the following equation [69]:

$$\frac{d^2\delta x_n}{dt^2} = u_0^2\left(\delta x_{n+1} + \delta x_{n-1} - 2\delta x_n\right) - \alpha\left[\left(\delta x_{n+1} - \delta x_n\right)^2 - \left(\delta x_n - \delta x_{n-1}\right)^2\right] + \beta\left[\left(\delta x_{n+1} - \delta x_n\right)^3 - \left(\delta x_n - \delta x_{n-1}\right)^3\right] \tag{1.33}$$

By considering the relative displacement $v_n = \delta x_{n+1} - \delta x_n$, this equation becomes:

$$\frac{d^2 v_n}{dt^2} = u_0^2\left(v_{n+1} + v_{n-1} - 2v_n\right) - \alpha\left[v_{n+1}^2 + v_{n-1}^2 - 2v_n^2\right] + \beta\left[v_{n+1}^3 + v_{n-1}^3 - 2v_n^3\right] \tag{1.34}$$

1.6.2 Supratransmission in a plama dust model

When driving the first particle of the lattice with a sinusoidal signal $v_0 = \Gamma cos\,(\omega t)$ which frequency ω lies in the forbidden band, Nkendji et al derived, through Eq. (1.34), at the limit $k = \pi$ of the first Brillouin zone, a nonlinear Schrödinger equation with the dispersion and nonlinear coefficients
$P_\pi = \frac{u_0^2}{2\omega_1}$, and $Q_\pi = \frac{2}{\omega_1}\left(\frac{4\alpha^2}{u_0^2} - 3\beta\right)$, respectively. The supratransmission threshold is derived as the maximum amplitude of the static breather solution of the nonlinear Schrödinger equation and is given by:

$$\Gamma_{th} = 2\sqrt{\frac{2u_0\,(\omega - \omega_1)}{3\beta - \frac{4\alpha^2}{u_0^2}}} \tag{1.35}$$

The numerical investigation of the supratransmission phenomenon in plasma dust has been performed [69] in a lattice of 40 particles, and the following observations have been done [see Fig1.17]:

- For a driving amplitude $\Gamma < \Gamma_{th} = 0.6325$, the wave vanishes during its propagation along the lattice
- For a driving amplitude $\Gamma \geq \Gamma_{th}$, a moving breather is generated and propagates along the lattice: the supratransmission occurred.

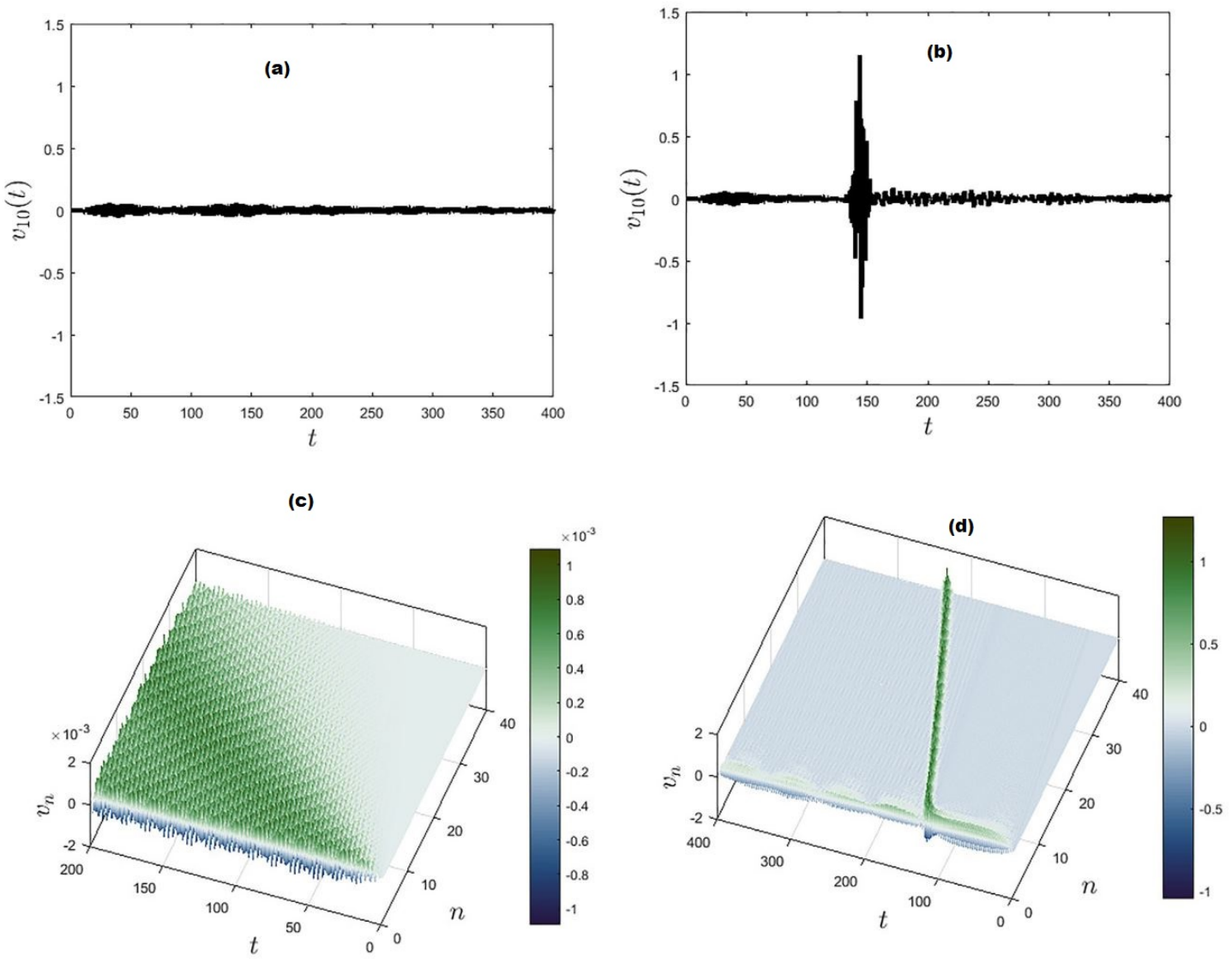

Figure 1.17: Evolution of the relative displacement of longitudinal dust grain oscillation. (a and c) temporal evolution of the amplitude of the 10th particle. (c and d) spatio-temporal evolution of the driving signal along the chain. The frequency $\omega = 2.1$; $\Gamma = 0.6324 < \Gamma_{th}$ (a and c) and $\Gamma = 0.6325 > \Gamma_{th}$ (b and d)

1.7 Context and problematic

Nonlinear phenomenon such as supratransmission, soliton generation, wave amplification and so on have been widely studied in nonlinear network, where the unit cell has one degree of freedom (as presented in the previous sections). The modeling of real systems displays a more complex structure which include a diversity between the unit cells constituting a lattice, dissipation and impurities. However, to consider

all these parameters together results in a very complex structures whose study is very complicated. For the investigation on NST, a significant advanced have been done by considering

- **the presence of impurities**: It has been shown that for a lattice with impurity, the supratransmission occurs with an amplitude lower than that of a homogeneous lattice, showing that the impurities have as main effect to lower the NST threshold [91],
- **the presence of dissipation in the lattice**: for a lattice with energy dissipation, more energy is needed to trigger the NST and as consequence, the NST threshold is seen enhance [114]

For all these studies on NST in 1D lattices, the unit cell has one degree of freedom and the driving signal is sinusoidal, so that the phenomenon is known to occur only through sinusoidal signals. Considering all these knowledge on the topic, and the limit of the accomplished works, several question still exist:

- Is it possible to observe the supratransmission phenomenon in 1D lattices possessing more than one degree of freedom per unit cell? If yes what are the effects of the different elements of the unit cell on that phenomenon?
- What happens when sinusoidal signals used to drive one end of the lattices are replaced by non-sinusoidal signals?

To answer to these questions, β-Fermi-Pasta-Ulam diatomic and monoatomic lattices driven by a sinusoidal and non-sinusoidal signals, respectively, will be considered.

1.8 Conclusion

At the end of this chapter, it appears that nonlinear lattices are useful tools for the study of complex phenomena such as wave propagation, modulational instability, and nonlinear supratransmission. The nonlinearity is revealed to be the main condition for the supratransmission occurrence in any system. A large number of studies on supratransmission phenomenon are currently found in literature and they

deepen our understanding of the phenomenon and its potential applications. Despite this number of studies, several questions remain without response and then, keep open the research field of the supratransmission.

CHAPTER II

MODELS AND METHODOLOGY

Introduction

In the previous chapter, we have presented various nonlinear models and their specificities, and we have given for each model the analytical procedure used to investigate the supratransmission phenomenon and the derived supratransmission thresholds. In this chapter, we present the models which are of interest and investigate analytically the supratransmission phenomenon. We shall also describe the analytical and numerical procedures used throughout this work.

2.1 Mathematical modelisation

The Fermi-Pasta-Ulam monoatomic and diatomic lattices will be the core models of our study. The β-FPU monoatomic lattice has been previously described in section 1.2.1.3.

The diatomic version of the described β-FPU is formed by two sub-lattices of masses m and M $(m < M)$ instead of a unique mass for all particles, as indicated in Fig. 2.1.

The Hamiltonian function of the system is given by:

$$H = \sum_j \left[\frac{1}{2} \mathcal{M}_j \left(\frac{du_j}{dt} \right)^2 + \phi(u_{j+1} - u_j) \right], \tag{2.1}$$

where $\phi(r) = \frac{1}{2}K_2 r^2 + \frac{1}{4}K_4 r^4$, K_2 and K_4 are positive constants representing harmonic and quartic potentials, respectively; $u_j = u_j(t)$ is the displacement from the equilibrium position of the jth particle with the mass $\mathcal{M}_j = M\delta_{j,2l} + m\delta_{j,2l+1}$ ($\delta_{j,p}$ is the Kronecker's delta which has the values 0 for $j \neq p$ and 1 otherwise; l is an

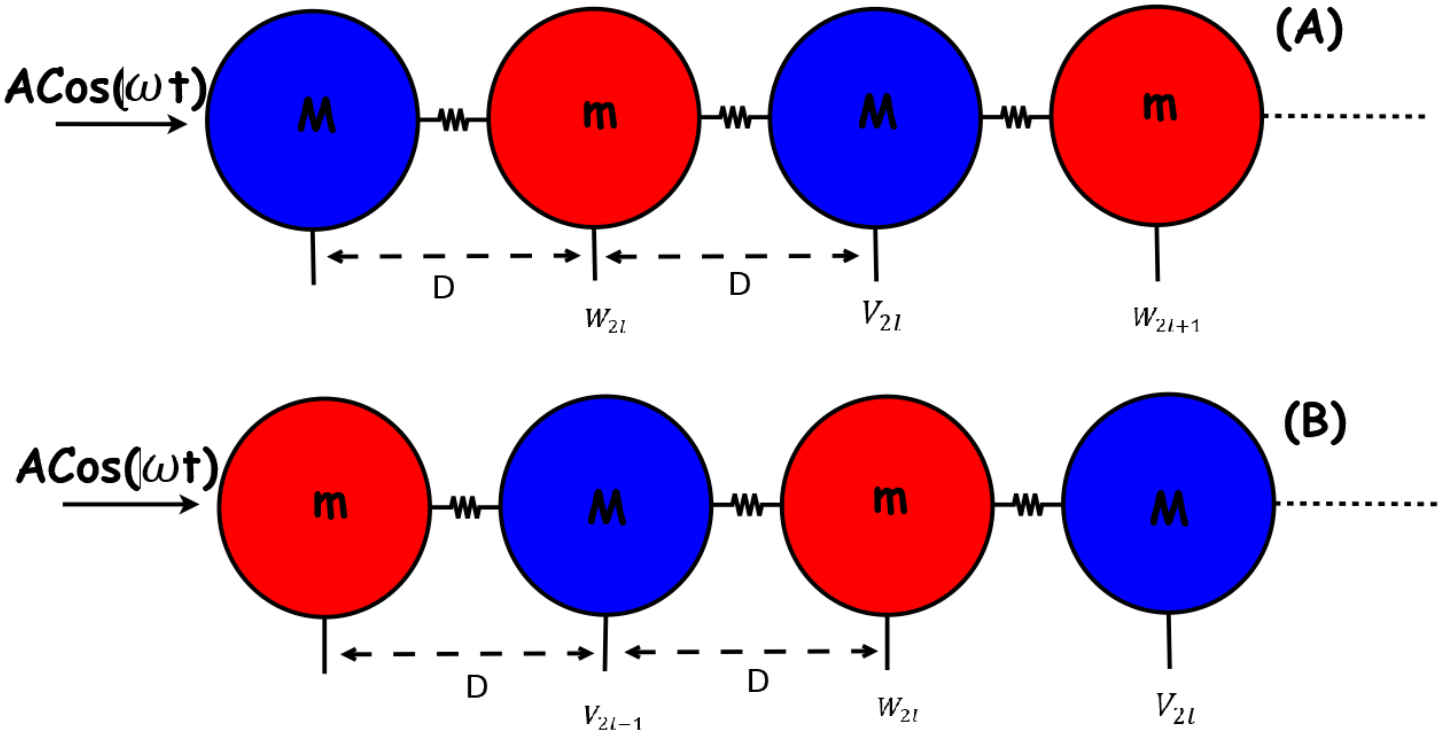

Figure 2.1: Diatomic FPU lattices. (a) light particle is the first particle; (b) heavy particle is the first particle.

integer) and, $u_j = V_j\delta_{j,2l} + W_j\delta_{j,2l+1}$. The derived equations of motion of the heavy (even) and light (odd) particles are given by:

$$\ddot{V}_n = J_2\left(W_n + W_{n-1} - 2V_n\right) + J_4\left[\left(W_n - V_n\right)^3 - \left(V_n - W_{n-1}\right)^3\right], \tag{2.2}$$

$$\ddot{W}_n = I_2(V_{n+1} + V_n - 2W_n) + I_4\left[\left(V_{n+1} - W_n\right)^3 - \left(W_n - V_n\right)^3\right], \tag{2.3}$$

where $I_2 = K_2/m$, $J_2 = K_2/M$, $I_4 = K_4/m$ and $J_4 = K_4/M$ and n is the index of the nth unit cell with spacing of $d = 2D$ (see Fig. 2.1).

Taking the linear form of Eqs. (2.2) and (2.3), and seeking plane wave solutions under the form $V_n(t) = V_0\exp\left[i(2knD - \omega t)\right]$ and $W_n(t) = W_0\exp\left[i(2knD - \omega t)\right]$, where $i^2 = -1$, k being the wave vector and ω the phonon frequency; the derived linear dispersion law is :

$$\omega_{\pm}(k) = \sqrt{I_2\left(1+\mu\right) \pm I_2\sqrt{2\mu\cos(2kD) + 1 + \mu^2}}, \tag{2.4}$$

where $\mu = m/M$ is the mass ratio.

The minus (plus) sign corresponds to the acoustic (optical) modes [66, 75, 75, 116]. At the wave number $k = 0$, the eigenfrequency spectrum has an upper cutoff $\omega_+(0) = \omega_{+max} = \sqrt{2I_2(1+\mu)}$. At $k = \frac{\pi}{2D}$, there exists a band gap between the upper cuttoff of the acoustic branch $\omega_-(\frac{\pi}{2D}) = \omega_{-max} = \sqrt{2J_2}$, and the lower cuttoff of the optical branch, $\omega+(\frac{\pi}{2D}) = \omega_{+min} = \sqrt{2I_2}$. Therefore, the previous linear dispersion relation admits two forbidden band gaps: one above the optical mode (light gray band : $\omega \in]\omega_{+max}, +\infty[$) called the upper forbidden band in the following, and the other between the acoustic and the optical mode (dark gray band : $\omega \in]\omega_{-max},\omega_{+min}[$) named the lower forbidden band, which are displayed on Fig. 2.2.

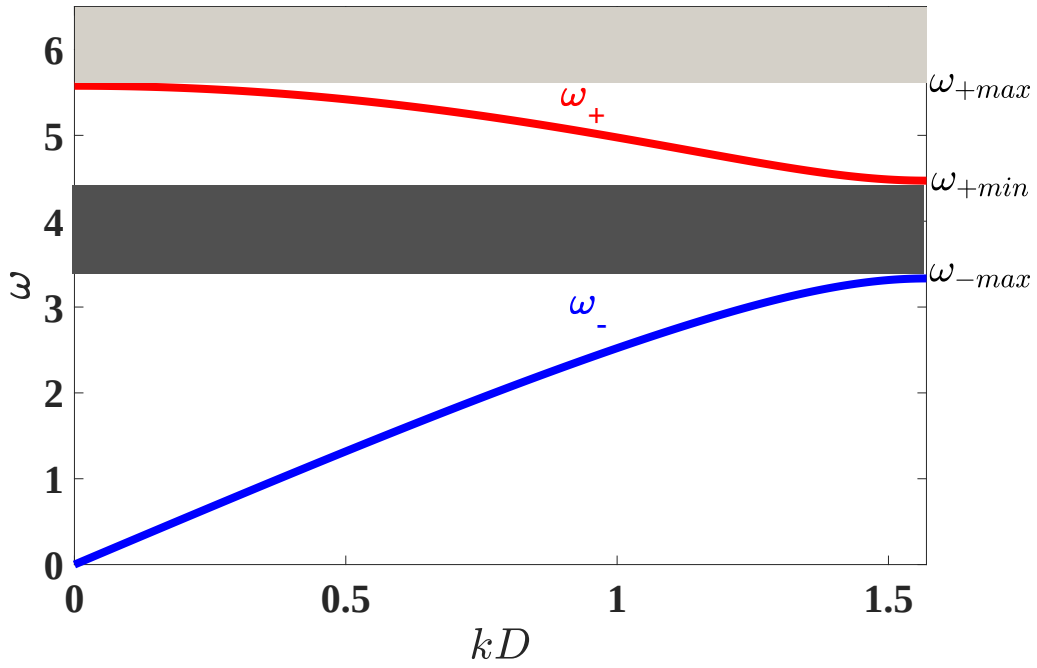

Figure 2.2: Linear dispersion relation. Blue and red curves represent acoustic (the lower branch) and optical (the upper branch) modes, respectively; $K_2 = 1$, $K_4 = 1$, $m = 0.1$, $M = 0.18$.

2.2 Supratransmission in FPU diatomic lattice

The behavior of vibrating particles under the effect of a signal whose frequency lies in the forbidden band is ordered by the nearest modes. We can distinguish for the diatomic lattice two behaviors according to the optical and acoustic modes, respectively: when the driving frequency is taken within the upper forbidden gap,

the behavior of the particles is that of optical mode and when it is taken within the lower forbidden band, the behavior of the particles is ordered by the band width given by $\omega_{+min} - \omega_{-max} = \sqrt{2I_2} - \sqrt{2J_2}$.

Furthermore, the study of NST in diatomic FPU lattice shall consider the two possible configurations of such a lattice: light particle at the first range and heavy particle at the first range (see Fig. 2.1). It is important to note that for the two cases, the lattice is the same, since when the first particle is light, the last particle is heavy, and inversely; the difference between the two cases is the mass of the driven particle (the lattice being driven at one end).

Methodology used for analytical study of supratransmission

To study analytically the supratransmission phenomenon, we proceed as follow:

- Seek pulse-type soliton solutions of the system of discrete equations,
- use approximations on the envelope and the carrier of the desired solution,
- deduce the partial nonlinear differential equation of this envelop and its static breather type solution,
- deduce the supratransmission threshold as the maximum amplitude of the static breather solution.

For the first part of the study of supratransmission, the FPU diatomic lattice considered is the version with a heavy particle at the first range.

2.2.1 Supratransmission in upper forbidden band: optical mode behavior

To investigate the supratransmission phenomenon in the upper forbidden band, we shall pay attention to its boundary. In particular, the upper forbidden band is bounded on the bottom at $k = 0$ (see Fig. (2.2). A weak value of the wave number k corresponds to a large value of wavelength so that the wave can no longer distinguish the discreteness of the lattice. The long wavelength limit can therefore be considered. Considering this approximation together with the slowly varying envelop hypothesis (in space and time) yields the following approximations:

$x = 2nD$, $u_n(t) = u(x,t)$, $u_{n\pm1}(t) = u(x \pm 2D, t)$. This continuum limit is applied to each type of particle separately since the different nature of particles of the two sub-lattices imposes a discontinuity to the overall movement. By considering the continuum approximation, we can write the Taylor expansion of $u(x \pm 2D, t)$ as:

$$u(x \pm 2D, t) = \sum_{l=1}^{4} \frac{(\pm 2D)^l}{l!} \partial_x^l u\,(x,t) + \mathcal{O}\left(D^5\right). \tag{2.5}$$

Since each particle is connected to its nearest neighbors, its displacement shall provoke that of these neighbors; decoupling ansatz is based on this natural fact and expresses the displacement of a given particle as a series expansion of the displacement of its neighbor. In the long wavelength limit, the decoupling ansatz method [79, 119] is used to approximate W as:

$$W = \lambda_i \left[V + \sum_{l=1}^{4} b_{l,i} \frac{D^l}{l!} \partial_x^l V \right] + \mathcal{O}\left(D^5\right), \tag{2.6}$$

where $\partial_x V = \partial V / \partial x = V_x$; λ_i, $b_{l,i}$ are constants which are determined by replacing Eq. (2.5) in Eqs. (2.2) and (2.3) and thereafter inserting in the resulting equations the expression of W given by Eq. (2.6).

Identifying the two resulting equations, we obtain two possible values for λ_i namely: $\lambda_1 = 1$ and $\lambda_2 = -1/\mu$, corresponding to acoustic and optical modes, respectively, and the values of the coefficients b_i for each mode as in [79, 119]. For the acoustic mode ($\lambda = 1$), we consider terms up to $\mathcal{O}(D^5)$ and derive the coefficients as :

$$b_{1,1} = 1, \quad b_{1,2} = \frac{2}{\mu\,(1+\mu)}, \quad b_{3,1} = 2\frac{2-\mu^2}{1+\mu^2}, \quad b_{4,1} = 4b_2\left(1 - \frac{3\mu}{(1+\mu)^2}\right) \tag{2.7}$$

For the optical mode ($\lambda = -1/\mu$) terms up to $\mathcal{O}(D^3)$ are considered, and the coefficients are given by:

$$b_{2,1} = 1, \quad b_{2,2} = \frac{2\mu}{1+\mu}, \quad b_{2,3} = b_{2,4} = 0. \tag{2.8}$$

Inserting in Eqs. (2.2) and (2.3) the Taylor expansion Eq. (2.5) and the decoupling ansatz procedure Eq. (2.6) with optical mode's coefficients; we obtain when

keeping only terms up to $\mathcal{O}(\epsilon^3)$ the following equation

$$V_{tt} + cV_{xx} + dV + qV^3 = 0, \tag{2.9}$$

where

$$c = \frac{2J_2D^2}{1+\mu}, d = 2I_2(1+\mu), q = \frac{2J_4(1+\mu)^3}{\mu^3}.$$

Taking the linear form of Eq. (2.9) ($V_{tt} + cV_{xx} + dV = 0$,)and looking for plane wave solutions on the form $V = V_0 \exp[i(kx - \Omega t)]$, the linear dispersion relation $\Omega^2 = d - ck^2$ can be derived. We can seek solution of Eq. (2.9) on the form [79,119]:

$$V(x,t) = \Phi(x,t) \exp\left[i(kx - \omega t)\right] + cc. \tag{2.10}$$

By inserting Eq. (2.10) into Eq. (2.9) and using the new variables $\eta = x - v_g t$ and $\tau = \epsilon t$, we derive the following nonlinear Schrödinger equation:

$$-i\Phi_\tau + P\Phi_{\eta\eta} + Q|\Phi|^2\Phi = 0, \tag{2.11}$$

where

$$P = -\frac{\nu}{2}, \quad Q = \frac{3q}{2\omega} \quad and \quad \nu = \frac{d^2\omega}{dk^2} = -\frac{v_g^2 + c}{\omega}.$$

We seek solution of Eq. (2.11) on the form of static breather solution given by $\Phi(\eta,\tau) = A(\eta)\exp(-i\omega_s\tau)$; where $\omega_s = \omega - \omega_{+max}$ for the upper forbidden band, and we obtain (see Appendix A) :

$$\Phi(\eta,\tau) = \sqrt{\frac{2\omega_s}{Q}}\,\mathrm{sech}\left(\pm\sqrt{\frac{\omega_s}{P}}\,(\eta - \eta_0)\right)\exp(-i\omega_s\tau). \tag{2.12}$$

The supratransmission threshold is derived through the maximum amplitude of the static solution given by:

$$V_{max} = 2\Phi_{max} = 2\sqrt{\frac{2\omega_s}{Q}}$$

and thus, we can write the supratansmission threshold as:

$$A_{th_{up}} = \sqrt{\frac{8\omega\mu^3\left(\omega - \omega_{+max}\right)}{3J_4\left(1+\mu\right)^3}}. \tag{2.13}$$

Therefore, when the driving frequency is taken within the upper forbidden band, the energy transmission can occur when the driving amplitude $A \geq A_{th}$, otherwise, the wave shall vanish as observed in Fig. 1.8-a.

2.2.2 Supratransmission threshold in the lower forbidden band

The lower forbidden band of a FPU diatomic lattice is located between the acoustic and the optical modes so that the behavior of particles strongly depends on the width of the band (large or narrow).

2.2.2.1 Large band gap : acoustic mode behavior

When the width of the forbidden band is sufficiently large, the interaction between the two modes can be neglected, and the hypothesis of decoupling between these modes shall be consider. The lower forbidden band is bounded at $k = \frac{\pi}{2D}$ [Fig. 2.2], and for this value of the wave number, the long wave-length limit and then the decoupling ansatz given in Eq. (2.6) are no longer valid.

In order to take into account the effects of discreteness of the system, the continuum approximation is replaced by the quasi-discrete approximation [120], and therefore, a more general form of the decoupling ansatz method for arbitrary wave-length is used. [120]. According to QDA, the solutions of Eqs. (2.2) and (2.3) are sought on the form :

$$\begin{aligned} V_n &= A_n e^{i(2knD-\omega t)} + cc \\ W_n &= B_n e^{i(2knD-\omega t)} + cc \end{aligned} \tag{2.14}$$

and assumed the continuum approximation $2nD \to x$ so that $A_n(t) \to A(x,t)$ and $B_n(t) \to B(x,t)$. After the Taylor expansion of A_{n+1} and B_{n-1} around the continuum variables $A(x,t)$ and $B(x,t)$ respectively, we can apply the decoupling ansatz [120] :

$$B(x,t) = \sigma e^{ikD}(A + b_1 D A_x + \frac{b_2}{2} D A_{xx} + b_3 D A_{xt} + b_0 |A|^2 A), \tag{2.15}$$

which gives two possible values of σ (see appendix B) which yield, for $k = \frac{\pi}{2D}$, $\sigma = 0$ and $\sigma = -\infty$. The last value of σ which is obtained for optical mode provides an infinite value for the envelop and then, renders a divergence. For the former ($\sigma = 0$)

obtained for acoustic mode, the coefficients b_1, b_2, b_3 and b_0 given in [120] can be derived and thereafter we obtain V_n and W_n as follow:

$$\begin{aligned} V_n &= (-1)^n A e^{-i\omega t} + cc, \\ W_n &= 0. \end{aligned} \tag{2.16}$$

Following the procedure described in [120], we obtain the nonlinear Schrödinger equation which is given for $\sigma = 0$ and $k = \frac{\pi}{2D}$ by:

$$-iA_\tau + P_a A_{\eta\eta} + Q_a |A|^2 A = 0, \tag{2.17}$$

where

$$P_a = \frac{\sqrt{2J_2}D^2}{1-\mu} \quad \text{and} \quad Q_a = \frac{3J_4}{\omega_{-max}}$$

.

Equation (2.17) is similar to that obtained in section (2.2) and its static solution can be written as:

$$A(\eta,\tau) = \sqrt{\frac{2\omega_s}{Q_a}}\,\mathrm{sech}\left(\pm\sqrt{\frac{\omega_s}{P}}\,(\eta-\eta_0)\right)\exp(-i\omega_s\tau). \tag{2.18}$$

Thus,

$$V(\eta,\tau) = \sqrt{\frac{2\omega_s}{Q_a}}\,\mathrm{sech}\left(\pm\sqrt{\frac{\omega_s}{P}}\,(\eta-\eta_0)\right)e^{(-i\omega_s\tau)}e^{i\theta} + CC, \tag{2.19}$$

where $\omega_s = \omega - \omega_{-max}$. The supratransmission threshold is given by:

$$A_{th_{low_1}} = \sqrt{\frac{8\omega_{-max}\,(\omega-\omega_{-max})}{3J_4}}. \tag{2.20}$$

2.2.2.2 Narrow forbidden phonon band gap : coupling mode effects

In case of small mass difference, the width of the band is weak. Because of the nonlinearity, there exist a strong coupling between the optical lower cuttoff mode and the acoustic upper cutoff mode at the boundary $k = \frac{\pi}{2D}$ of the first Brillouin zone [75]. The hypothesis of decoupling between the two modes is no longer valid, and the seeking of coupled modes static breathers shall be necessary to investigate the supratransmission phenomenon in this case.

We consider the following asymptotic expansion for V_n and W_n [75]:

$$\begin{aligned} V_n &= \epsilon V_{n,n}^{(1)} + \epsilon^2 V_{n,n}^{(2)} + \epsilon^3 V_{n,n}^{(3)} + ... \\ W_n &= \epsilon W_{n,n}^{(1)} + \epsilon^2 W_{n,n}^{(2)} + \epsilon^3 W_{n,n}^{(3)} + ... \end{aligned} \tag{2.21}$$

The Quasi-Discrete Approximation has early been studied by Hu et al [75], for a diatomic FPU lattice. Following this procedure, we consider the slow variables:

$$\begin{aligned} \eta &= \epsilon \left(2nD - v_g t\right) \\ \tau &= \epsilon^2 t, \end{aligned} \tag{2.22}$$

and the fast variable

$$\Phi_n(t) = 2knD - \omega t \tag{2.23}$$

When considering the expansion Eq. (2.21), the linear form of Eq. (2.2) and Eq. (2.3) are verified when the following conditions known as solvability conditions are verified: **at the order** ϵ^1

$$\begin{aligned} M\frac{\partial^2}{\partial t^2}V_{n,n}^{(1)} &= K_2\left(W_{n,n}^{(1)} + W_{n,n-1}^{(1)} - 2V_{n,n}^{(1)}\right) \\ m\frac{\partial^2}{\partial t^2}W_{n,n}^{(1)} &= K_2\left(V_{n,n}^{(1)} + V_{n,n+1}^{(1)} - 2W_{n,n}^{(1)}\right) \end{aligned} \tag{2.24}$$

at the order ϵ^2

$$\begin{aligned} M\frac{\partial^2}{\partial t^2}V_{n,n}^{(2)} &= K_2\left(W_{n,n}^{(2)} + W_{n,n-1}^{(2)} - 2V_{n,n}^{(2)}\right) \\ m\frac{\partial^2}{\partial t^2}W_{n,n}^{(2)} &= K_2\left(V_{n,n}^{(2)} + V_{n,n+1}^{(2)} - 2W_{n,n}^{(2)}\right) \end{aligned} \tag{2.25}$$

at the order ϵ^3

$$\begin{aligned} M\frac{\partial^2}{\partial t^2}V_{n,n}^{(3)} &= K_2\left(W_{n,n}^{(3)} + W_{n,n-1}^{(3)} - 2V_{n,n}^{(3)}\right) \\ m\frac{\partial^2}{\partial t^2}W_{n,n}^{(3)} &= K_2\left(V_{n,n}^{(3)} + V_{n,n+1}^{(3)} - 2W_{n,n}^{(3)}\right) \end{aligned} \tag{2.26}$$

When inserting Eq. (2.21) into Eqs. (2.2 and 2.3), and taking into account Eqs. (2.22 and 2.23), we derive $V_{n,n}^{(1)}$ and $W_{n,n}^{(1)}$ from the leading order (ϵ^1), at the limit

$k = \frac{\pi}{2D}$ of the first Brillouin zone as:

$$\begin{aligned} V_{n,n}^{(1)} &= (-1)^n A_{11}(\eta,\tau)\exp(-i\omega_{-max}t) + cc \\ W_{n,n}^{(1)} &= (-1)^n B_{11}(\eta,\tau)\exp(-i\omega_{+min}t) + cc. \end{aligned} \tag{2.27}$$

At the second order (ϵ^2), the solvability conditions yield $v_g = 0$; and at the third order (ϵ^3) we derived when taking into account Eq. (2.27) and the solvability conditions obtained from the second order, the following coupled equations

$$\begin{aligned} i\frac{\partial}{\partial\tau}A_{11} - \frac{K_2^2D^2}{2Mm\omega_{-max}\left(\omega_{+min}^2-\omega_{-max}^2\right)}\frac{\partial^2}{\partial\eta^2}A_{11} \\ - \frac{3K_4}{M\omega_{-max}}\left(|A_{11}|^2+2|B_{11}|^2\right)A_{11} = 0, \end{aligned} \tag{2.28}$$

$$\begin{aligned} i\frac{\partial}{\partial\tau}B_{11} - \frac{K_2^2D^2}{2Mm\omega_{+min}\left(\omega_{-max}^2-\omega_{+min}^2\right)}\frac{\partial^2}{\partial\eta^2}B_{11} \\ - \frac{3K_4}{m\omega_{+min}}\left(|B_{11}|^2+2|A_{11}|^2\right)B_{11} = 0. \end{aligned} \tag{2.29}$$

When using the new variables $\Phi = \epsilon A_{11}$ and $\Psi = \epsilon B_{11}$ into Eqs. (2.28 and 2.29), we obtain the coupled nonlinear Schrödinger equations depending to the initial variables $x_n = 2nD$ and t

$$\begin{aligned} i\frac{\partial}{\partial t}\Phi - P_1\frac{\partial^2}{\partial x_n^2}\Phi - Q_1\left(|\Phi|^2+2|\Psi|^2\right)\Phi = 0, \\ i\frac{\partial}{\partial t}\Psi + P_2\frac{\partial^2}{\partial x_n^2}\Psi - Q_2\left(|\Psi|^2+2|\Phi|^2\right)\Psi = 0, \end{aligned} \tag{2.30}$$

where

$$P_1 = \frac{K_2J_2D^2}{4\omega_{-max}(1-\mu)}, \quad P_2 = \frac{K_2J_2D^2}{4\omega_{+min}(1-\mu)},$$
$$Q_1 = \frac{3\omega_{-max}J_4}{2J_2}, \quad Q_2 = \frac{3\omega_{+min}J_4}{2J_2}.$$

- **Band with negligible coupling**

Since we are at the limit $k = \frac{\pi}{2D}$ we can do the approximation $\Psi = 0$ for the

acoustic mode and $\Phi = 0$ for the optical mode (see section (2.2.2.1)); we thus obtain for each case a nonlinear Schrödinger equation

$$i\frac{\partial}{\partial t}\Phi - P_1\frac{\partial^2}{\partial x_n^2}\Phi - Q_1|\Phi|^2\Phi = 0, \tag{2.31}$$

$$i\frac{\partial}{\partial t}\Psi + P_2\frac{\partial^2}{\partial x_n^2}\Psi - Q_2|\Psi|^2\Psi = 0. \tag{2.32}$$

Based on the PQ product, only Eq. (2.31) allows static breather solutions.

When seeking solution of Eq. (2.31) on the for $\Phi = a(\eta)e^{-i\omega_s t}$ and following the procedure indicated in appendix (A), we obtain a static breather solution of acoustic mode

$$\Phi(x_n, t) = \sqrt{\frac{2\omega_s}{Q_1}}\,\mathrm{sech}\left(\pm\sqrt{\frac{\omega_s}{P_1}}\,(x_n - x_0)\right)\exp(-i\omega_s t). \tag{2.33}$$

where $\omega_s = \omega - \omega_{-max}$.

Thereafter, we derived the supratransmission threshold

$$A_{th_{low_3}} = \sqrt{\frac{8\omega_{-max}\,(\omega - \omega_{-max})}{3J_4}}. \tag{2.34}$$

We can note that the threshold Eq. (2.34) obtained for acoustic mode excitation is identical to the threshold Eq. (2.20) early obtained in section (2.2.2.1)

- **Band with coupling effects**

When the width of the band gap is so small that the coupling effects become non-negligible, we shall seek static breather-breather solutions of Eq. (2.30) on the form

$$\begin{aligned}\Phi(x,t) &= A\,\mathrm{sech}\,(\gamma x)\,e^{-i\omega_{s_1}t},\\ \Psi(x,t) &= B\,\mathrm{sech}\,(\gamma x)\,e^{-i\omega_{s_2}t},\end{aligned} \tag{2.35}$$

where $\omega_{s_1} = \omega - \omega_{-max}$. ω_{s_2}, γ, A and B shall be defined by the solvability conditions (see appendix B).

When inserting Eq. (2.35) into Eq. (2.30), the solvability conditions yield:

$$\gamma^2 = \frac{\omega_{s_1}}{P_1}, \tag{2.36}$$

$$\omega_{s_2} = -\frac{\omega_{-max}\omega_{s_1}}{\omega_{+min}}, \tag{2.37}$$

$$A = \pm i\sqrt{\frac{4\omega_{s_2}}{3Q_2} + \frac{2\omega_{s_1}}{3Q_1}}, \tag{2.38}$$

$$B = \pm\sqrt{\frac{4\omega_{s_1}}{3Q_1} - \frac{2\omega_{s_2}}{3Q_2}}, \tag{2.39}$$

and thereafter, the supratransmission threshold is given by:

$$A_{th_{low_4}} = A_{th_{low3}}\sqrt{1 - \frac{2}{3}\left(\frac{\omega_{+min}^2 - \omega_{-max}^2}{\omega_{+min}^2}\right)} \tag{2.40}$$

2.2.3 Effects of the mass of the driven particle on the supratransmission threshold

In this section, the order of the particles array previously considered [Fig. 2.1.a] is switched into the diatomic lattice version which the driven particle (the first unit) has now the mass m [Fig. 2.1b].

The diatomic lattice consists on two sub-lattices having the masses m and M; the displacement of the nth particle of each sub-lattice are given by W_n and V_n respectively. Since the first particle have the mass m, the seeking of threshold amplitude of supratransmission occurrence shall be done through the solution W of the envelope equation, on contrary to the lattice with a particle of mass M as first particle, for which the solution V is needed. Our investigation on the effects of the mass of the driven particle on the supratransmission phenomenon shall be done in each forbidden band of the lattice, and for each of the scenario met in these bands.

2.2.3.1 Upper forbidden band

In this band, the decoupling ansatz procedure gives

$$W = \lambda_i \left[V + \sum_{l=1}^{4} b_{l,i} \frac{D^l}{l!} \partial_x^l V \right] + \mathcal{O}\left(D^5\right), \tag{2.41}$$

which can be approximated at the first order as

$$W = \lambda V, \tag{2.42}$$

where $\lambda = -1/\mu$. The supratransmission threshold which is the maximum amplitude of the static solution is then given by

$$B_{th_{up}} = |\lambda| A_{th_{up}} = |\lambda| \sqrt{\frac{8\omega\mu^3 \left(\omega - \omega_{+max}\right)}{3J_4 \left(1+\mu\right)^3}}. \tag{2.43}$$

2.2.3.2 Lower forbidden band

In the lower forbidden band, for a wide band gap, the decoupling ansatz procedure approximated at the first order gives:

$$B = \sigma e^{ikD} A, \tag{2.44}$$

where $\sigma = \frac{-\beta \pm \sqrt{\Delta}}{2\cos(kD)}$, $\Delta = \beta^2 + 4\frac{M}{m}\cos^2(kD)$, $\beta = \frac{M}{m} - 1$.

Around the limit $k = \pi/2D$ of the first Brillouin zone, we can do the approximation

$$kD = \frac{\pi}{2}\left(1 + \epsilon\right), \tag{2.45}$$

with $\epsilon << 1$. Taking into account Eq. (2.45), we can write

$$\cos(kD) \approx -\frac{\pi\epsilon}{2},$$
$$e^{ikD} \approx -\frac{\pi\epsilon}{2} + i,$$

and for the acoustic mode

$$\sigma = \frac{\pi\epsilon}{2\left(1-\mu\right)}. \tag{2.46}$$

and thereafter, we derived the supratransmission threshold as

$$B_{th_{low1}} = \frac{\pi\epsilon\sqrt{1+\frac{\epsilon^2\pi^2}{2}}}{2\left(1-\mu\right)}A_{th_{low1}}. \tag{2.47}$$

2.3 Wave transmission for a very narrow ($m/M > 66\%$) lower forbidden band of a diatomic FPU lattice

The lower forbidden band presents the particularity to be located between two pass bands, so that wave propagation in the lattice with frequency in this band is under the effects of these two modes. The effect of the coupling of the two modes, which are accentuated in the lower forbidden band, could induct new behaviours on the dynamic of particles in diatomic lattice, and more interestingly generated new phenomena. The adding of nonlinearity should surely impact the existing phenomena.

The diatomic dispersion law is given by:

$$\omega_{\pm}(k) = \sqrt{\frac{K_2\left(M+m\right) \pm K_2\sqrt{2mM\cos(2kD)+M^2+m^2}}{mM}}, \tag{2.48}$$

where the + (resp −) sign stands for optical (resp acoustic) mode. In the forbidden band, the wave number becomes complex, and shall be taken as

$$k = k_r + ik_i, \tag{2.49}$$

where k_r and k_i are real and imaginary parts of wave number respectively and i stands for the imaginary number characterized by $i^2 = -1$.

Inserting Eq (2.49) into Eq (2.48), we obtain the following expressions of imaginary part of wave number:

$$k_i = \frac{1}{2D}ach\left(\pm\frac{K_2^2\left(M^2+m^2\right)-\left(mM\omega^2-K_2\left(m+M\right)\right)^2}{2K_2^2mM}\right), \tag{2.50}$$

where the + and the − sign stand for the lower and the upper forbidden bands respectively.

For a given couple (m, M), the study of the imaginary part of wave number with

respect to the driving frequency reveals in the upper forbidden band, an increase of k_i with the growing of the driving frequency and in the lower forbidden band, the curve of k_i versus the driving frequency presents a bell shape, with the maximum value of k_i around the middle of this band (around $\omega = \frac{Max(\omega_-)+Min(\omega_+)}{2}$).

From Fig (2.3-b), we can deduce the coupling between the two modes (acoustic and optical) on all signals with driving frequency in the lower forbidden band. Moreover, the effects of one mode is greater than the other when the frequency is nearer this mode, and the effects of the two modes compensate each other for frequencies around the middle of the band. In addition, we note that the coefficient k_i is relatively weak in the lower forbidden band in comparison with the upper. The behavior of the lattice when driven by a signal which frequency lies in a narrow lower forbidden band shall be investigated numerically later in this work.

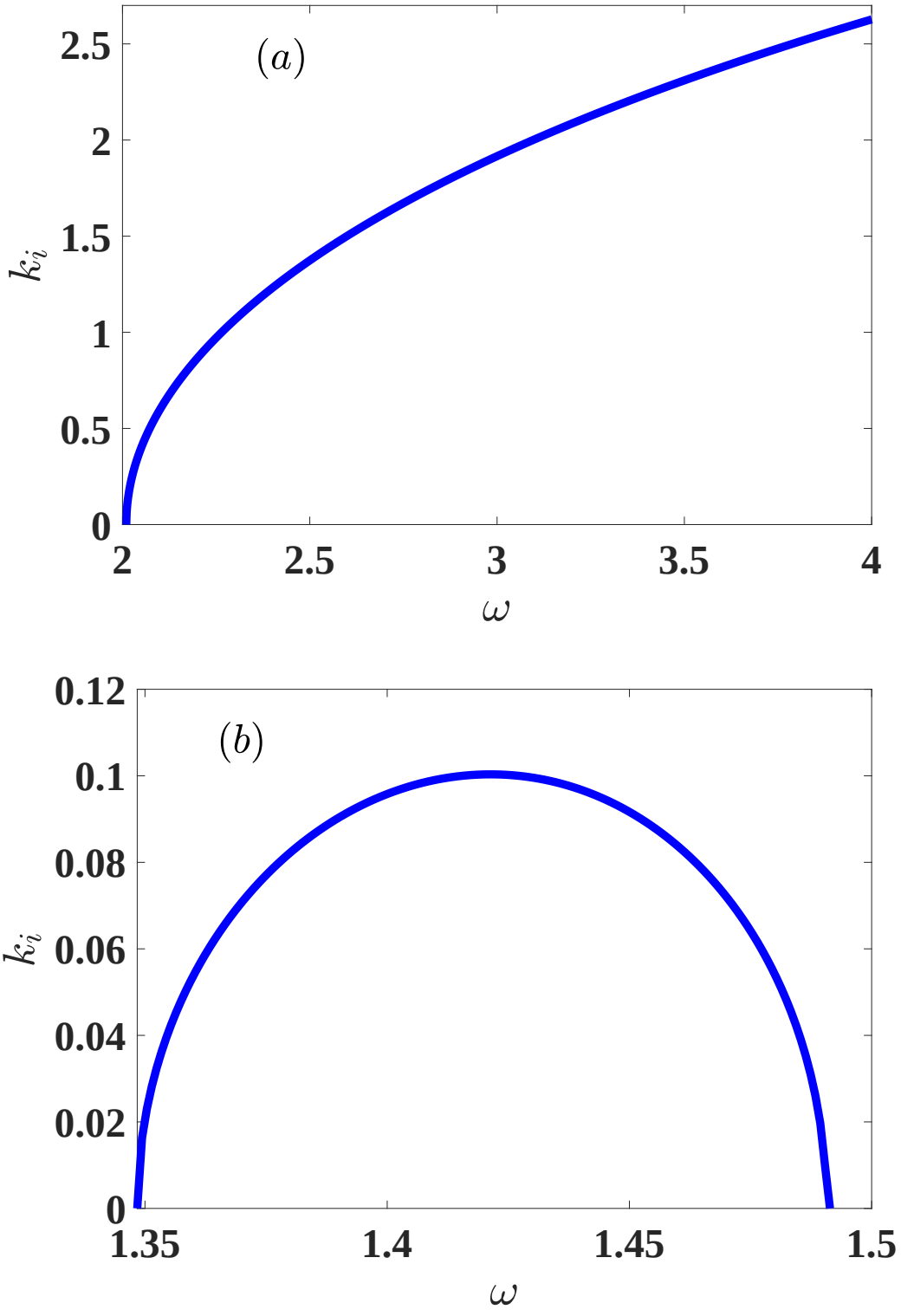

Figure 2.3: Imaginary part of wave number versus the driving frequency for the upper (a) and the lower (b) forbidden band. m=0.9, M=1.1

2.4 Shape-control's energy transmission in a monoatomic β-FPU lattice

In the section, we shall consider as core model a monoatomic β-FPU lattice as presented in Fig. 1.3.

2.4.1 Variable shape signals

The shape of a signal can vary through many procedures and can either or not preserve its symmetry during the variation. We can thus distinguish two cases: a symmetric shape variation and an asymmetric shape variation.

2.4.1.1 Symetric shape variation

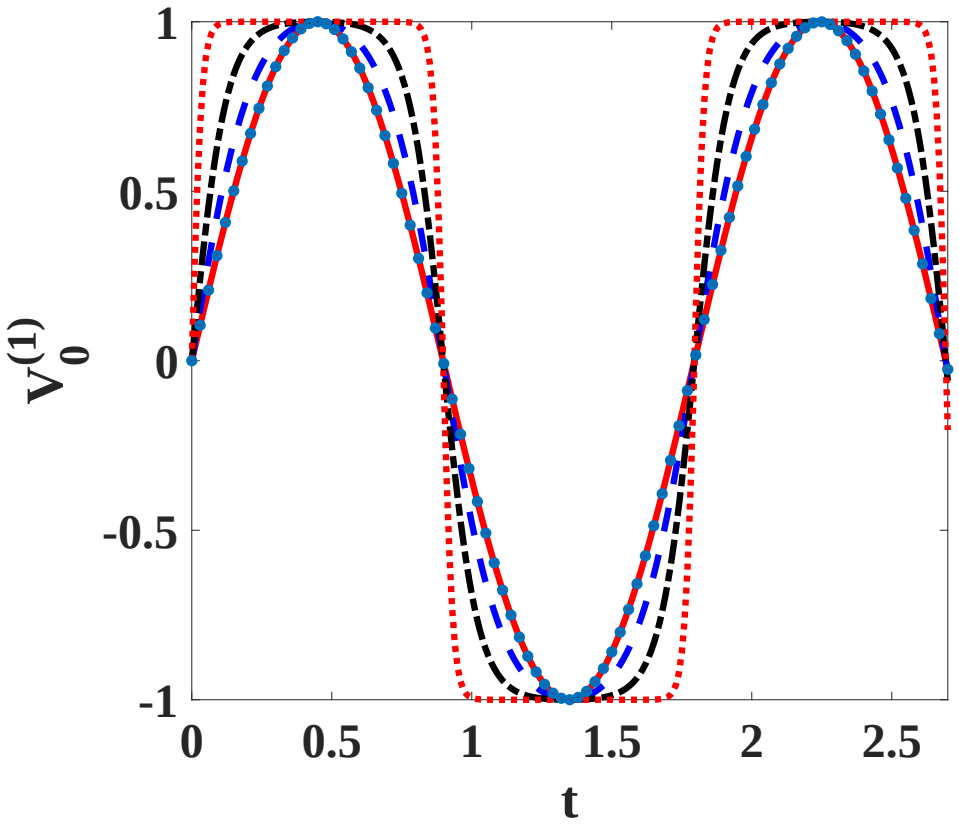

Figure 2.4: Variable shape signals $V_0^{(1)}$ and $V_0^{(2)}$ for different values of the shape parameter r: red dotted line ($r = 1 - 10^{-10}$), black dot-dashed line (r=0.99), blue dashed line (r=0.8), red solid line (r=0). The blue circles stand for sinusoidal signal $A_0 sin(\omega t)$. $A_0 = 1$, $\omega = 3.5$

We consider a variable shape Jacobi elliptic signal on the form:

$$V_0^{(1)}(t) = A_0 Sn\left(\frac{4K(r)\omega}{2\pi}t, r\right), \tag{2.51}$$

where sn is the Jacobi elliptic function, $K(r)$ is the complete elliptic function of first kind, and r is the shape parameter.

The signals $V_0^{(1)}$ have the frequency ω and the amplitude A_0, and take the well-known trigonometric forms $A_0 sin(\omega t)$ when setting the shape parameter r to zero.

The plotting of Eq. (2.51) for several values of r is displayed in Fig (2.4).

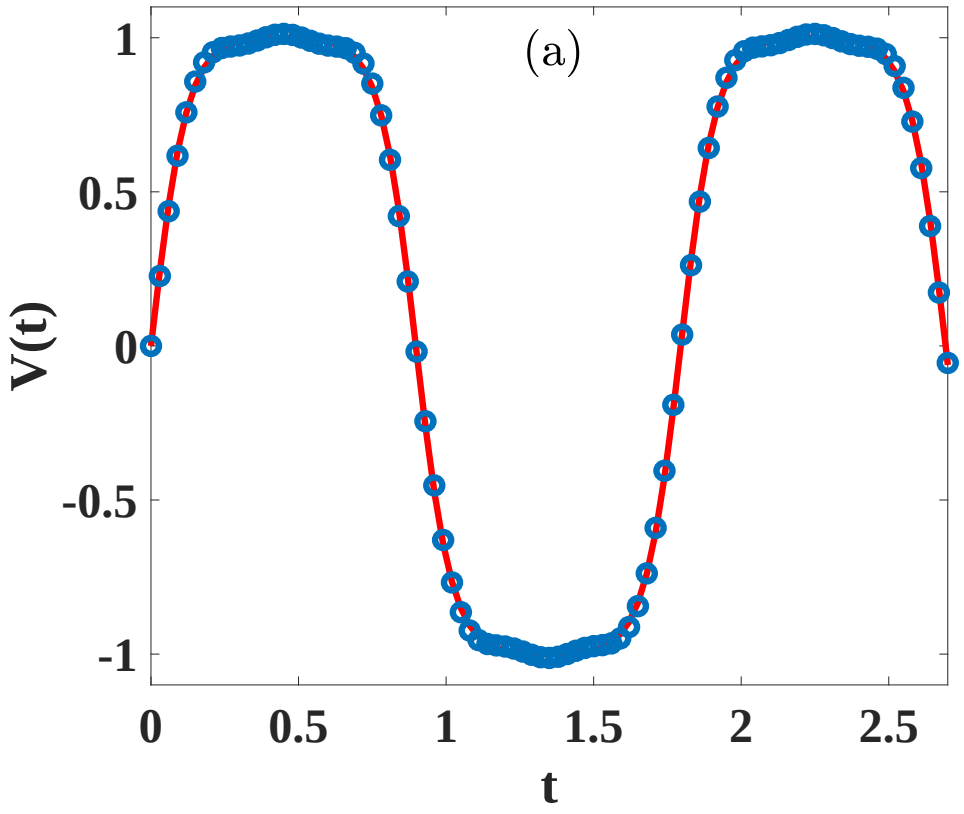

Figure 2.5: Signal $V_0^{(1)}$ (red lines) and its Fourier expansion $\tilde{V}_0^{(1)}$ limited to the first three terms (blue circles); $\omega = 3.5$, $r = 0.99$.

By using the Fourier expansion of the Jacobi elliptic function sn, $V_0^{(1)}(t)$ can be written as a sum of sinusoidal signals [96, 121], which, when keeping only the first three terms of this expansion, takes the form:

$$\tilde{V}_0^{(1)}(t) = A_0 \left(G_{1,1}\sin(\omega t) + G_{3,1}\sin(3\omega t) + G_{5,1}\sin(5\omega t)\right), \tag{2.52}$$

where

$$G_{i,1} = \frac{2\pi}{\sqrt{r}K}\frac{q^{i+\frac{1}{2}}}{(1-q^{2i+1})},$$

$i = 1, 3, 5$, $q = \exp(-\pi K'/K)$, K and K' are complete elliptic functions of first kind of argument r and $\sqrt{1-r^2}$ respectively, as see in Fig. 2.5. The accurateness of this approximation can be checked by comparing the original signal $V_0^{(1)}$ to its approximate form $\tilde{V}_0^{(1)}(t)$.

2.4.1.2 Modified Remoissenet-Peyrard signal

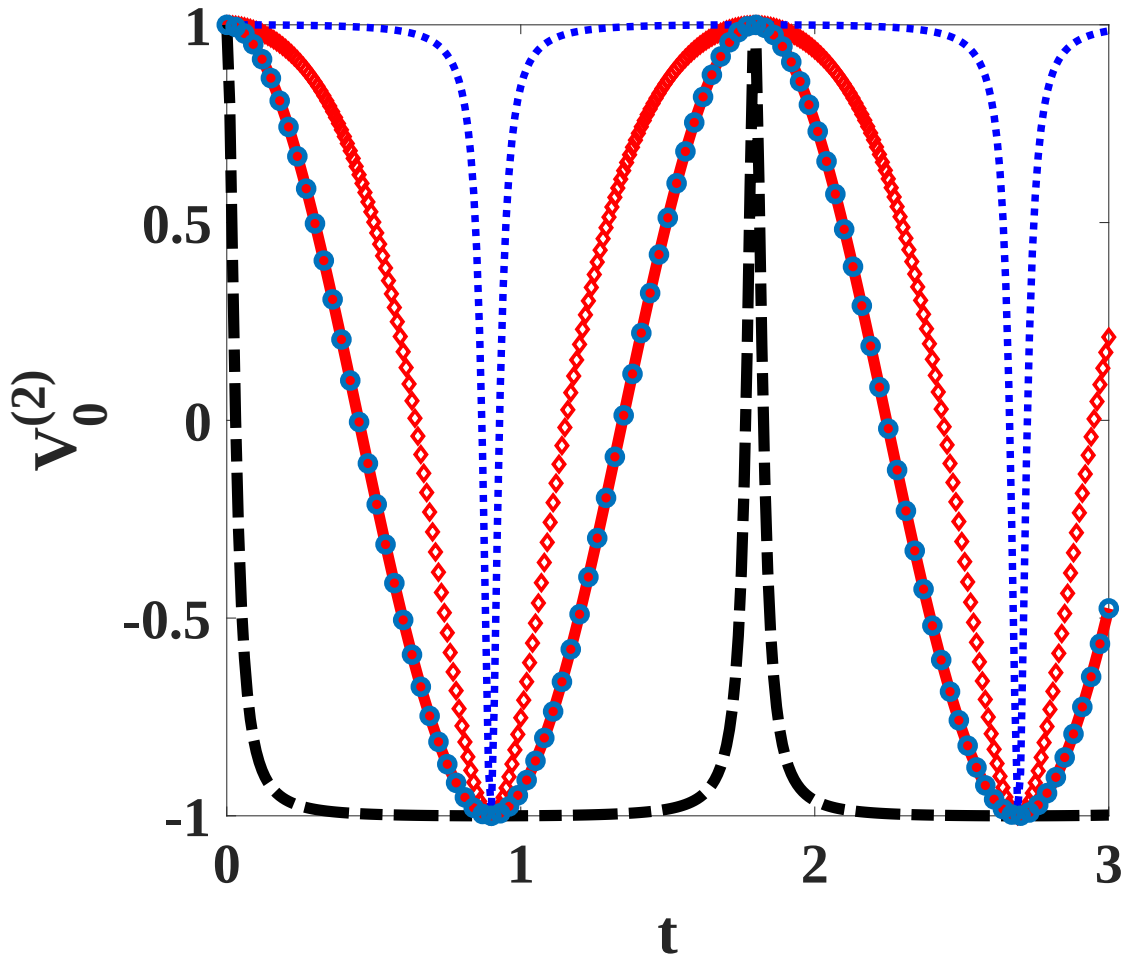

Figure 2.6: Variable shape signal V_2 for several values of the parameter r. Black dot-dashed line (r=-0.9), red solid line (r=0), red diamond (r=0.35), blue dotted line (r=0.9). Blue circles stand for the sinusoidal signal $A_0 cos\,(\omega t)$. $A_0 = 1$, $\omega = 3.5$.

We modified the Remoissenet-Peyrard potential to be centered at 0 and we have considered a periodic signal on the form of this modified potential given by:

$$V_0^{(2)}(t) = A_0 \frac{2r + \left(1 + r^2\right) cos\left(\omega t\right)}{1 + r^2 + 2r cos\left(\omega t\right)}, \tag{2.53}$$

where r is the shape parameter and ω is the driving frequency. We can easily check that $V_0^{(2)}(t)$ is reduced to the sinusoidal form $V(t) = A_0 cos(\omega t)$ when $r = 0$. The plotting of Eq. (2.53) for several values of r is shown in Fig. (2.6).

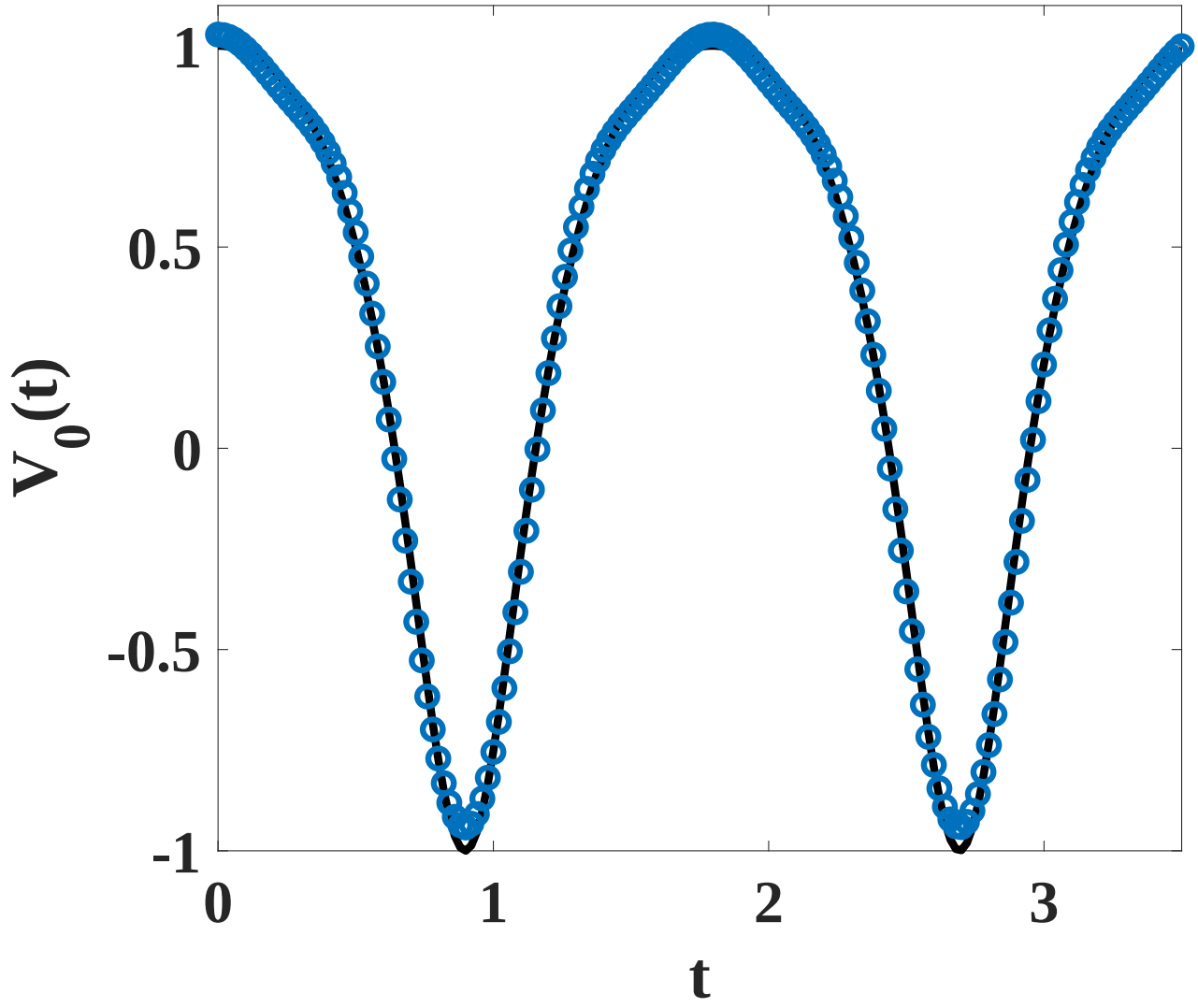

Figure 2.7: Remoissenet-Peyrard signal $V_0^{(2)}$ (black line) and its Fourier expansion $\tilde{V}_0^{(2)}$ limited to the first three terms (blue circles). $\omega = 3.5$, $r = 0.35$.

Following the procedure described by Ndjomatchoua et al [95], we can apply the Fourier expansion and approximate $V_0^{(2)}(t)$ as:

$$\tilde{V}_0^{(2)}(t) = A_0\left(G_{0,2} + G_{1,2}\sin(\omega t) + G_{2,2}\sin(2\omega t) + G_{3,2}\sin(3\omega t)\right), \tag{2.54}$$

where $G_{0,2} = r$, $G_{1,2} = 1 - r^2$, $G_{2,2} = -(1-r^2)r$ and $G_{3,2} = (1-r^2)r^2$.

This approximation is more accurate for $-0.5 \leq r \leq 0.5$. Figure 2.7 shows the accurateness of the approximate form of $V_2(t)$.

2.4.2 Analytical study of supratransmission with variable shape signal

To evidence the supratransmission phenomenon with non sinusoidal signal and especially the possibility of signal shape-controlled transmission, we shall consider the β-FPU lattice [Fig. 1.3] which dynamical equation is given by Eq. (3.6). This model is chosen as illustrative case for our study for the sake of simplicity and comparison purpose with literature results [3].

According to the Fourier expansion $\tilde{V}_1(t)$ and $\tilde{V}_2(t)$; Since the coefficients ($G_{i,\ell}$, $i = 1, 3, 5$, $\ell = 1, 2, 3$) are of the same order, and since we want to evidence the contribution of higher harmonic terms to the fundamental frequency's signal, we seek the solutions of Eq. (3.6) on the form

$$V_{0,n}^{(1)}(t) = A_n(t)\sum_{\ell=0}^{2} G_{1,(2\ell+1)} exp(j((2\ell+1)\omega t - knD)) + cc, \tag{2.55}$$

and

$$V_{0,n}^{(2)}(t) = A_n(t)\sum_{\ell=1}^{3} G_{2,\ell} exp(j(\ell\omega t - knD)) + cc, \tag{2.56}$$

respectively.

For the seek of simplicity, the triplets
$(G_{1,1}, G_{2,1}, G_{3,1})$ and $(G_{1,2}, G_{2,2}, G_{3,2})$ shall be replaced by $(\varrho_1, \varrho_2, \varrho_3)$. After inserting these *Ansatz* in Eq. (3.6), and when considering the slowly varying envelop approximation (in space and time), we use the continuum approximation ($A_n(t) \to A(x,t)$) and the Taylor's expansion. We obtain at the limit $q = \pi$ of the first Brillouin's zone when collecting terms on the powers of $\exp(j\omega t)$ the well

known nonlinear Schrödinger equation

$$-j\partial_t A + \left(\frac{m\omega^2 - 4K_2}{2m\omega}\right) A - \frac{K_2}{2m\omega}\partial_x^2 A - Q|A|^2 A = 0, \tag{2.57}$$

$$Q = \frac{6K_4}{m\omega}\left(\varrho_1^2 + 2\varrho_2^2 + 2\varrho_3^2 + \frac{\varrho_2^2\varrho_3}{\varrho_1}\right),$$

$\partial_t \equiv \partial/\partial t$, $\partial_x^2 \equiv \partial^2/\partial x^2$, $j^2 = -1$. Similarly to [3, 66, 122], the supratransmission threshold (A_{th}) which is obtained through the maximum amplitude of the static breather solution of Eq. (2.57). Here, the NLS equation is obtained by considering the term of $exp(j\omega t)$, which are of order 1, for the derivation of the static breather solution, it is logic to limit our selves on the order 1 of the Fourier approximation; the static breather solutions, for the case of the driven signal $V_0^{(1)}$ and $V_0^{(2)}$ are given by

$$V^{(1)}(x,t) = (-1)^n G_{1,1}\sqrt{\frac{m\omega^2 - 4K_2}{m\omega Q}}\,\mathrm{sech}\left(\sqrt{\frac{m\omega^2 - 4K_2}{K_2}}\,(x - x_0)\right)\cos(\omega t), \tag{2.58}$$

$$\begin{aligned} V^{(2)}(x,t) =& G_{0,2}\sqrt{\frac{m\omega^2 - 4K_2}{m\omega Q}}\,\mathrm{sech}\left(\sqrt{\frac{m\omega^2 - 4K_2}{K_2}}\,(x - x_0)\right) + \\ & (-1)^n G_{1,2}\sqrt{\frac{m\omega^2 - 4K_2}{m\omega Q}}\,\mathrm{sech}\left(\sqrt{\frac{m\omega^2 - 4K_2}{K_2}}\,(x - x_0)\right)\cos(\omega t), \end{aligned} \tag{2.59}$$

respectively; $x = na$ and x_0 being a constant. The supratransmission threshold is then expressed by:

$$A_{th}(r,\omega) = \gamma\sqrt{\frac{m\omega^2 - 4K_2}{6K_4\left(\varrho_1^2 + 2\varrho_2^2 + 2\varrho_3^2 + \frac{\varrho_2^2\varrho_3}{\varrho_1}\right)}}, \tag{2.60}$$

where $\gamma = \chi_1$ and $\gamma = |\lambda_0| + \lambda_1$ for symmetric $\left[V_0^{(1)}(t)\right]$ and asymmetric $\left[V_0^{(2)}(t)\right]$

shape signals respectively. When $r = 0$, we recover the NST threshold

$$A_{th} = \sqrt{\frac{m\omega^2 - 4K_2}{6K_4}} \tag{2.61}$$

previously found by Khomeriki et *al.* [3] with harmonic function $u_0(t) = A\cos(\omega t)$.

2.5 Numerical procedures

For the numerical exploration of the supratransmission phenomenon, we shall consider:

- a β-FPU diatomic lattice of 100 particles where the masses of light and heavy particles are initially fixed at $m = 0.1$ and $M = 0.18$, respectively. With these values of m and M, the lower and the upper band gap are located in $]3.333, 4.472[$ and $]5.578, +\infty[$ respectively. The first particle is subjected to a periodic excitation $V_0(t) = A\cos(\omega t)$ which frequency ω lies within the upper or lower forbidden band gap frequency while the remaining particles of the chain being initially at rest. In all the work, we shall take the parameter $D = 1$.To avoid initial shocks formation, the external driver is modified as $V_0(t) = A\left[1 - \exp(-t/\tau)\right]\cos(\omega t)$, with $\tau = 5$. To avoid the reflections at the boundary of the lattice, the 10 last particles are submitted to a dissipation with a damping coefficient value $\gamma = 5$. The system is numerically integrated by using the fifth-order Runge-Kutta formula with a fixed time step $\Delta t = 10^{-3}$. The supratransmission is assumed to occur (stopping criterion of the algorithm) as soon as $\max[u_{50}(t)]$ is above the driving amplitude A. The brute-force method combined with the bisection search is applied to determine the supratransmission threshold numerically [71]. In order to detect the onset of the supratransmission, the spatial evolution $u_n(t)$ and the behavior of particles $n = 50$ and $n = 51$ are monitored.

- For the study of the signal shape's effect on the supratransmission phenomenon, a β-FPU monoatomic lattice of 100 particles is considered. The first particle

is submitted to the variable shape signal

$$V_0(t) = \begin{cases} V_0^{(1)}(t), \\ V_0^{(2)}(t), \end{cases} \tag{2.62}$$

The onset of supratransmission is detected by evaluating the energy flux density between two consecutive particles [3, 93]:

$$J_{n,n+1} = (\dot{u}_n - \dot{u}_{n-1})\left[(u_n - u_{n-1}) + (u_n - u_{n-1})^3\right]. \tag{2.63}$$

To avoid initial shocks, the signal shall be introduced smoothly ($V_0(t) \to V_0[1 - \exp(-t/\tau)]$, with $\tau = 10$) in the system, with the chain initially at rest ($u_n(0) = \dot{u}_n(0) = 0$) [3, 116]. Reflexive waves coming from the boundary of the lattice are avoided by adding a dissipation with a damping coefficient value $\gamma = 5$ to the last ten cells.

2.5.1 Runge-Kutta algorithms

The Runge-Kutta algorithm is a numerical method used to solve ordinary differential equation of first order.

Let consider the following equation

$$\frac{d^2u_n}{dt^2} = \frac{K_2}{m}(u_{n-1} - 2u_n + u_{n+1}) + \frac{K_4}{m}\left[(u_n - u_{n-1}) + (u_n - u_{n+1})\right] \tag{2.64}$$

we can rewrite this equation as

$$\frac{dv_n}{dt} = g(u_n, v_n), \tag{2.65}$$

$$\frac{du_n}{dt} = f(u_n, v_n), \tag{2.66}$$

and on the vectorial form

$$\frac{d\vec{X}_n}{dt} = \vec{F}(\vec{X}_n), \tag{2.67}$$

where $\overrightarrow{X_n} = \begin{bmatrix} v_n \\ u_n \end{bmatrix}$ and $\overrightarrow{F}\begin{bmatrix} g(u_n, v_n) \\ f(u_n, v_n) \end{bmatrix}$; f and g being two functions defined by the parameters of the system.

- to integrate this equation by the fourth order Runge-Kutta algorithm between two instants t_0 and t_1, we proceed as follow:

  Let t_0 the initial instant, and h the integration step, the state of the system at the instant $t_0 + h$ is given by [123–126]:

$$(\overrightarrow{X_n})_{t_0+h} = (\overrightarrow{X_n})_{t_0} + \frac{1}{6}\left(\overrightarrow{L_1} + 2\overrightarrow{L_2} + 2\overrightarrow{L_3} + \overrightarrow{L_4}\right) \tag{2.68}$$

  where

$$\overrightarrow{L_1} = h\overrightarrow{F}\left(t_0, (\overrightarrow{X_n})_{t_0}\right) \tag{2.69}$$

$$\overrightarrow{L_2} = h\overrightarrow{F}\left(t_0 + \frac{h}{2}, (\overrightarrow{X_n})_{t_0} + \frac{\overrightarrow{L_1}}{2}\right) \tag{2.70}$$

$$\overrightarrow{L_3} = h\overrightarrow{F}\left(t_0 + \frac{h}{2}, (\overrightarrow{X_n})_{t_0} + \frac{\overrightarrow{L_2}}{2}\right) \tag{2.71}$$

$$\overrightarrow{L_4} = h\overrightarrow{F}\left(t_0 + h, (\overrightarrow{X_n})_{t_0} + \overrightarrow{L_3}\right) \tag{2.72}$$

- Using the $5th$ order Runge-Kutta algorithm, the state of the system at the instant $t_0 + h$ is given by:

$$(\overrightarrow{X_n})_{t_0+h} = (\overrightarrow{X_n})_{t_0} + c_1\overrightarrow{\psi_1} + c_2\overrightarrow{\psi_2} + c_3\overrightarrow{\psi_3} + c_4\overrightarrow{\psi_4} + c_5\overrightarrow{\psi_5} + c_6\overrightarrow{\psi_6} + c_7\overrightarrow{\psi_7}, \tag{2.73}$$

  where

$$\begin{aligned}
\psi_1 &= h\overrightarrow{F}(t_0 + c_1 h, (\overrightarrow{X_n})_{t_0}) \\
\psi_2 &= h\overrightarrow{F}(t_0 + c_2 h, (\overrightarrow{X_n})_{t_0} + a_{2,1}\psi_1), \\
\psi_3 &= h\overrightarrow{F}(t_0 + c_3 h, (\overrightarrow{X_n})_{t_0} + a_{3,1}\psi_1 + a_{3,2}\psi_2), \\
\psi_4 &= h\overrightarrow{F}(t_0 + c_4 h, (\overrightarrow{X_n})_{t_0} + a_{4,1}\psi_1 + a_{4,2}\psi_2 + a_{4,3}\psi_3), \\
\psi_5 &= h\overrightarrow{F}(t_0 + c_5 h, (\overrightarrow{X_n})_{t_0} + a_{5,1}\psi_1 + a_{5,2}\psi_2 + a_{5,3}\psi_3 + a_{5,4}\psi_4), \\
\psi_6 &= h\overrightarrow{F}(t_0 + c_6 h, (\overrightarrow{X_n})_{t_0} + a_{6,1}\psi_1 + a_{6,2}\psi_2 + a_{6,3}\psi_3 + a_{6,4}\psi_4 + a_{6,5}\psi_5), \\
\psi_7 &= h\overrightarrow{F}(t_0 + c_7 h, (\overrightarrow{X_n})_{t_0} + a_{7,1}\psi_1 + a_{7,2}\psi_2 + a_{7,3}\psi_3 + a_{7,4}\psi_4 + a_{7,5}\psi_5 + a_{7,6}\psi_5),
\end{aligned}$$

  and the parameters

c_1	a_{11}	a_{12}	a_{13}	a_{14}	a_{15}	a_{16}	a_{17}
c_2	a_{21}	a_{22}	a_{23}	a_{24}	a_{25}	a_{26}	a_{27}
c_3	a_{31}	a_{32}	a_{33}	a_{34}	a_{35}	a_{36}	a_{37}
c_4	a_{41}	a_{42}	a_{43}	a_{44}	a_{45}	a_{46}	a_{47}
c_5	a_{51}	a_{52}	a_{53}	a_{54}	a_{55}	a_{56}	a_{57}
c_6	a_{61}	a_{62}	a_{63}	a_{64}	a_{65}	a_{66}	a_{67}
c_7	a_{71}	a_{72}	a_{73}	a_{74}	a_{75}	a_{76}	a_{77}
	b_1	b_2	b_3	b_4	b_5	b_6	b_7

are found through the Butcher table [127, 128] and are given by:

0	0	0	0	0	0	0	0
1/5	1/5	0	0	0	0	0	0
3/10	3/40	9/40	0	0	0	0	0
4/5	44/55	−56/15	32/9	0	0	0	0
8/9	19372/6561	−25360/2187	64448/6561	−212/729	0	0	0
1	9017/3168	−355/33	46732/5247	49/176	−5103/18656	0	0
1	35/384	0	500/1113	125/192	−2187/6784	11/84	0
	5179/57600	0	7571/16695	393/640	−92097/339200	187/2100	1/40

Table 2.1: Butcher table for fifth order Runge-Kutta coefficients

2.5.2 Brute force method and dichotomic research

The Brute force method used to estimate numerically the supratransmission threshold consists to find the interval, as narrow as possible, of driving amplitude leading to the wave propagation although the external driving frequency lies in the forbidden band. To identify this interval, we shall process as follow [129]:

- We consider a driving signal $A_0 cos(\omega t)$, taking A_0 so small that the energy transmission cannot occurs,
- the driving amplitude is modified as $A_0 \to A_0 + a$, where $0 \leq a \ll A_0$, and the system is submitted to the new signal,
- the operation is repeated until the wave propagation occurs, and then, the interval leading to wave propagation is identified as $[A_0, A_0 + a]$.

Once this interval is found, it is subsequently refined through a dichotomic search algorithm and stopped when the precision of 10^{-6} is reached. The supratransmission is assumed to occur (stopping criterion of the algorithm) as soon as $\max[u_{50}(t)]$ is above the driving amplitude A.

Let $[A_{left}, A_{right}]$ the interval amplitude leading to wave propagation; to refine this interval through dichotomic research, we consider the function f defined as

$$f(A) = \begin{cases} 1 & if \max[u_{50}(t)] \geq A, \\ 0 & if \max[u_{50}(t)] \leq A, \end{cases} \tag{2.74}$$

where A is the driving amplitude. Let $A_{mid} = (A_{left} + A_{right})/2$, we have the following situations:

- if $f(A_{left}) = f(A_{mid})$, then $A_{mid} \leq A_{th} \leq A_{right}$, and thus A_{left} takes the new value A_{mid};
- if $f(A_{right}) = f(A_{mid})$, then $A_{left} \leq A_{th} \leq A_{mid}$, and A_{right} takes the new value A_{mid}.

the process is repeated until the wished precision ($|A_{left} - A_{right}| \leq 10^{-}6$) is reached; and the supratransmission threshold is given by

$$A_{th} = \frac{A_{left} + A_{right}}{2} \tag{2.75}$$

2.5.3 Fast-Fourier transform (FFT) algorithm

It is a numerical method based on the discrete Fourier transform. Let a function $V_n(t)$, the Fast Fourier Transform $\tilde{v}$ of the function $V_n(t)$ is given by [130–134]

$$\tilde{v}(\omega) = fft(V_n(t)) = \sum_{n=1}^{N} V_n e^{i\omega n}, \tag{2.76}$$

which is usually complex; for its representation, it is common to evaluate its modulus, the spectral power density (SPD) given by:

$$v(\omega) = |\tilde{v}(\omega)| \tag{2.77}$$

where v is a function of the angular frequency ω

2.6 Conclusion

The study of the supratransmission phenomenon in a β-FPU diatomic lattice requests several analytical procedures. The presence of two forbidden band gap frequencies and also the presence of two different masses per unit cell make the calculations very cumbersome and impose to review a number of known technics of derivation of supratransmission threshold. Otherwise, the dependence of the supratransmission threshold on the shape parameter r for the case of the β-FPU monoatomic lattice driven by a variable shape signal has also been evidenced, giving the possibility to reduce or to enhance the supratransmission threshold by varying the shape of the signal.

Chapter III

RESULTS AND DISCUSSION

Introduction

In the previous chapter, we have derived analytically several supratransmission thresholds corresponding to diverse situations met in the forbidden bands of an FPU diatomic lattice, and also by varying the shape of a driving signal in an FPU monoatomic lattice. In the present chapter, the supratansmission phenomenon shall be investigated numerically via the observation of the propagation of the signals along the lattices, the behavior of certain particles, and also via the estimation of the energy density of two consecutive particles. Moreover, the validity and the accurateness of the derived analytical thresholds shall be checked, precisely by comparing them to their numerical analogs.

3.1 Diatomic FPU model driven by a sinusoidal signal

3.1.1 Supratransmission in upper forbidden band

We consider the periodic excitation $V_0(t) = A\cos(\omega t)$ with driving frequency $\omega = 6.0$ and for two different values of driving amplitude ($A = 0.227$ and $A = 0.228$).

A sudden propagation of the wave in the system for the case $A = 0.228$ can be observed (Fig. 3.1). Thus, $A = 0.228$ corresponds to the threshold amplitude of the supratransmission phenomenon occurrence. This observation is confirmed by the behavior of particles V_{25} and W_{25} for the two values of driving amplitude displayed on Fig (3.2). We can observe a significant amplification of the driving amplitude when pass from $A = 0.227 < A_{th}$ to $A = 0.228 = A_{th}$. It can be noticed that a slight increase of 0.1% is enough to trigger the propagation of the incident wave

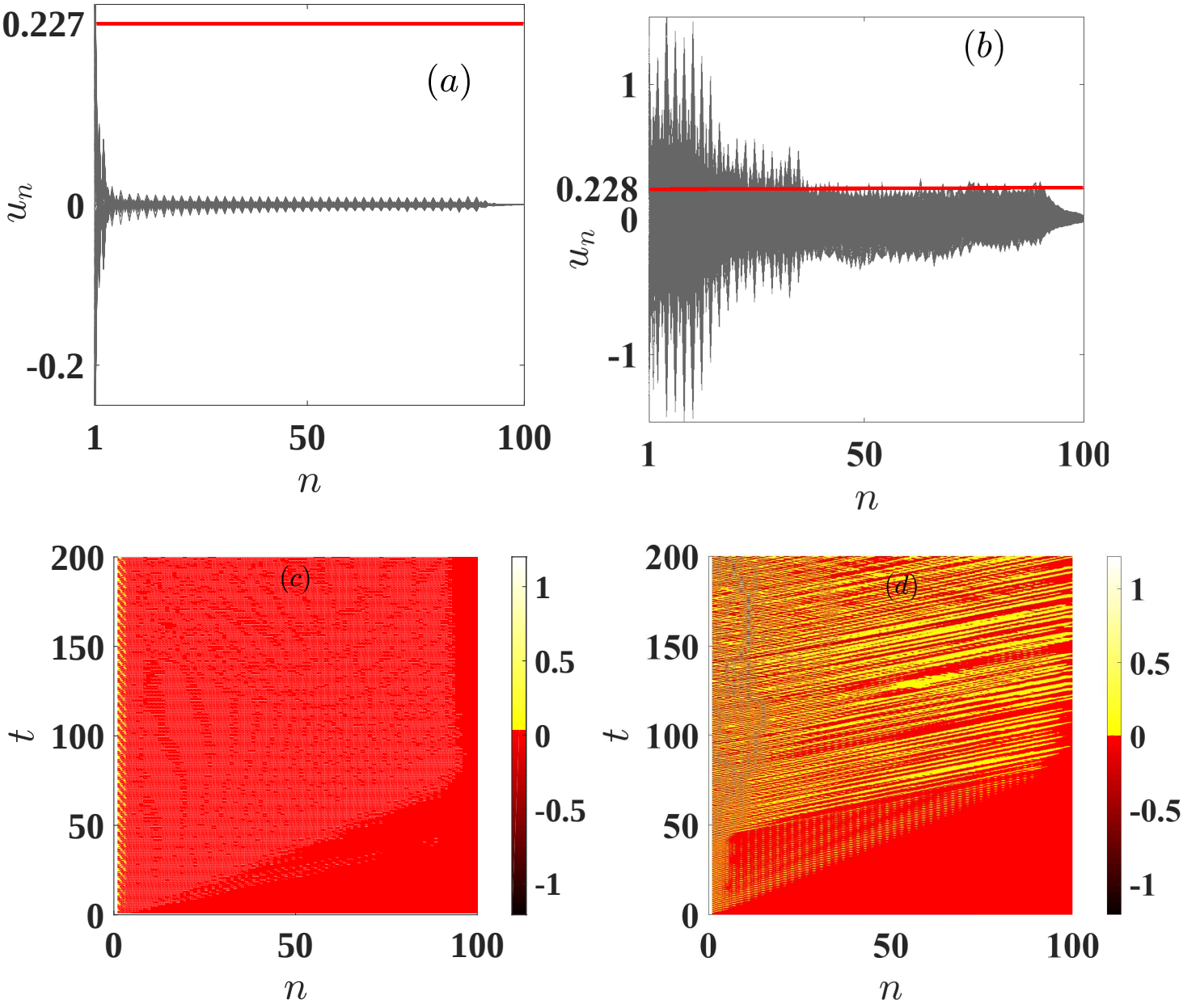

Figure 3.1: Spatial [(a),(b)] and spatio-temporal [(c),(d)] evolution of plane wave within the chain for driving amplitude $A = 0.227$ [(a),(c)] and $A = 0.228$ [(b),(d)]; $\omega = 6.0$, $m = 0.1$, $M = 0.18$, red line stand for the driving amplitude value.

along the lattice although ω is in the forbidden band gap.

The numerical and analytical thresholds as a function of driving frequency for three values of the parameter couples (m, M) $[(0.1, 0.18), (0.3, 0.5), (1, 1.5)]$ which correspond to mass ratio of 55%, 60% and 66% respectively are monitored.

Figure 3.3 shows a good agreement between analytical supratransmission threshold and its numerical analog. The increase of mass ratio m/M induces a net increase

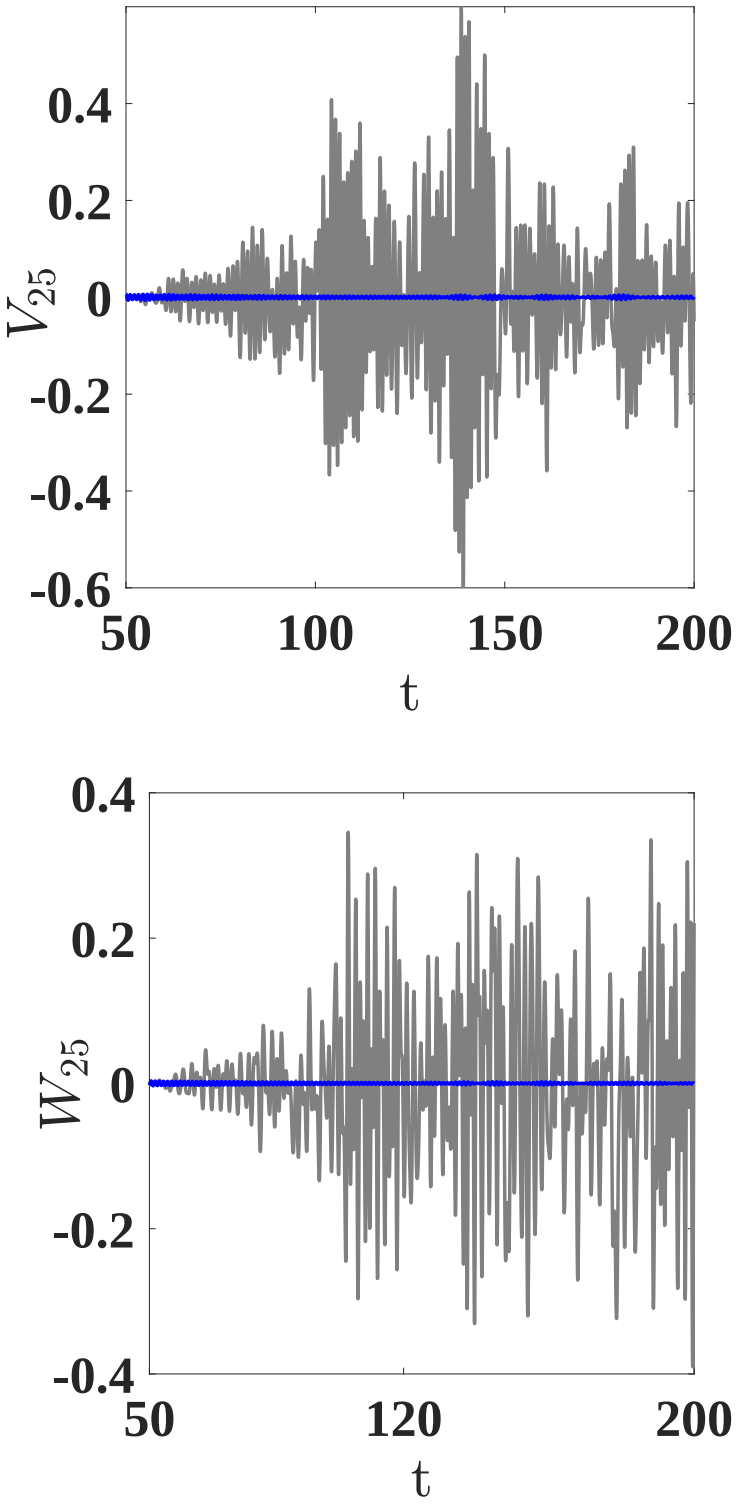

Figure 3.2: Behavior of the particles V_{25} and W_{25} for the insulating regime $A = 0.227$ (blue curves) and propagating regime $A = 0.228$ (gray curves), $\omega = 6.0$, $K_2 = 1$, $K_4 = 1$, $m = 0.1$, $M = 0.18$.

of the threshold, while the threshold always increases with the values of forbidden band gap frequencies.

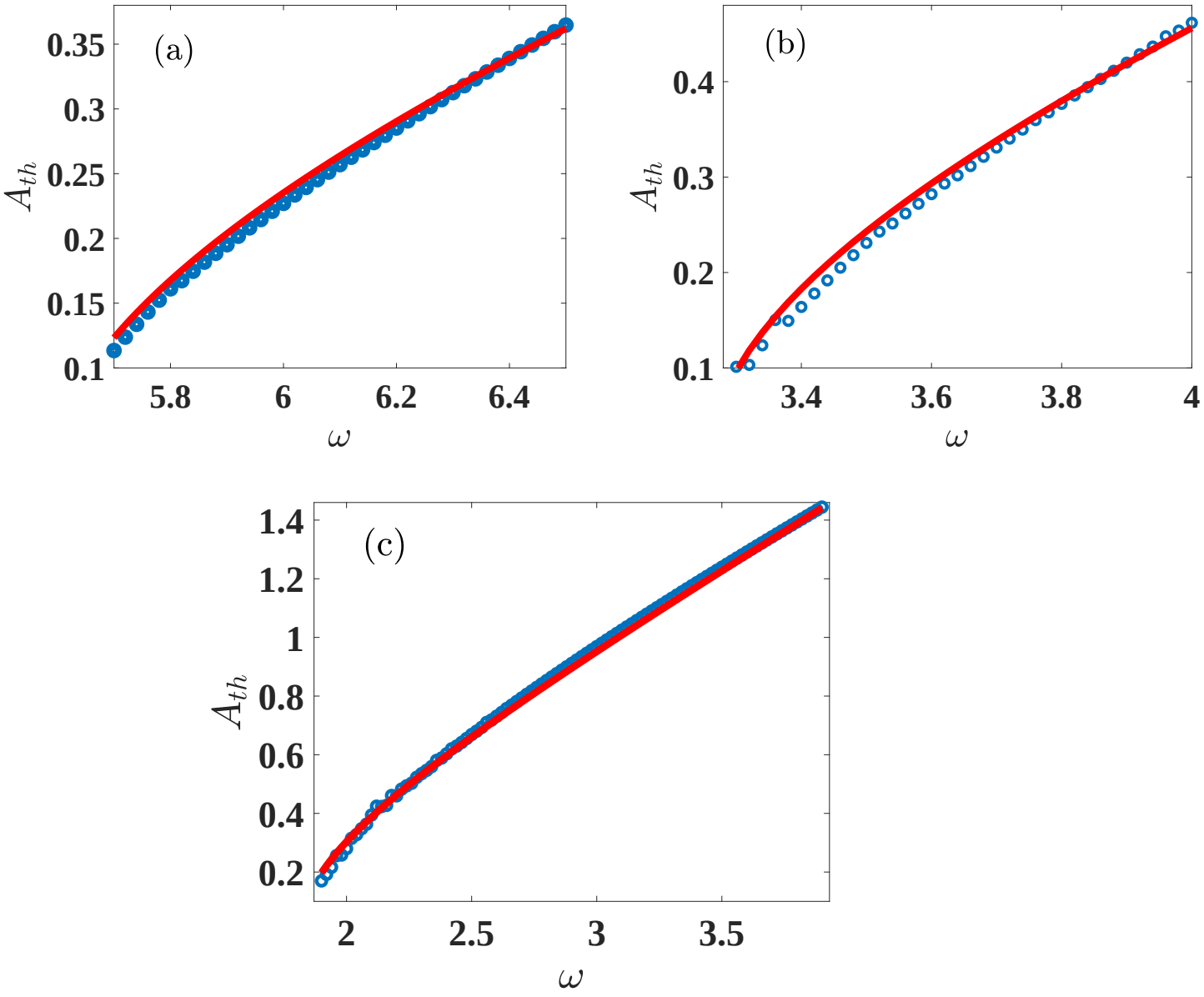

Figure 3.3: Threshold amplitude versus the driving frequency. Numerical (blue circles) and analytical (red solid lines) for (m,M) taking the values (0.1,0.18) (a); (0.3,0.5) (b) and (1,1.5) (c); $K_2 = 1$, $K_4 = 1$, $D = 1$.

3.1.2 Lower forbidden band gap frequencies

Submitting the lattice to the same periodic excitation as in upper forbidden band, with a driving frequency $\omega = 3.5$, the supratransmission phenomenon is noticed as a sudden transmission when slightly varying the driving amplitude from $A = 0.502$ to $A = 0.503$.

The behavior of particles V_{25} and W_{25} shown in Fig. 3.5 confirms the value of

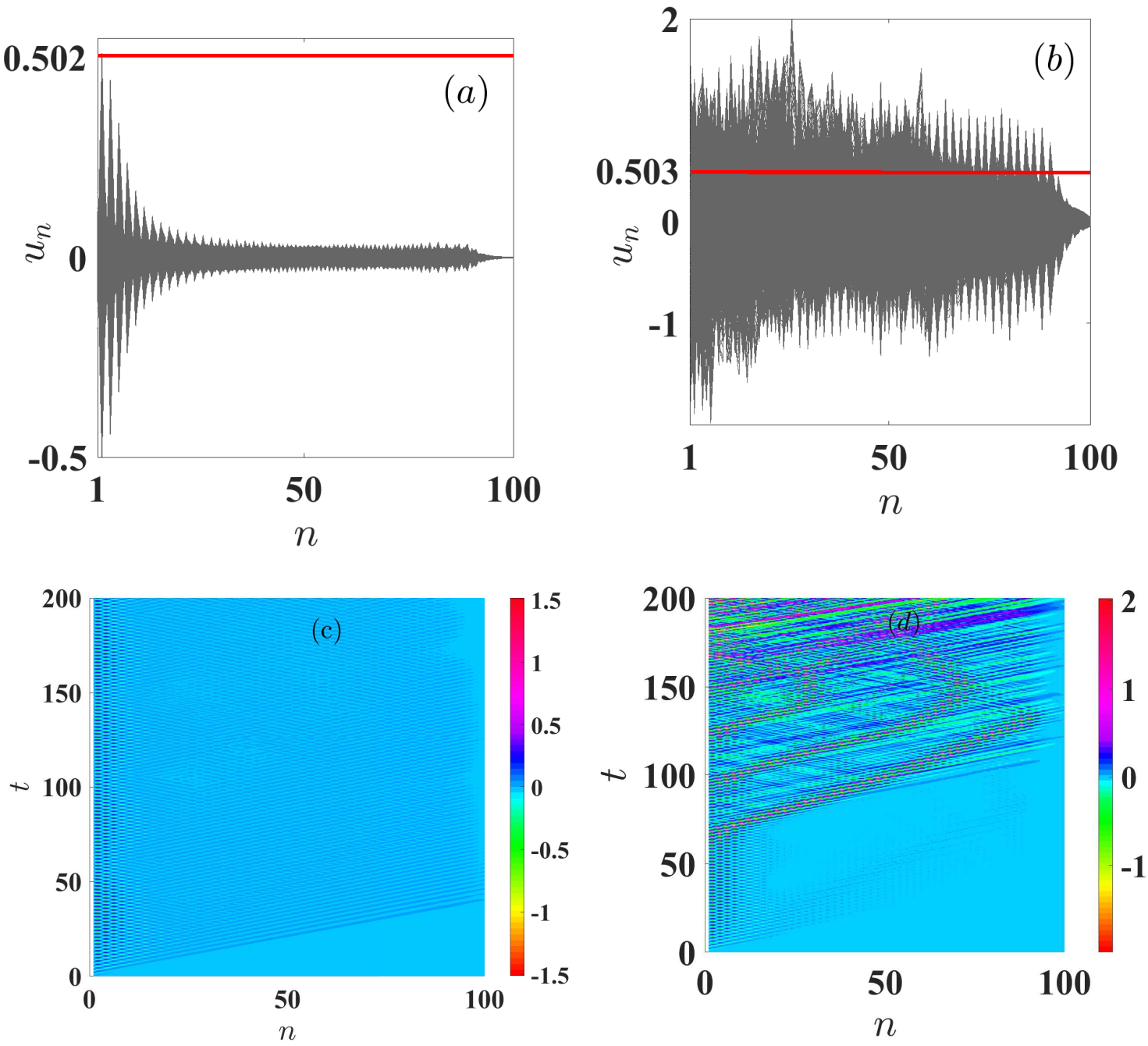

Figure 3.4: Spatial [(a),(b)] and spatio-temporal [(c),(d)] evolution of plane wave within the chain for driving amplitude $A = 0.502$) [(a),(c)] and $A = 0.503$ [(b),(d)]; $\omega = 3.5$, $m = 0.1$, $M = 0.18$, red line stand for the driving amplitude value.

the supratranmission threshold. To investigate the effects of the band width on the supratransmission phenomenon, we shall consider three couples of parameters (m, M): (0.1, 0.18), (0.3, 0.5) and (1, 1.5), which correspond to the mass ratio 55%, 60% and 66% respectively; the higher the mass ratio, the lower the band width.

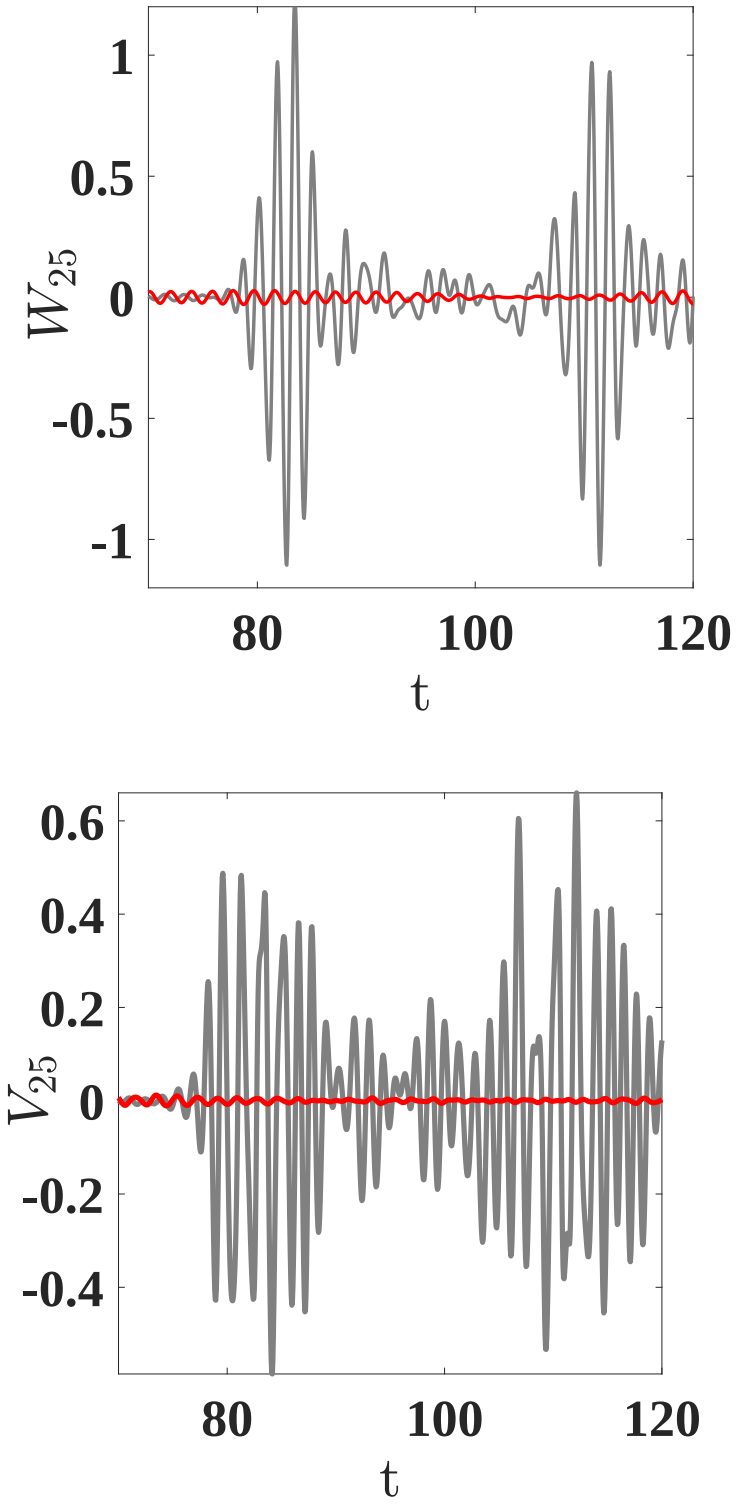

Figure 3.5: Behavior of the particles V_{25} and W_{25} for the insulating regime $A = 0.502$ (red curves) and propagating regime $A = 0.503$ (gray curves); $\omega = 3.5$, $K_2 = 1$, $K_4 = 1$, $m = 0.1$, $M = 0.18$.

3.1.2.1 Wide band gap

The numerical threshold amplitude as a function of driving frequency is plotted along with its analytical analog Eq. (2.20) for the three couple of parameters (m, M) [Fig. 3.6]. The increase of the mass ratio m/M induces a net decrease of the

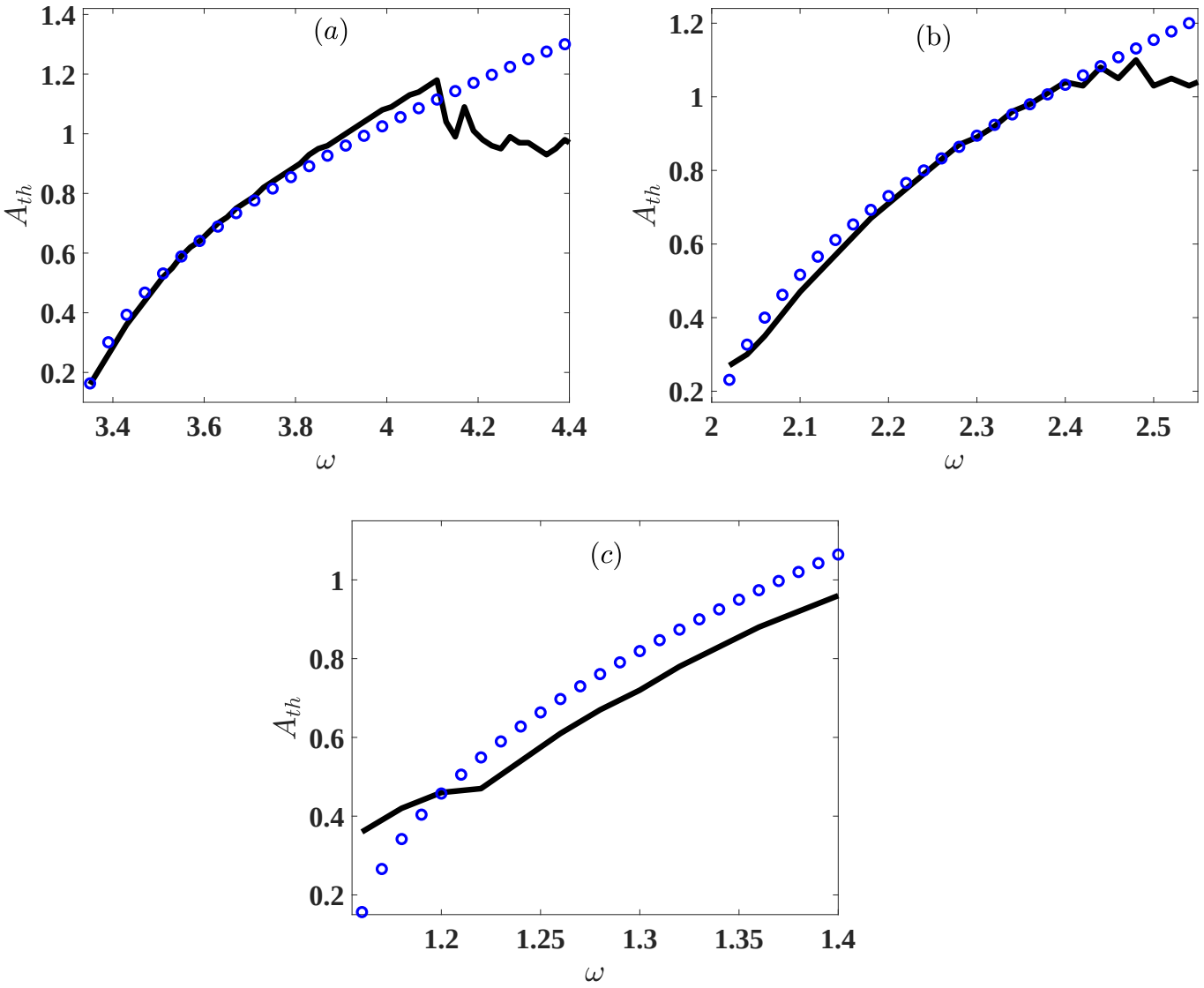

Figure 3.6: Threshold amplitude versus driving frequency. Numerical results (gray solid line) and analytical threshold (blue circles) for (m,M) taking the values (0.1,0.18) (a), (0.3,0.5) (b) and (1,1.5) (c); $K_2 = 1$, $K_4 = 1$, $D = 1$.

threshold, while the threshold always increases with the values of forbidden band gap frequencies. In Fig. 3.6, a good agreement is observed between the numerical and the analytical threshold Eq. (2.20) as the frequencies increase in the lower

forbidden band. From Fig. 3.6, we can also deduct that the analytical thresholds are more accurate for lower values of the mass ratio m/M. A growing disagreement can be noticed when the mass ratio increases beyond 60%, corresponding to narrow band gaps for which this threshold is no more valid.

3.1.2.2 Narrow forbidden band: effect of the coupled modes on the supratransmission threshold

The study of threshold with respect to driving frequency in lower forbidden band revealed a disagreement between numerical and analytical results as the mass threshold ratio m/M increases. We can also notice that when this ratio increases, the width of lower forbidden band decreases. A narrow band gap frequencies, which suppose a great proximity between the upper and the lower cutoff frequency of the acoustic and optical mode respectively results in a coupling between these two modes [75].

The plotting of Eq. (2.34) and Eq. (2.40) with respect to the driving frequency is displayed in Fig. 3.7, where we can see a good agreement with the numerical results of Eq. (2.34) for small mass ratio (acoustic mode behavior), and Eq. (2.40) for large mass ratio m/M (coupled mode behavior).

3.1.3 Effects of the mass of the driven particle on the supratransmission threshold

In this section, the order of the particles array previously considered [Fig. 2.1a] is switched into the diatomic lattice version so that the driven particle (the first unit) has now the mass m [Fig. 2.1b]. The lattice is driven at that end by the same wave given in section (3.1.1). We plotted for the three couples (m,M) the supratransmission threshold as a function of driving frequency for the upper (lower) forbidden band together with their analytical analogs Eq. (2.43) (Eq. (2.47).

We can notice from Fig. 3.8 that the supratransmission threshold drastically changes when passing from a line with heavy driven particle to a line with light driven particle in both the two forbidden bands.

In lower forbidden band, a light driven particle results in a decrease of the threshold in comparison with the case of heavy driven particle; whereas in upper forbidden band we observe the opposite situation. Figure 3.8 also displays a good agreement,

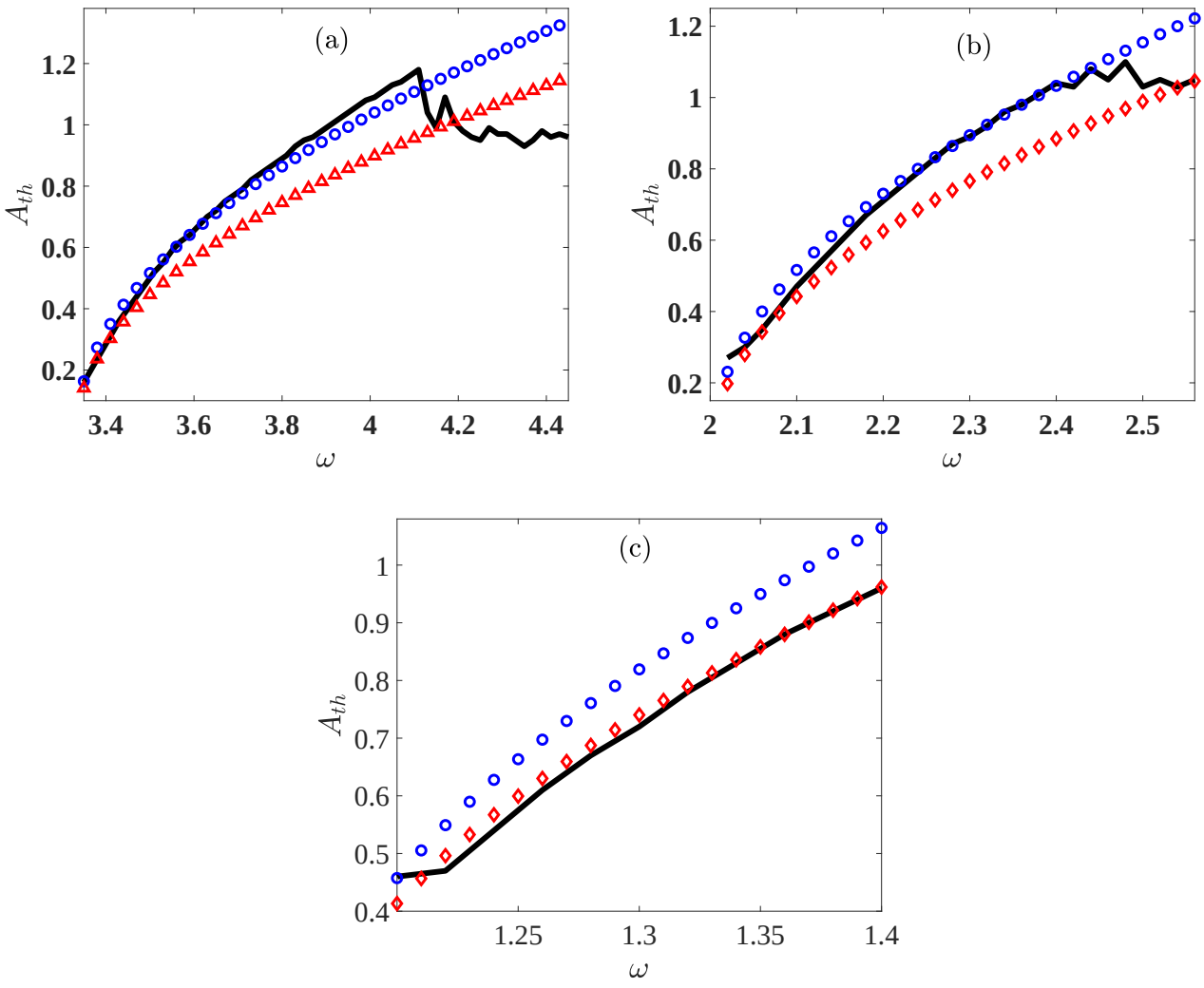

Figure 3.7: Threshold amplitude versus the driving frequency. Numerical (black solid lines) and analytical thresholds $A_{th_{low3}}$ (blue circles) and $A_{th_{low4}}$ (red diamonds) for (m,M) taking the values (0.1,0.18) (a); (0.3,0.5) (b) and (1,1.5) (c); $K_2 = 1$, $K_4 = 1$.

in both the two forbidden bands, between analytical thresholds for lattice with light driven particle and their numerical analogs.

Our tentative to find an analytical threshold for the light driven particle in the lower forbidden band with coupling effects provides results significantly different to the numerical simulations and have not be presented in this work.

The different analytical procedures used to derive the supratransmission threshold in the two forbidden bands and their accurateness are summarized in table 3.1.

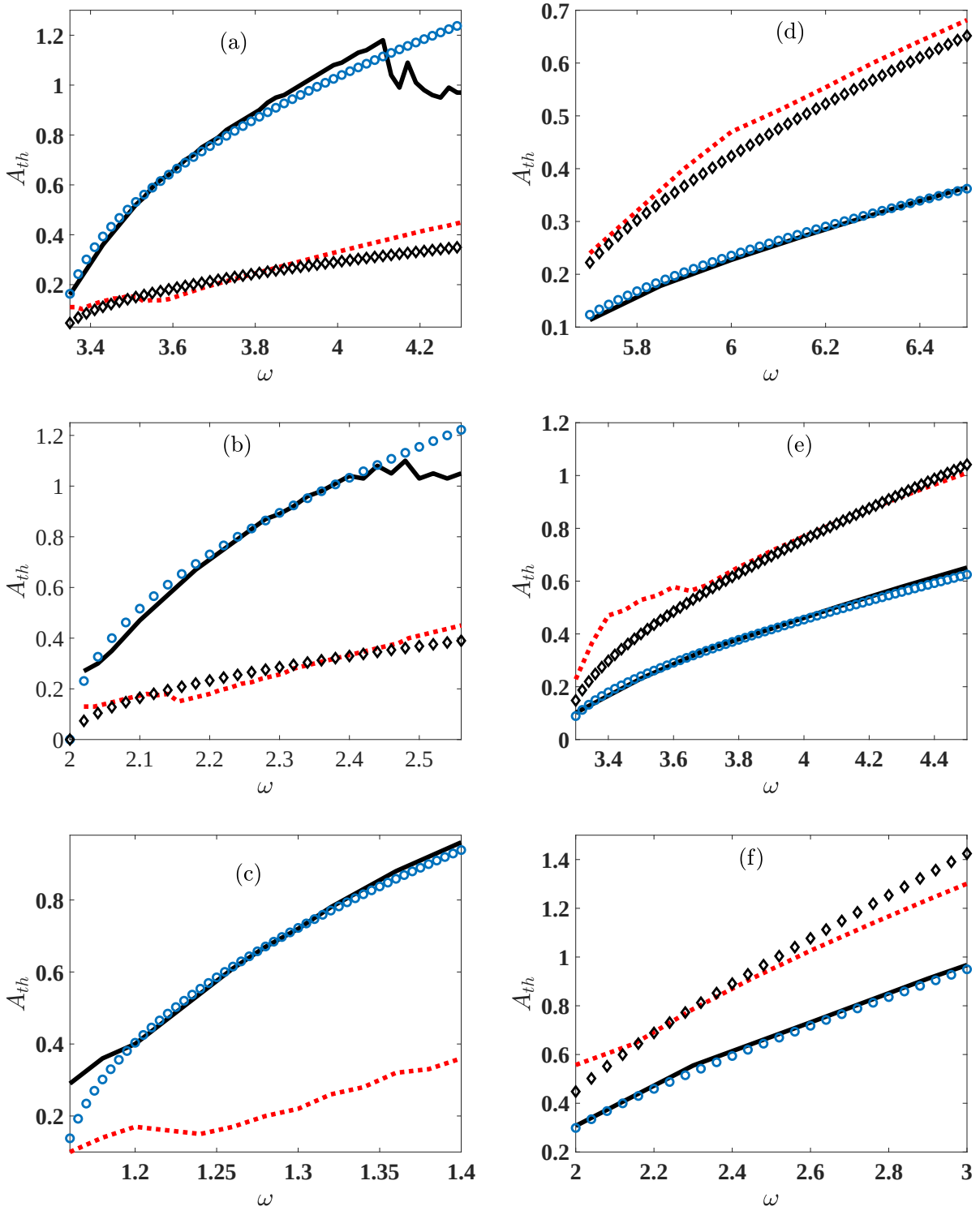

Figure 3.8: Threshold amplitude versus the driving frequency for three couples (m,M): (0.1,0.18) (a) and (d); (0.3,0.5) (b) and (e); (1,1.5) (c) and (f). (a),(b),(c) for lower forbidden band; (d),(e),(f) for upper forbidden band. Black solid lines (red dashed lines) represent the numerical cases of heavy driven particle (light driven particle); and blue circles (black diamonds) their analytical analogs. $K_2 = 1$, $K_4 = 1$, $\epsilon = 0.08$.

Analytical technics	Upper forbidden band for $\mu \leq 60\%$	Upper forbidden band for $\mu > 60\%$	forbidden band between acoustic and optical modes for $\mu \leq 60\%$	forbidden band between acoustic and optical modes for $\mu > 60\%$
Decoupling ansatz with $k \to 0$	✓	✓	N.A.	N.A.
Decoupling ansatz with k arbitrary	N.A.	N.A.	✓	✗
Coupled modes	N.A.	N.A.	✓	✓

Table 3.1: Comparison and accurateness of analytical procedures. The parameters μ and k are the mass-ratio (m/M) and wave vector, respectively. ✓: applicable technic with accurate results, ✗: applicable technic but does not track closely the numerical results, N.A.: not applicable.

3.1.4 Bridging diatomic and monoatomic cases

At the limit $m = M$, the dispersion diagram of the diatomic lattice displays only one forbidden band which boundary, as well as that of the mono-atomic lattice is known to be $\omega_{max} = \sqrt{4/m}$ [3]. The location of the forbidden band, which is the same in the two cases, corresponds to the upper forbidden band of the diatomic lattice so that the valid threshold in the limit $m = M$ of the diatomic lattice shall be obtained by replacing M by m in Eq. (2.13). We can thus write this threshold on the form

$$A_{th_{up}} = \sqrt{\frac{m\omega\left(\omega - \omega_{max}\right)}{3K_4}}. \tag{3.1}$$

$$A_{th_{mono1}} = \sqrt{\frac{m\omega^2 - 4K_2}{6K4}}, \tag{3.2}$$

$$A_{th_{mono2}} = \sqrt{\frac{16(m\omega^2 - 3K_2)}{81K_4}}, \tag{3.3}$$

The comparison between the analytical threshold Eq. (3.1) and those obtained for the mono-atomic case for the small and large amplitudes [Eq.(3.2) and Eq. (3.3)] [3, 71] respectively, is displayed in Fig. 3.9 (a). The thresholds estimated numerically are plotted as well. The simulations are performed for $m = M = 0.18$ and reveal for numerical estimations [Fig 3.9(b)], a good agreement between the

mono-atomic case and the limit $m = M$ of the diatomic case.

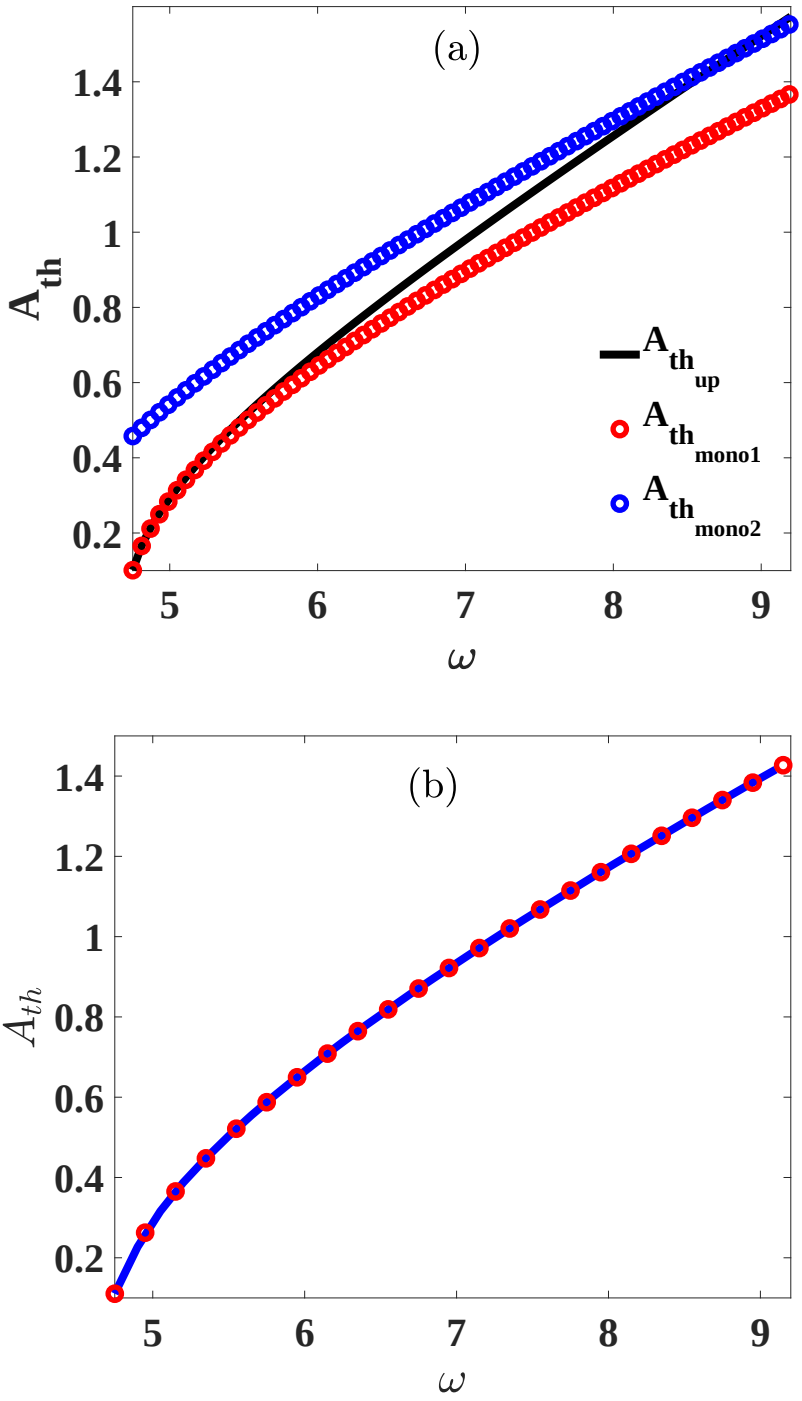

Figure 3.9: Threshold amplitude versus driving frequency, for mono-atomic case and for the limit $m = M$ of diatomic case. (a) for analytical thresholds and (b) for numerical simulations, $K_2 = 1$, $K_4 = 1$.

For frequencies close to ω_{max} (far from ω_{max}), a good agreement is observed between the limit $m = M$ [Eq. (3.1)] and the small amplitude [Eq. (3.2)] (and the

large amplitude [Eq. (3.3)]) thresholds of the monoatomic lattice.

3.2 Wave transmission for a very narrow lower ($m/M > 66\%$) forbidden band of diatomic FPU lattice

3.2.1 Linear diatomic lattice

We study the imaginary part of the wave number k_i with respect to the couple (m, M). We shall take in the upper forbidden band, a frequency not so far from the cutoff frequency (we shall take $\omega = Max(\omega_+) + \frac{Max(\omega_+)}{10}$).

In the lower forbidden band, the frequency shall be taken at the middle of the band to have the maximum value of k_i ($\omega = \frac{Max(\omega_-)+Min(\omega_+)}{2}$).

From Fig (3.10) we also observe that the coefficient k_i is relatively weak in the lower forbidden band compared to the upper forbidden band. For the same couple $(0.9, 1.1)$, $k_i = 0.1003$ in the lower whereas $k_i = 0.8907$ in the upper.

As a consequence, the evanescence of a signal whose driving frequency is in the lower forbidden band cannot be complete for many couples (m, M) for which the coefficient k_i is very weak. To confirm this affirmation, we shall submit the first particle of the lattice to a periodic excitation given by

$$U(t) = A_0 cos(\omega t), \tag{3.4}$$

where the frequency ω is taken in turn in the upper and the lower forbidden bands. To avoid the initial shock, we shall take the periodic excitation as $A_0 cos(\omega t)(1 - exp(i(t/\tau)))$ with $\tau = 5$. We shall also apply to the ten last cells a dissipation $\gamma = 5$ to avoid the reflexive wave to propagate in the lattice.

Figure (3.11) shows, for the same couple (0.9,1.1), a complete evanescence in the upper forbidden band where the amplitude of the signal decreases exponentially till a value lower than $A_0 = 0.01$, whereas in the lower forbidden band, a wave which firstly decreases in amplitude before stabilizing itself and propagates with a constant amplitude of $A_0 = 0.12$ within the line.

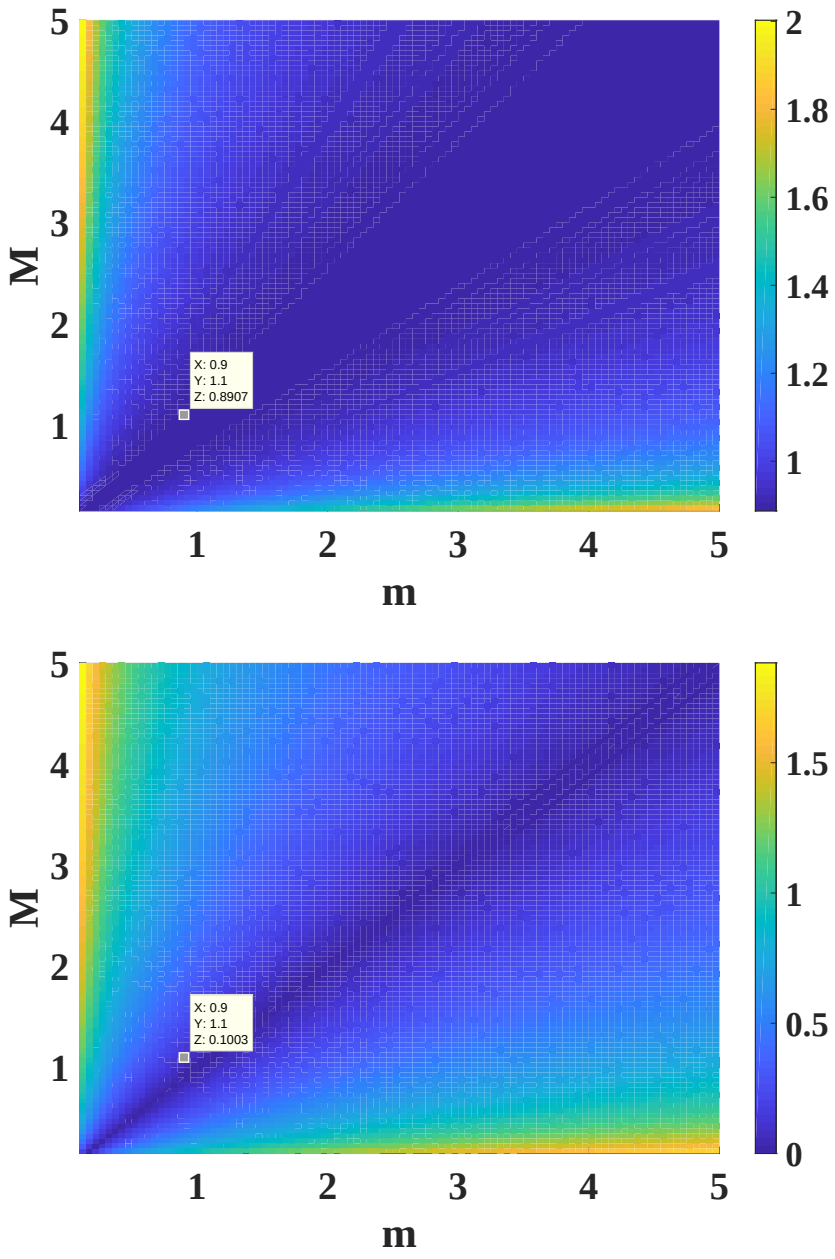

Figure 3.10: Imaginary part of wave number versus the couple (m, M) for the upper (a) and the lower (b) forbidden band.

3.2.2 Nonlinear diatomic FPU lattice

To study wave evanescence in the nonlinear chain, we shall submit the lattice to the same signal used in section (3.2.1). In the upper forbidden band, the wave is known to decay exponentially for all mass couples (m, M) when the driving frequency is lower than the supratransmission threshold, this part is not of great interest and shall not be studied more. The study in the lower forbidden band is more interesting

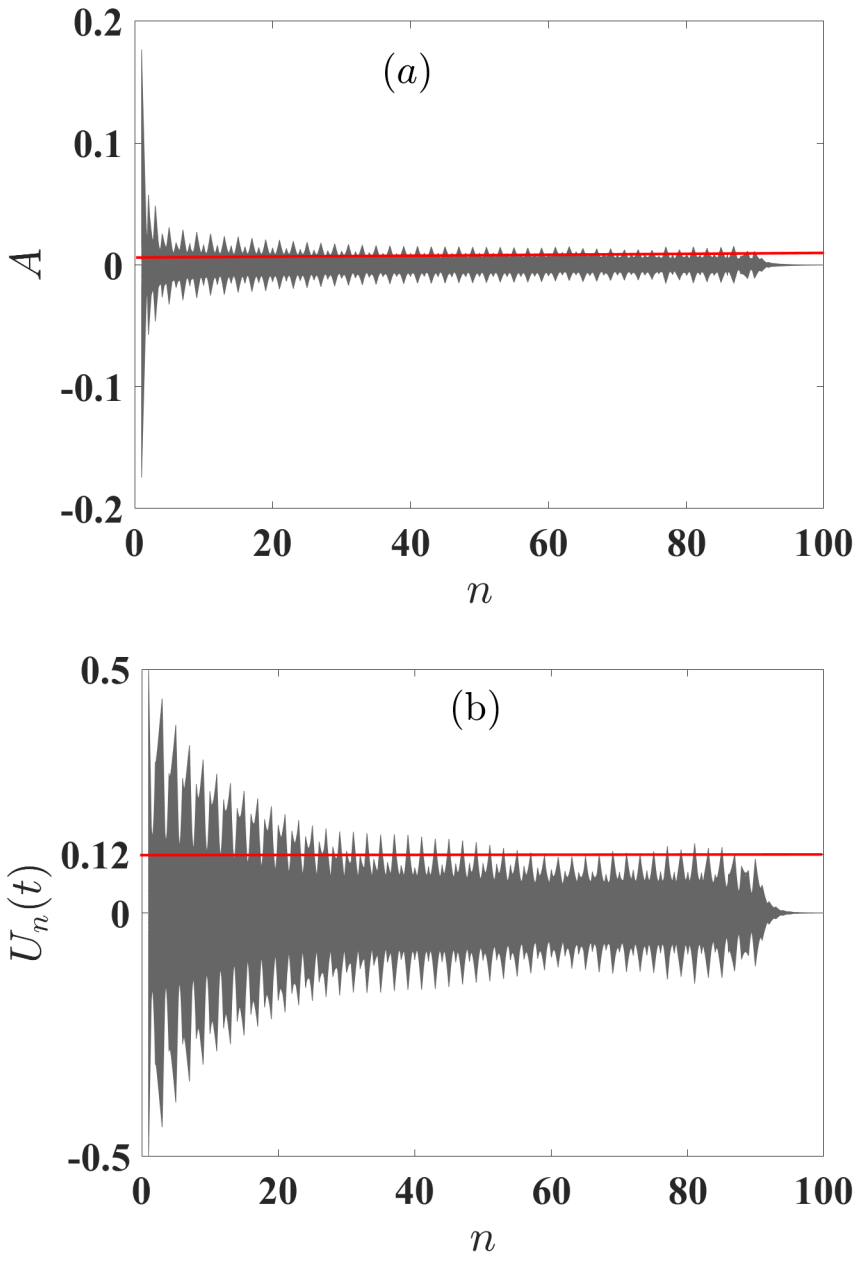

Figure 3.11: Spatial evolution of a signal within the lattice for the upper (a) and the lower (b) forbidden bands. We have taken $\omega = 2.4$ for the upper forbidden band and $\omega = 1.419$ in the lower; $A_0 = 0.35$ for the two cases.

because of the observation of peculiar behavior in linear regimes. The same driving frequency ($\omega = \frac{Max(\omega_-)+Min(\omega_+)}{2}$) which lay in the forbidden band of both the linear and the nonlinear dispersion law shall be used; and a driving amplitude, lower to the supratransmission threshold shall be considered. The spatial evolution of the wave displayed in Fig (3.12) shows the propagation of an attenuated signal which, after a transitory evanescence, stabilizes itself to a constant amplitude close to $A = 0.17$.

This is more than the case of the linear lattice, where the propagating amplitude was around $A = 0.12$ for the same driving amplitude of $A_0 = 0.35$. Thus, the nonlinearity accentuates the phenomenon by increasing the propagating amplitude.

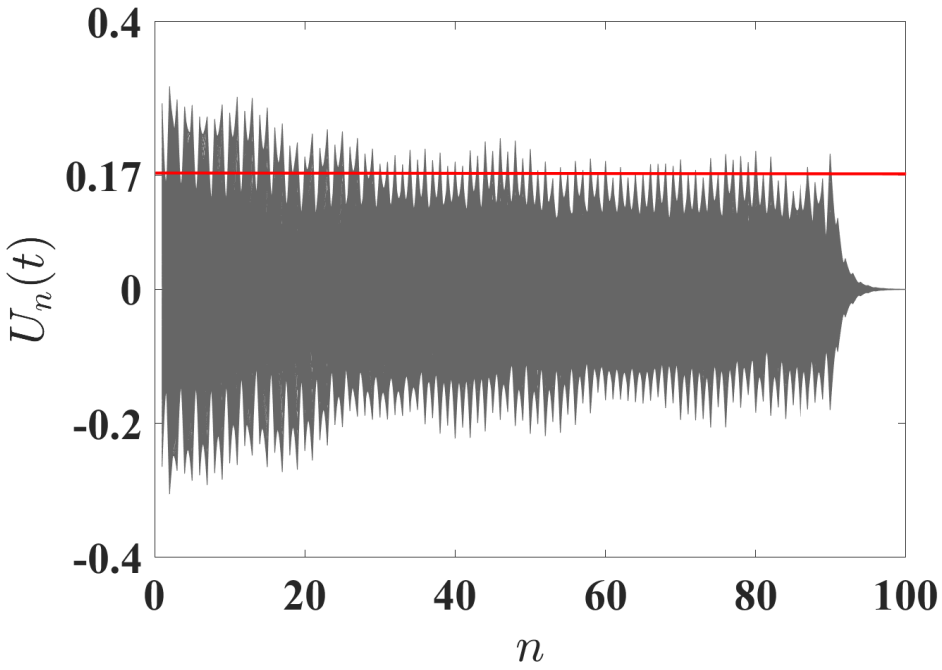

Figure 3.12: Spatial evolution of a signal within a nonlinear diatomic lattice. The driving frequency $\omega = 1.419$ lies in the lower forbidden band., $A_0 = 0.35$.

These results are not predicted in the linear theory, which predicts a complete evanescence as soon as the frequency lay in forbidden bands.

3.3 Energy transmission Control

The nonlinear supratransmission allows energy to flow through the medium with the condition $\omega > 2$. Following the literature [71], the NST threshold is estimated numerically by the brute-force method combined with the dichotomic search with a precision of 10^{-6}. This energy flow below and above the threshold is studied with the energy density flux between two consecutive particles [122, 135]

$$J_{n,n+1} = (\dot{u}_n - \dot{u}_{n-1})\left[(u_n - u_{n-1}) + (u_n - u_{n-1})^3\right] \tag{3.5}$$

The size of the lattice is fixed at 100 particles. To avoid initial shocks, the signal shall be introduced smoothly ($u_0(t) \to u_0[1 - \exp(-t/\tau)]$, with $\tau = 10$) in the system, with the chain initially at rest ($u_n(0) = \dot{u}_n(0) = 0$) [3, 71, 122]. The reflected waves coming back from the boundary $n = N$ are attenuated by adding a dissipative term ($-\gamma\dot{u}_n$, with $\gamma = 5$) to the last ten particles [3, 66, 71].

Additionally, to validate the analytical threshold represented by Equation (2.60), a comparative analysis with its numerical counterpart is conducted, plotting both against the driving frequency for both symmetric and asymmetric signal deformations.

This comparison is illustrated in Fig. 3.13, revealing a noteworthy concurrence between the analytical and numerical solutions. Such agreement underscores the reliability and accuracy of the analytical model in capturing the essential dynamics of the system across varying signal shapes and deformations.

Moreover, plotting the energy density as a function of the shape parameter for fixed values of the driving amplitude illustrates:

- a sharp increase (revealing the NST triggering) for the case of symmetric shape deformation [Fig. 3.14(a)],
- a sharp increase (NST triggering), followed by a zone of nonzero density (energy transmission), and thereafter a sharp decrease (suppression of NST) for the case of asymmetric shape deformation [Fig. 3.14(b)].

The effect of shape parameter r on the supratansmission threshold can also be seen in the variation of the threshold with respect to r displayed in Fig. 3.16 where we can observe a decreasing of the threshold with the increase of r for the symmetric deformation and the increase of this threshold with the absolute value of the shape parameter for the case of asymmetric shape deformation.

The NST threshold value $A = A_{th} = 1.229$ early found for an FPU lattice driven by a sinusoidal signal of frequency $\omega = 3.5$ [3], emerges distinctly ($J_{50,51} > 0$) for $r = 0$ [Fig. 3.14(c)]. Surprisingly, Fig. 3.14(a) reveals an energy propagation for a driving amplitude $A = 1.1$ triggered at a critical shape parameter value $r = 0.984$ of the signal $u_0^{(1)}$. In contrast, when considering the signal $u_0^{(2)}$ with an amplitude of $A = 1.4$ [Fig. 3.14(b)], the wave transmission does not occur when the shape

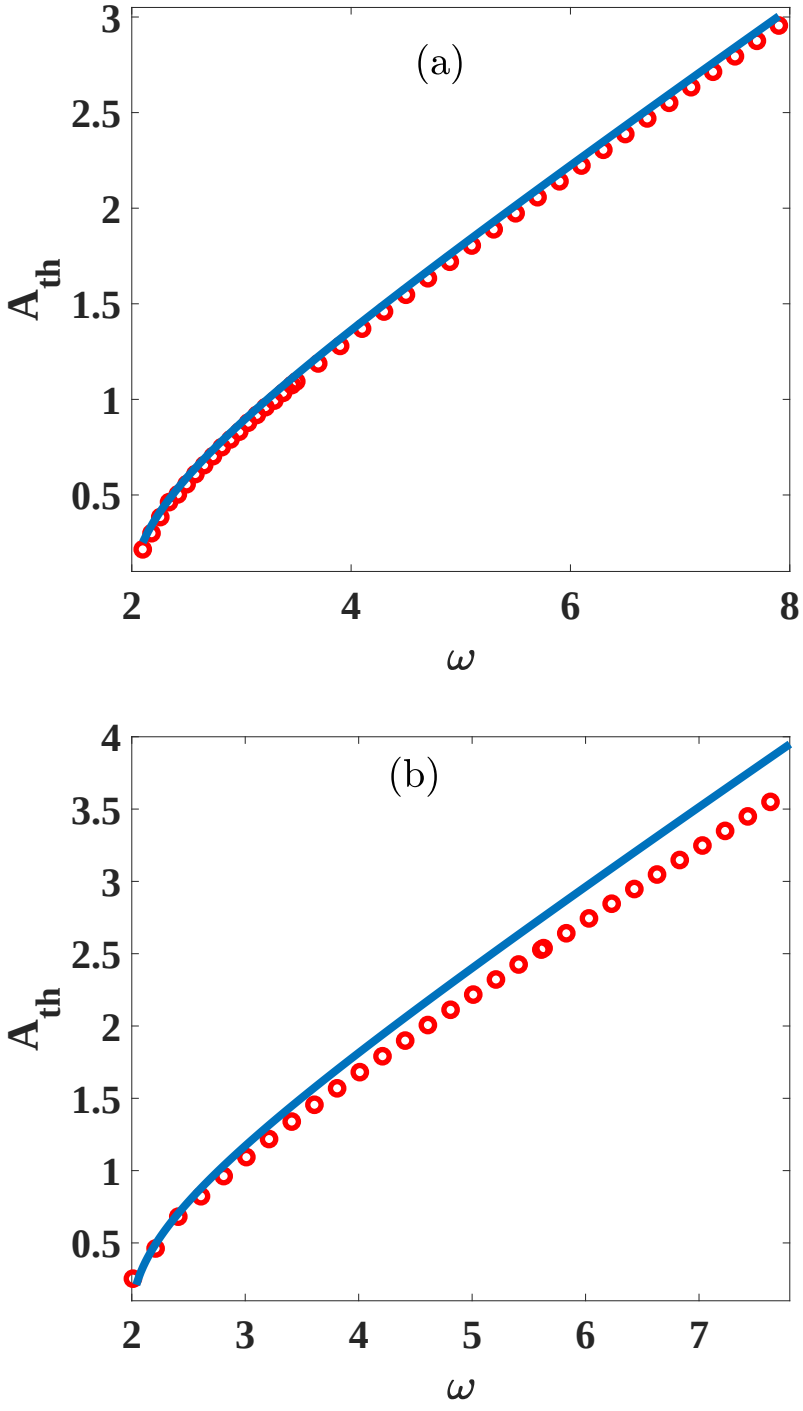

Figure 3.13: Analytical (blue solid lines) and numerical (red circles) thresholds Vs driving frequency for symmetric (a) and asymmetric (b) shape deformation; $r = 0.5$ (a) and $r = 0.99$ (b).

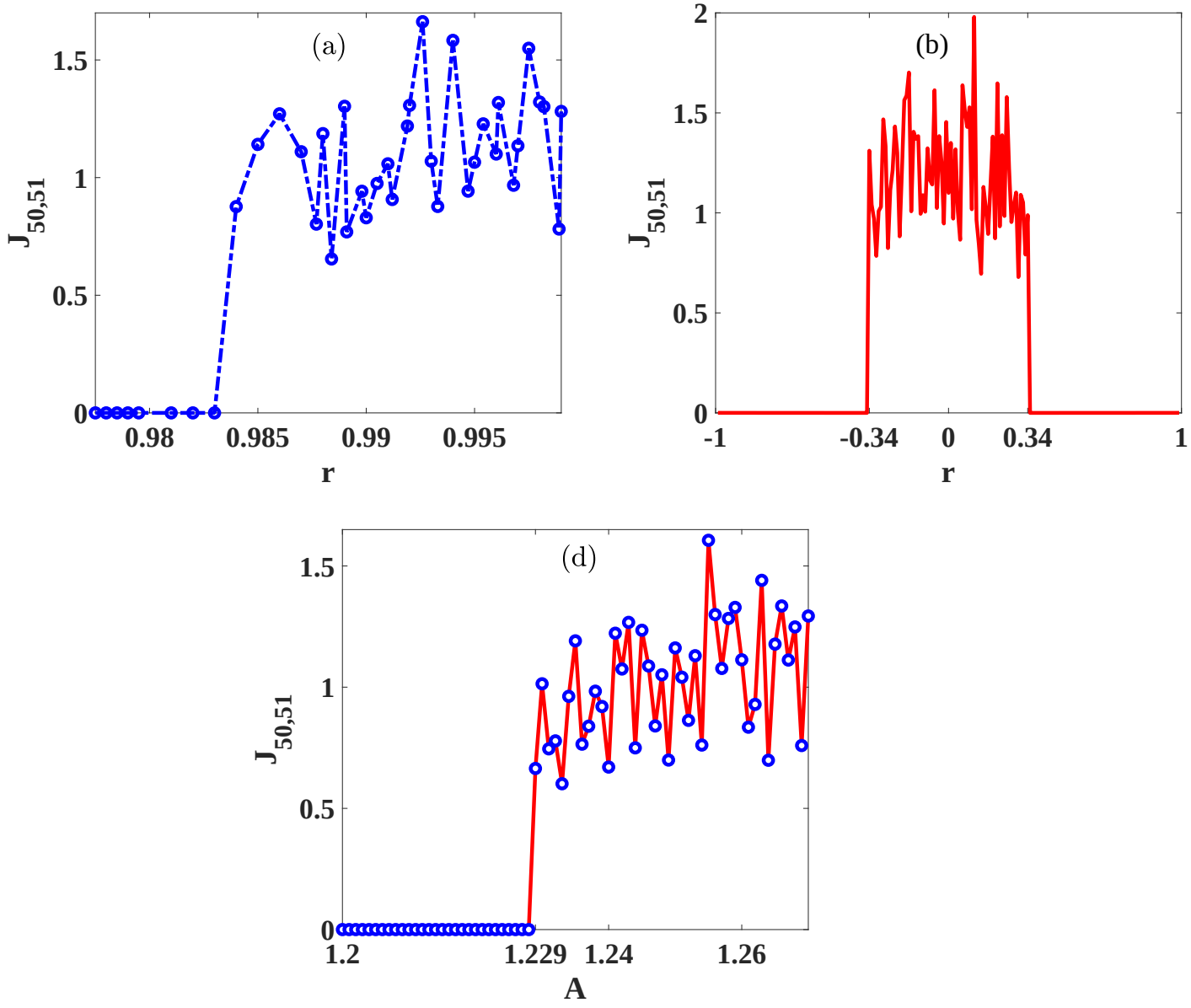

Figure 3.14: Energy density $J_{50,51}$ Vs the shape parameter for symmetric deformation (a) and asymmetric deformation (b). Energy density Vs the driving amplitude for shape parameter $r = 0$ (c). $A_0 = 1.1$(a) and $A = 1.4$ (b). For all the three sub-figures, $\omega = 3.5$.

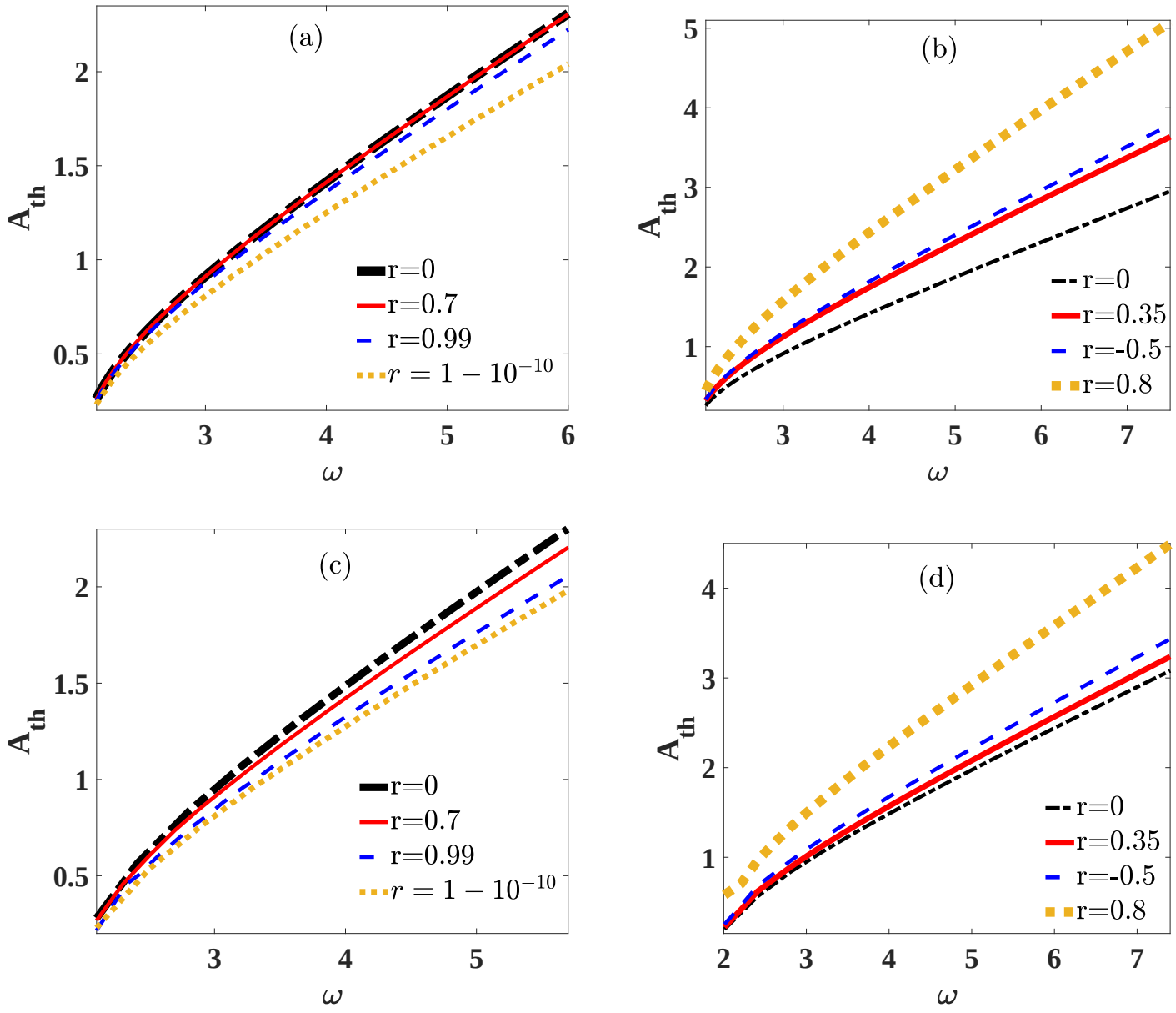

Figure 3.15: Analytical (a), (b) and numerical (c), (d) threshold Vs driving frequency for several value of r. (a) and (c) symmetric, (b) and (d) asymmetric deformation.

parameter is beyond $|r| = 0.35$. Furthermore, the findings underscore the intricate relationship between the supratransmission threshold and the shape parameter, particularly highlighting distinct trends based on the symmetry of shape deformation. Specifically, it becomes apparent that in instances of symmetric shape deformation, there is a discernible decrease in the supratransmission threshold as the shape parameter increases. Conversely, for asymmetric deformations, an opposite trend emerges, wherein the supratransmission threshold tends to increase with the abso-

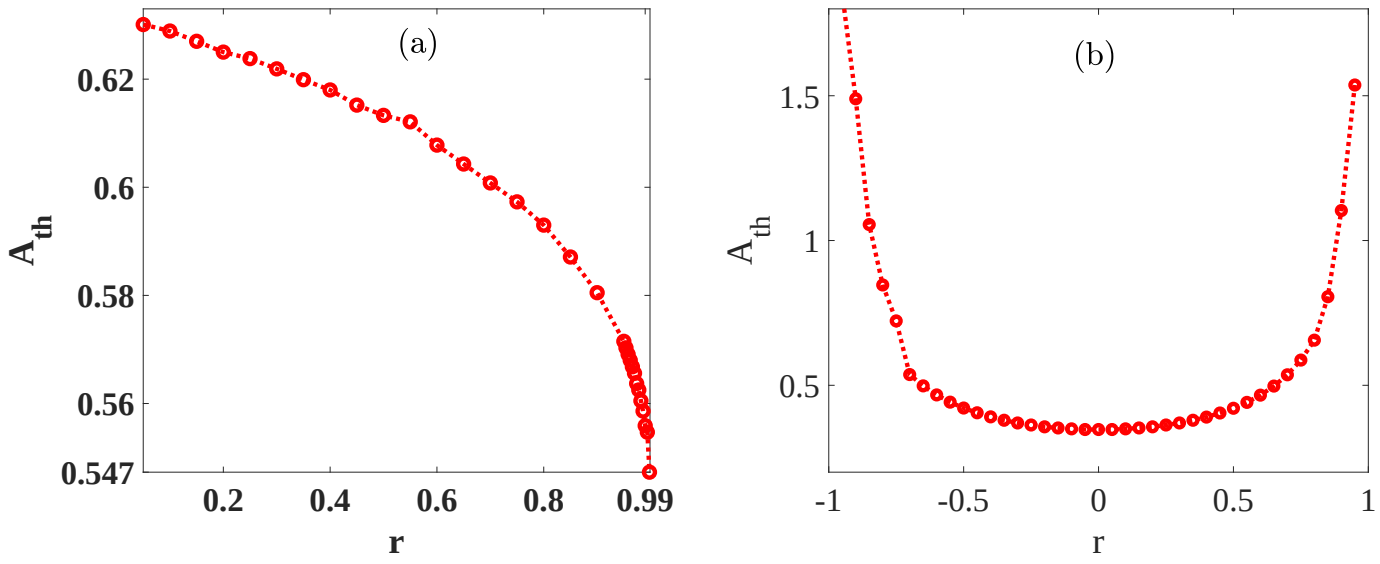

Figure 3.16: Numerical threshold Vs shape parameter r for symmetric (a), and asymmetric (b) deformation. For the two curves, $\omega = 2.5$.

lute value of the shape parameter, as evidenced in Fig. 3.15. These observations emphasize the profound influence exerted by the shape characteristics of the periodic signal on the phenomenon of supratransmission.

Discussion

In prior studies, researchers examined the presence and resilience of nonlinear static localized modes within different diatomic lattices, particularly those exhibiting frequencies falling within the forbidden band gap [56–59, 82]. This section now illustrates how these modes possess the ability to propagate throughout the lattice, a phenomenon commonly referred to as supra-transmission.

The nonlinear supratransmission phenomenon, previously observed in numerous mono-atomic systems [2–4,63,70–72] has also been evidenced here in one-dimensional diatomic β-FPU lattice. In contrast to the mono-atomic case [3, 136], there are several forbidden frequency band gaps, thus making the investigation more difficult. As highlighted by Mekontchou et *al.*, [71], only a few monoatomic models exhibit the supratransmission at all the forbidden frequency bands [71]. This study advocates further investigations of other diatomic case models.

Similarly to what was found in previous studies [2–4,63,70–74], the phenomenon

occurs when the amplitude of the sinusoidal excitation is greater than a certain value known as the threshold. In contrast to existing studies on di/tri-atomic models [137, 138], the supratransmission threshold has been derived analytically with acceptable accuracy by leveraging existing mathematical techniques for soliton investigation in nonlinear diatomic systems [78, 79, 119, 120, 139].

The investigation of nonlinear supra-transmission in structures featuring multiple elements within the unit cells, driven by differences in force constants and the presence of varying particle masses, was undertaken by both Zhang et al. [137] and Wu and Wang [138]. However, unlike the current study, Zhang et al. [137] based their conclusions solely on numerical simulations, lacking analytical rigor. Conversely, Wu and Wang [138] failed to fully consider the impact of the mass ratio, a crucial factor demonstrated in the present study to significantly impede the onset of supra-transmission. This oversight becomes apparent through the observed increases in the threshold value, indicating the necessity of accounting for mass ratio effects in understanding supra-transmission dynamics accurately. By addressing these shortcomings and leveraging analytical techniques, the present study provides a more comprehensive understanding of the underlying mechanisms governing supra-transmission in complex lattice structures, thereby contributing to the advancement of this field of research.

The intricate coupling between the motion of particles with alternating masses (m-M) in the diatomic β-FPU lattice renders the rotating wave approximation, commonly utilized in monoatomic FPU models [3], ineffective for accurately determining the threshold of supra-transmission occurrence. Despite our efforts to apply the same method, analytical results yielded by this approach did not closely align with the numerically exact threshold. However, through the decoupling ansatz method [78, 79, 119, 120, 139], we successfully derived an envelope equation capable of providing a threshold in the upper forbidden band that exhibits significant agreement with its numerical counterpart within the same gap.

It's worth noting that while the threshold derived in the upper forbidden band explicitly relies on the mass ratio μ, our analysis demonstrates its robust validity and accuracy across the spectrum of μ values. This finding underscores the usefulness of the decoupling ansatz method as a valuable tool for elucidating the

dynamics of supra-transmission in complex lattice structures, offering insights that transcend specific parameter configurations and facilitating a deeper understanding of the underlying physics governing nonlinear wave propagation phenomena.

The threshold obtained for the lower forbidden band through the continuum form of the decoupling ansatz method [79], was not in agreement with the numerical simulations. This is due to the fact that at the boundary of the lower forbidden band on the dispersion law, located at $k = \pi/2D$, the long wavelength limit, valid for $k = 0$ (boundary of the upper forbidden band) becomes less accurate. Fortunately, a more general form, valid for arbitrary wavelength exists for the decoupling ansatz [120]. This form provides an analytical threshold, which is in good agreement with the numerical results. It is also easy to check that for $k = 0$, we obtain, through that general form the results of section (2.2). Moreover it can be noticed that this threshold is not an explicit function of mass ratio μ and is in good agreement with numerical results for small values of this ratio ($\mu \leq 60\%$). This accordance confirms the hypothesis of acoustic mode vibration in the lower forbidden band and the decoupling between the optical and the acoustic modes. However, for values of the driving frequency sufficiently close to ω_{+min}, the coupling effects become very significative and result in a decrease of the threshold with the increase of the driving frequency as we can observe in Figs.3.6 (a,b), 3.7 (a,b) and 3.8 (a,b). In other words, the anomalous observed through the decreasing of the threshold are due to the coupling effects between the optical and acoustic mode; this observation is confirmed by the case of narrow band gap where the thresholds obtained when the coupling is taken into account are globally lower than those obtained without coupling effects.

For large values of mass ratio ($\mu > 60\%$), the coupling between acoustic and optical modes in the lower forbidden band, which has been previously investigated by Hu et al [75] has been considered to derive the supratransmission threshold, since the threshold Eq. (2.20) is no more in accordance with numerical results. The threshold Eq. (2.40), derived when taking into account the coupling between the two modes displays an explicit dependence on the frequency of these two modes and a good agreement with the numerical results proves the actual presence of a coupling which strength increases with the increasing of the mass ratio. Moreover,

we observe that using this coupling mode procedure, we can also derive, as one of the results, the same threshold Eq. (2.34) obtained when neglecting the coupling between the two modes.

A surprising and very interesting aspect of this work is the changing of the supratransmission threshold when switching the order of particles. In fact, this switch does not affect the physical properties of the lattice (apart from the mass of the driven particle) but is found relevant for the study of the supratransmission phenomenon in diatomic lattices. The choice of the driven particle (light or heavy) is thus crucial for the study of supratransmission and more generally for the study of the dynamic of diatomic lattices under external excitation. The consequences of such a behavior on real physical systems modeled by diatomic lattice could be very interesting.

Through the study on the supratransmission phenomenon with changing shape signals, we discovered that, contrary to popular belief, supratransmission is a phenomenon that depends on more than just the driving amplitude. The shape of the signal is an important parameter in the study of the phenomenon and should be considered in all studies on the subject.

Adjustment of the threshold, especially lowering it, is crucial in the quest for a purer waveform of solitonic pulses, as well as improving the efficiency and flexibility of hypersensitive detectors [53, 115] and emitting solitonic pulses in a range of applications. The usage of defect can achieve an important threshold reduction [91]. Although achieving a good result, such approaches do not lend itself easy to implement due to the need of modifying the system itself at specific lattice locations [91]. This study demonstrated that a well selected shape for the exciting signal can achieve a satisfying result without modifying the system.

Other original methods were employed to transmit periodic wave with an amplitude bellow the threshold. This wave can propagate if another incident harmonic driving is added at the left-end [89], or a noise added in the initial incident driving [90]. The present study showed that the shape variation suffices to achieve wave energy flow in the lattice.

To experimentally verify the theoretical prediction of this work, such deformable signal may be easily built in a laboratory, for example, using electrical circuits (e.g.,

see Ref. [95]).

The difference in behavior between the two analyzed signals regarding the NST threshold is not due to symmetry but rather stems from the interaction among various harmonics observed in the Fourier expansion. Specifically, for the symmetric signal, the coefficients of the super-harmonics are exclusively positive, leading to cooperative effects that amplify the amplitude of the fundamental harmonic up to that of sinusoidal signal $A\sin(\omega t)$. This amplification boosts its energy, subsequently resulting in the reduction of the NST threshold. Conversely, for the asymmetric signal, the coefficients of super-harmonics can vary in sign, resulting in competitive effects that diminish the amplitude of the fundamental harmonic below A. Consequently, more energy is required to initiate supratransmission, thereby enhancing the NST threshold. By mean of FFT [130–134], this phenomenon can be visualized through the spectral representation of $u_0^{(1)}$ and $u_0^{(2)}$ [Fig. 3.17].

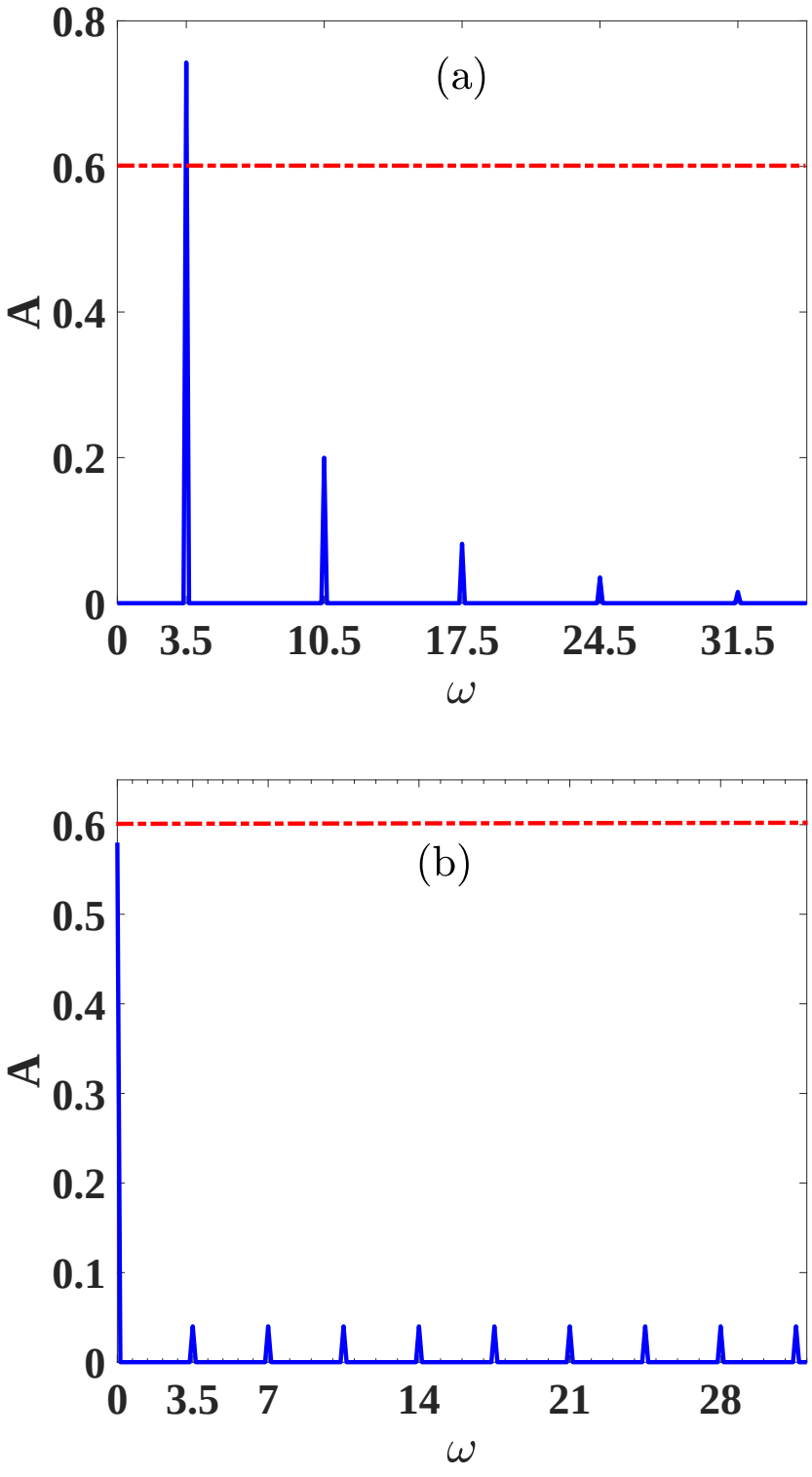

Figure 3.17: Spectral density of the signals $u_0^{(1)}$ (a) and $u_0^{(2)}$ (b). $\omega = 3.5$, $A = 0.6$, $r = 0.9999$. Red dashed lines stand for the driving amplitude values.

3.4 Conclusion

In this chapter, we investigated the Nonlinear supratransmission (NST) phenomenon using numerical simulations. We focused on a diatomic lattice driven by a sinusoidal signal with a frequency within the forbidden bands gap for the first part, and on a monoatomic FPU lattice driven by a variable shape signal with frequency within the forbidden band for the second part. Through numerical simulations, we determined NST thresholds for each case. Knowing that numerical simulations serve as valuable tools for studying complex systems [140–143], offering solutions close to exact solutions and serving as a means to test the accuracy of any analytical techniques, our work, by demonstrating a good agreement between the numerical thresholds and their analytical counterparts derived in the previous chapter, highlight the accuracy of the analytical procedures used. This agreement enhances our understanding of the NST phenomenon in FPU lattices.

GENERAL CONCLUSION

By ending this study where the purpose was the energy control in the forbidden phonon bands of FPU lattices, we can say that, for given driving amplitude and frequency, this control can be efficiently accomplished either by changing the lattice configuration or by changing the shape of the driving signal. Precisely, for the study of diatomic FPU lattice driven by sinusoidal signals, it is demonstrated that the supratransmission can occur in the upper and the lower forbidden band, and, the threshold amplitudes above which the phenomenon occurs have been derived for both forbidden band numerically and analytically. The accurateness of the numerical and analytical methods is established by estimating the threshold as a function of driving amplitude for several values of the ratio m/M and also with the study of the limit case $m = M$ which shows a good agreement with the existing theory. Moreover, our investigation unveils a noteworthy observation: switching the order of particles within the chain, from a configuration with a heavy first particle to one with a light first particle, results in distinct supratransmission thresholds within both forbidden bands. This peculiar behavior underscores the asymmetric nature of diatomic lattices. Furthermore, we discern in the lower forbidden band, a dependency of supratransmission on band width, shedding light on the nuanced characteristics of these lattice structures. Consequently, our study emphasizes the importance of employing multiple analytical approaches when studying diatomic lattices to fully capture their complex behavior

Otherwise, for a monoatomic FPU, the notion of supratransmission has been expanded by proving that an appropriate signal shape may induce (or block) energy flow through the lattice below (or above) the NST threshold, revealing that nonlinear supratransmission is dependent not only on driving amplitude but also on signal

form. These results show that for a given amplitude and frequency in the forbidden band, there is not one, but an infinity of supratransmission thresholds, depending on the shape of the driving signal. The origin of the variation of the supratransmission threshold when varying the shape of a signal is now a great subject of interest; from our research, it seems to be the consequence of the interaction of harmonic component with can enhance or reduce the amplitude of the fundamental harmonic; for the studied cases, we found that the cooperative effects observed for the symmetric signal are beneficial for the fundamental harmonic whereas competitive effects observed for the asymmetric signal are detrimental for the fundamental harmonic. However, is this valid for all symmetric signals and all asymmetric signals? In the next studies, we aim to:

- investigate the main properties of symmetric and asymmetric signals (linear as well as nonlinear signals) in order to derive a more general rule of classification of signals into NST threshold increasing and decreasing signals,
- explore the behavior of waves in forbidden bands, in particular in the lower forbidden band of an FPU diatomic lattice when the coupling effects become very strong,
- explore the supratransmission phenomenon in a system submitted to several periodic excitations.

Appendix

Appendix A: Resolution of nonlinear Schrodinger equation: static solution

$$-iG_t + PG_{\eta\eta} + Q|G|^2G = 0 \tag{3.6}$$

we find solution of Eq. (3.6) as static solution, so we shall take it on the form

$$G(x,t) = A(x)e^{-i\omega_s t} \tag{3.7}$$

with $\omega_s = \omega - \omega_c$
$v_g = 0 \Rightarrow \eta = x$ inserting Eq. (3.7) in Eq. (3.6) give

$$-\omega_s A e^{-\omega_s t} + PA_{xx}e^{-i\omega_s t} + QA^3e^{-i\omega_s t} = 0 \tag{3.8}$$

and then

$$-\omega_s A + PA_{xx} + QA^3 = 0 \tag{3.9}$$

multiplying (3.9) by $2A_x$, and integrating term by term, we obtain

$$-\omega_s A^2 + PA_x^2 + \frac{Q}{2}A^4 = A_0 \tag{3.10}$$

where A_0 is a constant. since $\lim_{x\to\infty} A = \lim x \to \infty A_x = 0$, the constant $A_0 = 0$ (3.10) can be rewritten as

$$A_x^2 = \frac{\omega_s A^2 - \frac{Q}{2}A^4}{P} \tag{3.11}$$

$\Rightarrow$

$$\frac{dA}{\sqrt{\frac{\omega_s}{P}A^2 - \frac{Q}{2P}A^4}} = \pm dx \tag{3.12}$$

$\Rightarrow$

$$\frac{\sqrt{\frac{Q}{2\omega_s}}dA}{\sqrt{\frac{\omega_s}{P}}\sqrt{\frac{Q}{2\omega_s}}A\sqrt{1 - \frac{Q}{2\omega_s}A^2}} = \pm dx \tag{3.13}$$

let $B = \sqrt{\frac{Q}{2\omega_s}}A$, $\Rightarrow$ $dB = \sqrt{\frac{Q}{2\omega_s}}dA$

$$\frac{dB}{\sqrt{\frac{\omega_s}{P}}B\sqrt{1 - B^2}} = \pm dx \tag{3.14}$$

and after integration, we obtain

$$-\sqrt{\frac{P}{\omega_s}}argsech(B) = x - x_0 \tag{3.15}$$

where x_0 is an integration constant we can easily derive

$$B = Sech\left(\pm\sqrt{\frac{\omega_s}{P}}(x - x_0)\right) \tag{3.16}$$

and

$$A = \sqrt{\frac{2\omega_s}{Q}}Sech\left(\pm\sqrt{\frac{\omega_s}{P}}(x - x_0)\right) \tag{3.17}$$

and finaly

$$G(x,t) = \sqrt{\frac{2\omega_s}{Q}}Sech\left(\pm\sqrt{\frac{\omega_s}{P}}(x - x_0)\right)e^{-i\omega_s t} \tag{3.18}$$

Appendix B: Static breather-breather solutions of coupled nonlinear Schrödinger equations

$$\begin{cases} i\Phi_t - P_1\Phi_{xx} - Q_1\left(|\Phi|^2 + 2|\Psi|^2\right)\Phi = 0 \\ i\Psi_t - P_2\Psi_{xx} - Q_2\left(|\Psi|^2 + 2|\Phi|^2\right)\Psi = 0 \end{cases} \tag{3.19}$$

Let's seek solutions of Eq. (3.19) as static breather-breather solutions on the form:

$$\begin{aligned}\Phi &= A\,\mathrm{sech}\,(\gamma x)\,e^{-i\omega_{s_1}t}\\ \Psi &= B\,\mathrm{sech}\,(\gamma x)\,e^{-i\omega_{s_2}t}\end{aligned} \tag{3.20}$$

Inserting Eq. (3.20) into Eq. (3.19) yields:

$$\begin{cases}\omega_{s_1} - P_1\left[2\gamma^2\tanh^2(\gamma x) - \gamma^2\right] - Q_1\left[A^2\,\mathrm{sech}^2(\gamma x) + 2B^2\,\mathrm{sech}^2(\gamma x)\right] = 0\\ \omega_{s_2} - P_2\left[2\gamma^2\tanh^2(\gamma x) - \gamma^2\right] - Q_2\left[B^2\,\mathrm{sech}^2(\gamma x) + 2A^2\,\mathrm{sech}^2(\gamma x)\right] = 0\end{cases} \tag{3.21}$$

Multiplying Eq. (3.21) by $\cosh^2(\gamma x)$ yields:

$$\begin{cases}\left(\omega_{s_1} + P_1\gamma^2\right)\cosh^2(\gamma x) - 2P_1\gamma^2\sinh^2(\gamma x) = Q_1\left(A^2 + 2B^2\right)\\ \left(\omega_{s_2} + P_2\gamma^2\right)\cosh^2(\gamma x) - 2P_2\gamma^2\sinh^2(\gamma x) = Q_2\left(B^2 + 2A^2\right)\end{cases} \tag{3.22}$$

Equation (3.22) allows solution if and only if

$$\begin{aligned}\omega_{s_1} + P_1\gamma^2 &= 2P_1\gamma^2 = Q_1\left(A^2 + 2B^2\right)\\ \omega_{s_2} + P_2\gamma^2 &= 2P_2\gamma^2 = Q_2\left(B^2 + 2A^2\right)\end{aligned} \tag{3.23}$$

that is

$$\begin{cases}\omega_{s_1} + P_1\gamma^2 = 2P_1\gamma^2,\\ \omega_{s_1} + P_1\gamma^2 = Q_1\left(A^2 + 2B^2\right),\end{cases} \tag{3.24}$$

and

$$\begin{cases}\omega_{s_2} + P_2\gamma^2 = 2P_2\gamma^2,\\ \omega_{s_2} + P_2\gamma^2 = Q_2\left(B^2 + 2A^2\right).\end{cases} \tag{3.25}$$

The first equations of the system Eq. (3.24) yields:

$$\gamma^2 = \frac{\omega_{s_1}}{P_1}, \tag{3.26}$$

From the first equation of the system Eq. (3.25), when taking into account $P_2 = -\frac{P_1\omega_{-max}}{\omega_{+min}}$, we derive

$$\omega_{s_2} = -\frac{\omega_{s_1}\omega_{-max}}{\omega_{+min}} \tag{3.27}$$

The resolution of the system formed by the last equations of systems Eq. (3.24) and

Eq. (3.25) gives

$$B^2 = \frac{4\omega_{s_1}}{3Q_1} - \frac{2\omega_{s_2}}{3Q_2}, \tag{3.28}$$

$$A^2 = \frac{4\omega_{s_2}}{3Q_2} - 2\frac{2\omega_{s_1}}{3Q_1} \tag{3.29}$$

Bibliography

[1] Ramaz Khomeriki. Nonlinear band gap transmission in optical waveguide arrays. *Physical Review Letters*, 92(6):063905, 2004.

[2] F Geniet and J Leon. Energy transmission in the forbidden band gap of a nonlinear chain. *Physical Review Letters*, 89(13):134102, 2002.

[3] Ramaz Khomeriki, Stefano Lepri, and Stefano Ruffo. Nonlinear supratransmission and bistability in the fermi-pasta-ulam model. *Physical Review E*, 70(6):066626, 2004.

[4] K. Tse Ve Koon, J. Leon, P. Marquié, and P. Tchofo-Dinda. Cutoff solitons and bistability of the discrete inductance-capacitance electrical line: Theory and experiments. *Phys. Rev. E*, 75(6):389–406, 2007.

[5] Flach, Sergej, and Christoph R. Willis, Discrete breathers. Physics Reports 295.5-6 (1998): 181-264.

[6] Oleg M Braun and Yuri S Kivshar. The frenkel-kontorova model: concepts, methods, and applications. 2004.

[7] Serge Aubry. The twist map, the extended frenkel-kontorova model and the devil's staircase. *Physica D: Nonlinear Phenomena*, 7(1-3):240–258, 1983.

[8] Michel Peyrard and Alan R Bishop. Statistical mechanics of a nonlinear model for dna denaturation. *Physical Review Letters*, 62(23):2755, 1989.

[9] Mahmoud I Hussein, Michael J Leamy, and Massimo Ruzzene. Dynamics of phononic materials and structures: Historical origins, recent progress, and future outlook. *Applied Mechanics Reviews*, 66(4):040802, 2014.

[10] Serge Aubry. Discrete breathers: localization and transfer of energy in discrete hamiltonian nonlinear systems. *Physica D: Nonlinear Phenomena*, 216(1):1–30, 2006.

[11] Anna Maria Morgante, Magnus Johansson, Georgios Kopidakis, and Serge Aubry. Standing wave instabilities in a chain of nonlinear coupled oscillators. *Physica D: Nonlinear Phenomena*, 162(1-2):53–94, 2002.

[12] Michel Remoissenet. Waves called solitons: concepts and experiments, springer science & business media. 2013.

[13] Salerno, Mario. Soliton dynamics in nonlinear lattices. Physics Reports 182.2-3 (1989): 79-159.

[14] PG Kevrekidis, KØ Rasmussen, and AR Bishop. The discrete nonlinear schrödinger equation: a survey of recent results. *International Journal of Modern Physics B*, 15(21):2833–2900, 2001.

[15] AJ Sievers and S Takeno. Intrinsic localized modes in anharmonic crystals. *Physical Review Letters*, 61(8):970, 1988.

[16] Lucas Lindsay, DA Broido, and TL Reinecke. First-principles determination of ultrahigh thermal conductivity of boron arsenide: a competitor for diamond? *Physical Review Letters*, 111(2):025901, 2013.

[17] Philippe Ghosez. First-principles study of the dielectric and dynamical properties of barium titanate. *Doctor Thesis, Universite Catholique de Louvain*, 1997.

[18] Richard Cisek, Virginijus Barzda, Harry E Ruda, and Alexander Shik. Nonlinear optical properties of semiconductor nanowires. *IEEE Journal of Selected Topics in Quantum Electronics*, 17(4):915–921, 2010.

[19] Mark G Kuzyk, RC Moore, and LA King. Second-harmonic-generation measurements of the elastic constant of a molecule in a polymer matrix. *Journal of the Optical Society of America B*, 7(1):64–72, 1990.

[20] Vincent Laude, Abdelkrim Khelif, Sarah Benchabane, Mikael Wilm, Thibaut Sylvestre, Bertrand Kibler, Arnaud Mussot, John M Dudley, and Hervé Maillotte. Phononic band-gap guidance of acoustic modes in photonic crystal fibers. *Physical Review BâĂŤCondensed Matter and Materials Physics*, 71(4):045107, 2005.

[21] Rosa Martínez-Sala. Sound attenuation by sculpture. *nature*, 378:241, 1995.

[22] Zhengyou Liu, Xixiang Zhang, Yiwei Mao, YY Zhu, Zhiyu Yang, Che Ting Chan, and Ping Sheng. Locally resonant sonic materials. *science*, 289(5485):1734–1736, 2000.

[23] Ilya V Shadrivov, Alexander B Kozyrev, DanielW van der Weide, and Yuri S Kivshar. Nonlinear magnetic metamaterials. *Optics Express*, 16(25):20266–20271, 2008.

[24] John D Joannopoulos, Steven G Johnson, Joshua N Winn, and Robert D Meade. Molding the flow of light. *Princet. Univ. Press. Princeton, NJ [ua]*, 2008.

[25] Marin Soljacic, Elefterios Lidorikis, Mihai Ibanescu, Steven G Johnson, JD Joannopoulos, and Yoel Fink. Optical bistability and cutoff solitons in photonic bandgap fibers. *Optics express*, 12(8):1518–1527, 2004.

[26] Yuri S Kivshar and Michel Peyrard. Modulational instabilities in discrete lattices. *Physical Review A*, 46(6):3198, 1992.

[27] Vladimir E Zakharov and Lev A Ostrovsky. Modulation instability: The beginning. *Physica D: Nonlinear Phenomena*, 238(5):540–548, 2009.

[28] Eric Tala-Tebue, Aurelien Kenfack-Jiotsa, Marius Hervé Tatchou-Ntemfack, and Timoléon Crépin Kofané. Modulational instability in a pair of non-identical coupled nonlinear electrical transmission lines. *Communications in Theoretical Physics*, 60(1):93, 2013.

[29] E Kengne, ST Chui, and WM Liu. Modulational instability criteria for coupled nonlinear transmission lines with dispersive elements. *Physical Review E*, 74(3):036614, 2006.

[30] D Barday and M Remoissenet. Modulational instability and gap solitons in a finite josephson transmission line. *Physical Review B*, 43(9):7297, 1991.

[31] Yuriy A Kosevich and Stefano Lepri. Modulational instability and energy localization in anharmonic lattices at finite energy density. *Physical Review B*, 61(1):299, 2000.

[32] Thierry Dauxois, Stefano Ruffo, Ennio Arimondo, and Martin Wilkens. Dynamics and thermodynamics of systems with long-range interactions: An introduction. 2002.

[33] K Tse Ve Koon, P Marquié, and P Tchofo Dinda. Experimental observation of the generation of cutoff solitons in a discrete l c nonlinear electrical line. *Physical Review E*, 90(5):052901, 2014.

[34] Fernanda Sayuri Yamasaki, Lauro Paulo Silva Neto, Jose Osvaldo Rossi, and Joaquim J Barroso. Soliton generation using nonlinear transmission lines. *IEEE transactions on plasma science*, 42(11):3471–3477, 2014.

[35] DL Sekulic, MV Sataric, MB Zivanov, and JS Bajic. Soliton-like pulses along electrical nonlinear transmission line. *Elektronika ir Elektrotechnika*, 121(5):53–58, 2012.

[36] Yaroslav V Kartashov, Boris A Malomed, and Lluis Torner. Solitons in nonlinear lattices. *Reviews of Modern Physics*, 83(1):247, 2011.

[37] Fabien Kenmogne, David Yemélé, and Paul Woafo. Electrical dark compacton generator: Theory and simulations. *Physical Review E*, 85(5):056606, 2012.

[38] JL Marin and S Aubry. Breathers in nonlinear lattices: numerical calculation from the anticontinuous limit. *Nonlinearity*, 9(6):1501, 1996.

[39] Guillaume James. Travelling breathers and solitary waves in strongly nonlinear lattices. *Philosophical Transactions of the Royal Society A: Mathematical, Physical and Engineering Sciences*, 376(2127):20170138, 2018.

[40] Tassos Bountis and Jeroen M Bergamin. Discrete breathers in nonlinear lattices: A review and recent results. *Galaxies and Chaos*, pages 75–90, 2003.

[41] Carlos Lawrence Gninzanlong, Frank Thomas Ndjomatchoua, and Clément Tchawoua. Forward and backward propagating breathers in a dna model with dipole-dipole long-range interactions. *Physical Review E*, 102(5):052212, 2020.

[42] Carlos Lawrence Gninzanlong, Frank Thomas Ndjomatchoua, and Clément Tchawoua. Discrete breathers dynamic in a model for dna chain with a finite stacking enthalpy. *Chaos: An Interdisciplinary Journal of Nonlinear Science*, 28(4), 2018.

[43] Michael Mekontchou Foudjio, Frank Thomas Ndjomatchoua, Carlos Lawrence Gninzanlong, and Clément Tchawoua. Collective escape and homoclinic bifurcation phenomena in a nonlinear oscillators chain. *Communications in Nonlinear Science and Numerical Simulation*, 114:106690, 2022.

[44] Karsten Ahnert and Arkady Pikovsky. Compactons and chaos in strongly nonlinear lattices. *Physical Review E*, 79(2):026209, 2009.

[45] Dirk Hennig. Periodic, quasiperiodic, and chaotic localized solutions of a driven, damped nonlinear lattice. *Physical Review E*, 59(2):1637, 1999.

[46] B Senyange, B Many Manda, and Ch Skokos. Characteristics of chaos evolution in one-dimensional disordered nonlinear lattices. *Physical Review E*, 98(5):052229, 2018.

[47] Pavel V Zakharov, Elena A Korznikova, Artem A Izosimov, and Andrey S Kochkin. The influence of crystal anisotropy on the characteristics of solitary waves in the nonlinear supratransmission effect: Molecular dynamic modeling. *Computation*, 11(10):193, 2023.

[48] JE Macías-Díaz and A Puri. An application of nonlinear supratransmission to the propagation of binary signals in weakly damped, mechanical systems of coupled oscillators. *Physics Letters A*, 366(4-5):447–450, 2007.

[49] JE Macías-Díaz and A Puri. On the transmission of binary bits in discrete josephson-junction arrays. *Physics Letters A*, 372(30):5004–5010, 2008.

[50] Jorge Eduardo Macías-Díaz. Persistence of nonlinear hysteresis in fractional models of josephson transmission lines. *Communications in Nonlinear Science and Numerical Simulation*, 53:31–43, 2017.

[51] Bertrand Bodo, Saverio Morfu, Patrick Marquié, and BZ Essimbi. Noise induced breather generation in a sine–gordon chain. *Journal of Statistical Mechanics: Theory and Experiment*, 2009(01):P01026, 2009.

[52] Bertrand Bodo, Saverio Morfu, Patrick Marquié, and Matthieu Rosse. A klein-gordon electronic network exhibiting the supratransmission effect. *Electron. Lett*, 46(2):123–124, 2010.

[53] D Chevriaux, R Khomeriki, and J Leon. Theory of a josephson junction parallel array detector sensitive to very weak signals. *Physical Review B*, 73(21):214516, 2006.

[54] Pavel Vasilyvich Zakharov et al. The effect of nonlinear supratransmission in discrete structures: A review. *Comput. Res. Model*, 15(3):599–617, 2023.

[55] Dahai He, Bao-quan Ai, Ho-Kei Chan, Bambi Hu, et al. Heat conduction in the nonlinear response regime: Scaling, boundary jumps, and negative differential thermal resistance. *Physical Review E*, 81(4):041131, 2010.

[56] N Boechler, G Theocharis, Stéphane Job, Panayotis G Kevrekidis, Mason A Porter, and C Daraio. Discrete breathers in one-dimensional diatomic granular crystals. *Physical Review Letters*, 104(24):244302, 2010.

[57] P Maniadis, AV Zolotaryuk, and GP Tsironis. Existence and stability of discrete gap breathers in a diatomic β fermi-pasta-ulam chain. *Physical Review E*, 67(4):046612, 2003.

[58] Andrey V Gorbach and Magnus Johansson. Discrete gap breathers in a diatomic klein-gordon chain: Stability and mobility. *Physical Review E*, 67(6):066608, 2003.

[59] Kazuyuki Yoshimura. Existence and stability of discrete breathers in diatomic fermi–pasta–ulam type lattices. *Nonlinearity*, 24(1):293, 2010.

[60] J Leon and A Spire. Gap soliton formation by nonlinear supratransmission in bragg media. *Physics Letters A*, 327(5-6):474–480, 2004.

[61] Duilio De Santis, Claudio Guarcello, Bernardo Spagnolo, Angelo Carollo, and Davide Valenti. Supratransmission-induced traveling breathers in long josephson junctions. *Communications in Nonlinear Science and Numerical Simulation*, 115:106736, 2022.

[62] F Geniet and J Leon. Nonlinear supratransmission. *Journal of Physics: Condensed Matter*, 15(17):2933, 2003.

[63] Fabien Kenmogne, Guy Bertrand Ndombou, David Yemélé, and Anaclet Fomethe. Nonlinear supratransmission in a discrete nonlinear electrical transmission line: Modulated gap peak solitons. *Chaos, Solitons & Fractals*, 75:263–271, 2015.

[64] H Susanto and N Karjanto. Calculated threshold of supratransmission phenomena in waveguide arrays with saturable nonlinearity. *Journal of Nonlinear Optical Physics & Materials*, 17(02):159–165, 2008.

[65] Hadi Susanto. Boundary driven waveguide arrays: supratransmission and saddle-node bifurcation. *SIAM Journal on Applied Mathematics*, 69(1):111–125, 2008.

[66] Christian Simadji Ngamou, Frank Thomas Ndjomatchoua, Michael Mekontchou Foudjio, Carlos Lawrence Gninzanlong, and Clément Tchawoua. Supratransmission phenomenon in a fermi-pasta-ulam diatomic lattice. *Physical Review E*, 108(5):054216, 2023.

[67] A Kamdoum Kuitche, AB Togueu Motcheyo, Thomas Kanaa, and C Tchawoua. Supratransmission in transversely connected nonlinear pendulum pairs. *Chaos, Solitons & Fractals*, 160:112196, 2022.

[68] AB Togueu Motcheyo and JE Macías-Díaz. Energy transmission in the forbidden band-gap of a nonlinear chain with global interactions. *Journal of Physics A: Mathematical and Theoretical*, 53(50):505701, 2020.

[69] E Nkendji Kenkeu, AB Togueu Motcheyo, Thomas Kanaa, and C Tchawoua. Wave propagation with longitudinal dust grain oscillations in dusty plasma crystals. *Physics of Plasmas*, 29(4), 2022.

[70] Behrooz Yousefzadeh and A Srikantha Phani. Supratransmission in a disordered nonlinear periodic structure. *Journal of Sound and Vibration*, 380:242–266, 2016.

[71] Michael Mekontchou Foudjio, Frank Thomas Ndjomatchoua, Carlos Lawrence Gninzanlong, and Clément Tchawoua. Collective escape and supratransmission phenomena in a nonlinear oscillators chain. *Chaos: An Interdisciplinary Journal of Nonlinear Science*, 30(12), 2020.

[72] Jorge Eduardo Macías-Díaz. Numerical study of the transmission of energy in discrete arrays of sine-gordon equations in two space dimensions. *Physical Review E*, 77(1):016602, 2008.

[73] Merab Malishava and Ramaz Khomeriki. All-phononic digital transistor on the basis of gap-soliton dynamics in an anharmonic oscillator ladder. *Physical Review Letters*, 115(10):104301, 2015.

[74] Merab Malishava. All-phononic amplification in coupled cantilever arrays based on gap soliton dynamics. *Physical Review E*, 95(2):022203, 2017.

[75] Bambi Hu, Guoxiang Huang, and Manuel G Velarde. Dynamics of coupled gap solitons in diatomic lattices with cubic and quartic nonlinearities. *Physical Review E*, 62(2):2827, 2000.

[76] K Kesavasamy and N Krishnamurthy. Lattice vibrations in a linear triatomic chain. *American Journal of Physics*, 46(8):815–819, 1978.

[77] Cang He, Kian-Meng Lim, Fang Zhang, and Jin-hui Jiang. Dual-tuning mechanism for elastic wave transmission in a triatomic lattice with string stiffening. *Wave Motion*, 112:102951, 2022.

[78] PC Dash and K Patnaik. Solitons in nonlinear diatomic lattices. *Progress of Theoretical Physics*, 65(5):1526–1541, 1981.

[79] St Pnevmatikos, M Remoissenet, and N Flytzanis. Propagation of acoustic and optical solitons in nonlinear diatomic chains. *Journal of Physics C: Solid State Physics*, 16(11):L305, 1983.

[80] Mason A Porter, Chiara Daraio, Eric B Herbold, Ivan Szelengowicz, and PG Kevrekidis. Highly nonlinear solitary waves in periodic dimer granular chains. *Physical Review E*, 77(1):015601, 2008.

[81] Sen-yue Lou and Guoxiang Huang. Experimental study of the solitons in nonlinear diatomic macro-lattice. *Modern Physics Letters B*, 9(19):1231–1241, 1995.

[82] F Palmero, Lars Q English, Xuan-Lin Chen, Weilun Li, Jesús Cuevas-Maraver, and PG Kevrekidis. Experimental and numerical observation of dark and bright breathers in the band gap of a diatomic electrical lattice. *Physical Review E*, 99(3):032206, 2019.

[83] Abdou K Farota and Mansour M Faye. Experimental study of the fermi–pasta–ulam recurrence in a bi-modal electrical transmission line. *Physica Scripta*, 88(5):055802, 2013.

[84] T Kofane, B Michaux, and M Remoissenet. Theoretical and experimental studies of diatomic lattice solitons using an electrical transmission line. *Journal of Physics C: Solid State Physics*, 21(8):1395, 1988.

[85] Petrutza Anghel-Vasilescu, Jerome Dorignac, Frédéric Geniet, Jerome Leon, and Majid Taki. Nonlinear supratransmission in multicomponent systems. *Physical Review Letters*, 105(7):074101, 2010.

[86] AB Togueu Motcheyo and JE Macías-Díaz. Nonlinear bandgap transmission with zero frequency in a cross-stitch lattice. *Chaos, Solitons & Fractals*, 170:113349, 2023.

[87] Alaa Bader and OV Gendelman. Supratransmission in a vibro-impact chain. *Journal of Sound and Vibration*, 547:117493, 2023.

[88] Jian-Guo Cui, Mu-Qing Niu, Li-Qun Chen, and Tianzhi Yang. Asymmetric propagation of acoustic waves in a conical granular chain. *Communications in Nonlinear Science and Numerical Simulation*, 116:106885, 2023.

[89] AB Togueu Motcheyo, C Tchawoua, and JD Tchinang Tchameu. Supratransmission induced by waves collisions in a discrete electrical lattice. *Physical Review E*, 88(4):040901, 2013.

[90] Serge Bruno Yamgoué, Savério Morfu, and Patrick Marquié. Noise effects on gap wave propagation in a nonlinear discrete l c transmission line. *Physical Review E*, 75(3):036211, 2007.

[91] Xinyun Liu, Mei Wen, Xiezhi Mao, and Xinlong Wang. Optimal and efficient generation of sine-gordon breathers. *Physical Review E*, 104(1):014209, 2021.

[92] Joseph Lydon, Georgios Theocharis, and Chiara Daraio. Nonlinear resonances and energy transfer in finite granular chains. *Physical Review E*, 91(2):023208, 2015.

[93] Magnus Johansson, Georgios Kopidakis, Stefano Lepri, and Serge Aubry. Transmission thresholds in time-periodically driven nonlinear disordered systems. *Europhysics Letters*, 86(1):10009, 2009.

[94] H Simo and Paul Woafo. Bifurcation structure of a van der pol oscillator subjected to nonsinusoidal periodic excitation. *International Journal of Bifurcation and Chaos*, 22(01):1250003, 2012.

[95] Frank T Ndjomatchoua, Thierry LM Djomo, Florent F Kemwoue, Carlos L Gninzanlong, Maxime P Kepnang, Martin S Siewe, Clément Tchawoua, Sansao A Pedro, and Timoleon C Kofane. Amplitude response, melnikov's criteria, and chaos occurrence in a duffing's system subjected to an external periodic excitation with a variable shape. *Chaos: An Interdisciplinary Journal of Nonlinear Science*, 32(8), 2022.

[96] Ricardo Chacón, Pedro J Martínez, Jesús María Marcos, FJ Aranda, and JA Martínez. Ratchet universality in the bidirectional escape from a symmetric potential well. *Physical Review E*, 103(2):022203, 2021.

[97] R Chacón, JA Martínez, and JJ Miralles. Impulse-induced optimum control of escape from a metastable state by periodic secondary excitations. *Physical Review E*, 85(6):066207, 2012.

[98] Frank Thomas Ndjomatchoua, Carlos Lawrence Gninzanlong, Thierry Landry Michel Mbong Djomo, Maxime Fabrice Pebeu Kepnang, and Clément Tchawoua. Enhanced signal response in globally coupled networks of bistable oscillators: Effects of mean field density and signal shape. *Physical Review E*, 107(6):064208, 2023.

[99] Wulfram Gerstner and Werner M Kistler. Spiking neuron models: Single neurons, populations, plasticity. 2002.

[100] W. Gerstner, W. M. Kistler, R. Naud, and L. Paninski, "Neuronal Dynamics: From Single Neurons to Networks and Models of Cognition," (Cambridge University Press, 2014).

[101] Wulfram Gerstner, Werner M Kistler, Richard Naud, and Liam Paninski. Neuronal dynamics: From single neurons to networks and models of cognition. 2014.

[102] Ken A Dill and Hue Sun Chan. From levinthal to pathways to funnels. *Nature structural biology*, 4(1):10–19, 1997.

[103] R. P. Behringer and J. T. Jenkins, Frictional Mechanics: Particles, Packs, and Forces, Physics Today 60, 32 (2007).

[104] Govind P Agrawal. Nonlinear fiber optics. pages 195–211, 2000.

[105] Morikazu Toda. Vibration of a chain with nonlinear interaction. *Journal of the Physical Society of Japan*, 22(2):431–436, 1967.

[106] Morikazu Toda. Theory of nonlinear lattices. 20, 2012.

[107] Ryogo Kubo, Morikazu Toda, and Natsuki Hashitsume. Statistical physics ii: nonequilibrium statistical mechanics. 31, 2012.

[108] Philip W Anderson. Absence of diffusion in certain random lattices. *Physical Review*, 109(5):1492, 1958.

[109] OV Pountougnigni, R Yamapi, G Filatrella, and C Tchawoua. Noise and disorder effects in a series of birhythmic josephson junctions coupled to a resonator. *Physical Review E*, 99(3):032220, 2019.

[110] OV Pountougnigni, R Yamapi, C Tchawoua, V Pierro, and G Filatrella. Detection of signals in presence of noise through josephson junction switching currents. *Physical Review E*, 101(5):052205, 2020.

[111] Guoying Zhao, Feng Tao, and Weizhong Chen. Soliton excitation in the pass band of the transmission line based on modulation. *Chinese Physics B*, 25(4):044101, 2016.

[112] Fabien Kenmogne, David Yemélé, Jacques Kengne, and Désiré Ndjanfang. Transverse compactlike pulse signals in a two-dimensional nonlinear electrical network. *Physical Review E*, 90(5):052921, 2014.

[113] Essimbi BZ and Barashenkov IV. Gap soliton excitations in a bi-inductance electrical line. *Journal of the Physical Society of Japan*, 71(2):448–452, 2002.

[114] Frank T Ndjomatchoua, Clément Tchawoua, Francois MM Kakmeni, Bruno P Le Ru, and Henri EZ Tonnang. Waves transmission and amplification in an electrical model of microtubules. *Chaos: An Interdisciplinary Journal of Nonlinear Science*, 26(5), 2016.

[115] Ramaz Khomeriki and Jerome Leon. Light detectors bistable nonlinear waveguide arrays. *Physical Review Letters*, 94(24):243902, 2005.

[116] L Brillouin. Periodic structure: electronic filters and crystal lattices. 1946.

[117] Dominique Chevriaux. *Supratransmission et bistabilité nonlinéaire dans les milieux à bandes interdites photoniques et électroniques*. PhD thesis, Université Montpellier II-Sciences et Techniques du Languedoc, 2007.

[118] Yuriy A Kosevich. Nonlinear sinusoidal waves and their superposition in anharmonic lattices. *Physical Review Letters*, 71(13):2058, 1993.

[119] C Tchawoua, TC Kofane, and AS Bokosah. Dynamics of solitary waves in diatomic chains with long-range kac-baker interactions. *Journal of Physics A: Mathematical and General*, 26(22):6477, 1993.

[120] N Flytzanis, M Remoissenet, et al. Soliton dynamics of nonlinear diatomic lattices. *Physical Review B*, 33(4):2308, 1986.

[121] Ayşe Kiper. Fourier series coefficients for powers of the jacobian elliptic functions. *Mathematics of computation*, 43(167):247–259, 1984.

[122] Christian Simadji Ngamou, Thomas Franck Ndjomatchoua, and Clément Tchawoua. Periodic driving shape controls energy transmission. *Physical Review E*, 109(L052201), 2024.

[123] John Charles Butcher. A history of runge-kutta methods. *Applied numerical mathematics*, 20(3):247–260, 1996.

[124] David Goeken and Olin Johnson. Runge–kutta with higher order derivative approximations. *Applied numerical mathematics*, 34(2-3):207–218, 2000.

[125] John Charles Butcher. The numerical analysis of ordinary differential equations: Runge-kutta and general linear methods. 1987.

[126] Ruitao Lin, Chan Wang, Fang Liu, and Yueliang Xu. A new numerical method of nonlinear equations by four order runge-kutta method. pages 1295–1299, 2010.

[127] Mohammed S Mechee and Yasen Rajihy. Generalized rk integrators for solving ordinary differential equations: A survey& comparison study. *Global Journal of Pure and Applied Mathematics*, 13(7):2923–2949, 2017.

[128] Erwin Fehlberg. New high-order runge-kutta formulas with step size control for systems of first-and second-order differential equations. *ZAMM-Journal of Applied Mathematics and Mechanics/Zeitschrift für Angewandte Mathematik und Mechanik*, 44(S1 S1):T17–T29, 1964.

[129] M Miyama and S Kumano. Numerical solution of q2 evolution equations in a brute-force method. *Computer Physics Communications*, 94(2-3):185–215, 1996.

[130] Christopher Bingham, Michael Godfrey, and John Tukey. Modern techniques of power spectrum estimation. *IEEE Transactions on audio and electroacoustics*, 15(2):56–66, 1967.

[131] Paul Heckbert. Fourier transforms and the fast fourier transform (fft) algorithm. *Computer Graphics*, 2(1995):15–463, 1995.

[132] Henri J Nussbaumer and Henri J Nussbaumer. The fast fourier transform. 1982.

[133] E Oran Brigham. The fast fourier transform and its applications. 1988.

[134] Glenn D Bergland. A fast fourier transform algorithm using base 8 iterations. *Mathematics of Computation*, 22(102):275–279, 1968.

[135] Magnus Johansson, Georgios Kopidakis, Stefano Lepri, and Serge Aubry. Transmission thresholds in time-periodically driven nonlinear disordered systems. *Europhysics Letters*, 86(1):10009, 2009.

[136] Jorge E Macías-Díaz and Anastasios Bountis. Supratransmission in β-fermi–pasta–ulam chains with different ranges of interactions. *Communications in Nonlinear Science and Numerical Simulation*, 63:307–321, 2018.

[137] Qiwei Zhang, Hongbin Fang, and Jian Xu. Programmable stopbands and supratransmission effects in a stacked miura-origami metastructure. *Physical Review E*, 101(4):042206, 2020.

[138] Zhen Wu and Kon-Well Wang. On the wave propagation analysis and supratransmission prediction of a metastable modular metastructure for nonreciprocal energy transmission. *Journal of Sound and Vibration*, 458:389–406, 2019.

[139] J Lajzerowicz, JJ Niez, AR Bishop, and T Schneider. Solitons and condensed matter physics. pages 195–8, 1978.

[140] Steven H Strogatz. Nonlinear dynamics and chaos: with applications to physics, biology, chemistry, and engineering. 2018.

[141] Francis C Moon and Michael Shlesinger. Chaotic and fractal dynamics: An introduction for applied scientists and engineers. 1993.

[142] Michael Tabor. Chaos and integrability in nonlinear dynamics: An introduction, wileyinterscience. *Chaos and Integrability in Nonlinear Dynamics: An Introduction*, 1989.

[143] Landa, Peter S. , Dynamics of nonlinear systems." Springer Science and Business Media, 2013.